MODELING OF THE DYNAMICS OF MULTI-AXLE STEERED VEHICLES

A THESIS SUBMITTED TO
THE GRADUATE SCHOOL OF NATURAL AND APPLIED SCIENCES
OF
MIDDLE EAST TECHNICAL UNIVERSITY

BY

KEREM BAYAR

IN PARTIAL FULFILLMENT OF THE REQUIREMENTS
FOR
THE DEGREE OF MASTER OF SCIENCE
IN
MECHANICAL ENGINEERING

JULY 2006

Approval of the Graduate School of Natural and Applied Sciences

Prof. Dr. Canan Özgen
Director

I certify that this thesis satisfies all the requirements as a thesis for the degree of Master of Science.

Prof. Dr. Kemal İDER
Head of Department

This is to certify that we have read this thesis and that in our opinion it is fully adequate, in scope and quality, as a thesis for the degree of Master of Science.

Prof. Dr. Y. Samim ÜNLÜSOY
Supervisor

Examining Committee Members

Prof. Dr. Y. Samim Ünlüsoy (METU, ME) _____

Prof. Dr. Tuna Balkan (METU, ME) _____

Asst. Prof. Dr. İlhan Konukseven (METU, ME) _____

Instr. Dr. Yiğit Yazıcıoğlu (METU, ME) _____

Asst. Prof. Dr. Murat Köksal (Hacettepe U, ME) _____

I hereby declare that all information in this document has been obtained and presented in accordance with academic rules and ethical conduct. I also declare that, as required by these rules and conduct, I have fully cited and referenced all material and results that are not original to this work.

Name, Last name : Kerem Bayar

Signature :

ABSTRACT

MODELING OF THE DYNAMICS OF MULTI-AXLE STEERED VEHICLES

Bayar, Kerem
M.S., Department of Mechanical Engineering
Supervisor: Prof. Dr. Y. Samim Ünlüsoy

July 2006, 92 pages

Four wheel steering (4WS) is a concept proven to be beneficial in low speed applications requiring large steering angles, which is the case in city traffic or parking. By steering the rear wheels in the opposite direction to the front ones, maneuverability can be improved. However, a conflict is encountered at high speeds for all the steering strategies developed. If sharper response is achieved, this is at the expense of undesirably large vehicle sideslip angles. On the other hand, small vehicle sideslip angles are associated with heavy understeering behavior. It is not possible to improve both simultaneously in case of two-axle 4WS vehicles.

The object of this study is the simulation of various steering configurations for multi-axle vehicles in an attempt to find a means of solving the problem of 4WS and to determine the best steering strategy. In addition to two-axle vehicles which have been extensively studied in literature, three- and four-axle vehicles are taken into consideration. By extending the strategies used for 4WS two-axle vehicles, new strategies are established for three and four-axle vehicles. An integrated non-linear ride and handling model in Matlab & Simulink environment considering sprung and

unsprung mass motions, wheel and tire dynamics, is used for simulations. It is shown by case studies that, with the application of the derived strategies for three and four-axle vehicles, lateral acceleration and yaw velocity responses can be improved without degrading vehicle sideslip angle.

Keywords: 4WS, Three-Axle Vehicle, Four-Axle Vehicle, Multi-Axle Steering, Steering Strategy, Handling

ÖZ

ÇOK AKSTAN YÖNLENDİRİLEN ARAÇLARIN DİNAMİK MODELLENMESİ VE ANALİZİ

Bayar, Kerem
Yüksek Lisans, Makina Mühendisliği Bölümü
Tez Yöneticisi: Prof. Dr. Y. Samim Ünlüsoy

Temmuz 2006, 92 sayfa

Bu güne kadar çalışmalar ve uygulamalar, yol araçlarında dört tekerlekten yönlendirmenin, düşük hızlarda geniş yönverme açıları gereken durumlarda; yani şehir trafiğinde ya da park esnasında yarar sağladığını kanıtlamıştır. Arka tekerlekler ön tekerleklerin tersi yönde döndürülerek araçların manevra kabiliyetleri gelistirilebilmiştir. Ancak şu ana kadar önerilen yönlendirme stratejilerinin tümünde, yüksek hızlarda bir çelişki ile karşılaşılmıştır. Araçtan daha iyi viraj davranışı, ancak araç yüzme açısının arttırılması durumunda elde edilebilmektedir. Diğer taraftan, araç yüzme açısının azaltılması, aracın viraj alma yeteneğini olumsuz yönde etkilemektedir.

Bu çalışmanın amacı, çok aksli araçlarda yukarda belirtilen problemi gidermenin mümkün olup olmayacağını incelemek ve çeşitli yönlendirme stratejiler arasından en iyisini seçmektir. Literatürde kapsamlı olarak incelenmiş iki akslı araçların yanı sıra üç ve dört akslı araçlar göz önüne alınmıştır. İki akslı, dört tekerlekten yönlendirilen araçlar için kullanılan stratejiler genişletilerek, üç ve dört akslı araçlar için yeni stratejiler elde edilmiştir. Simülasyonlar için yaylı ve yaysız kütle hareketlerini,

tekerlek ve lastik dinamiğini içeren, lineer olmayan entegre bir sürüş ve yol tutuş modeli kullanılmıştır. Durum çalışmaları, üç ve dört akslı araçlarda ara akslar üzerindeki tekerleklerin de yönlendirilmesi yoluyla, araçların dönme hızlarının ve yanal ivmelerinin araç yüzme açısı arttırılmadan yükseltilebileceğini göstermiştir.

Anahtar Kelimeler: Dört Tekerlekten Yönlendirme, Üç Akslı Araç, Dört Akslı Araç, Çok Akstan Yönlendirme, Yönlendirme Stratejisi, Yol Tutuş

ACKNOWLEDGEMENTS

I express my deepest gratitude to my supervisor Prof. Dr. Y. Samim Ünlüsoy for his guidance, advice, criticism, encouragements and insight throughout the research. Special thanks go to my parents, M. Akif Bayar and F. Leyla Bayar, for their moral support and incredible sacrifices throughout my whole life. I offer sincere thanks to my elder brother Fırat Bayar for his guidance and support in moral and academic respect. Thanks also go to my colleagues Emir Kutluay and Gökhan Tekin for their appreciable help in my study.

TABLE OF CONTENTS

LIST OF TABLES

Table

LIST OF FIGURES

Figure

LIST OF SYMBOLS

a_l	lateral acceleration
A_f	frontal area
A_s	friction reduction factor
c_i	damping coefficient of suspension
C_D	drag coefficient
C_f	cornering stiffness of front wheels
C_i	cornering stiffness
C_l	tire longitudinal stiffness
C_m	cornering stiffness of wheels on intermediate axle
C_r	cornering stiffness orear wheels
e	rolling resistance static coefficient
F_{si}	suspension force
F_{xi}	longitudinal force generated by tire
F_{yi}	lateral force generated by tire
F_{zi}	dynamic load on tire
F_{zis}	static load on tire
g	rolling resistance velocity dependent coefficient
h	height of center of gravity from ground
I_x	mass moment of inertia, x-axis
I_y	mass moment of inertia, y-axis
I_z	mass moment of inertia, z-axis
I_ω	spin inertia of wheel
k_{si}	spring coefficient of the i^{th} suspension
k_t	spring coefficient of tire
K_{ri}	anti roll bar stiffness
K_{fr}	front roll stiffness
K_{rr}	rear roll stiffness
K_{roll}	roll stiffness

L	wheelbase
m_i	unsprung mass
M	sprung mass
n	distance between roll center and center of gravity
p	roll velocity
q	pitch velocity
r	yaw velocity
r_w	rolling radius of tire
R_a	air resistance
s_i	longitudinal slip
t	track
t_s	distance between suspension mounting points
T	drive or brake torque
V_i	velocity component in wheel plane
V_s	sliding velocity
V_x	forward velocity
V_y	lateral velocity
V_z	vertical velocity
z_i	unsprung mass vertical displacement
z_{oi}	road input
α	slip angle
β	vehicle sideslip angle
ϕ	roll angle
δ_f	front axle steering angle
δ_m	intermediate axle steering angle
δ_r	rear axle steering angle
δ_i	steering angle of the
μ_0	static tire road friction coefficient
ω_i	rotational speed

subscript i	i^{th} wheel, axle, tire, or suspension

Abbreviations:

FWS : Front Wheel Steering
4WS : Four Wheel Steering
6WS : Six Wheel Steering
8WS : Eight Wheel Steering
GUI : Graphical User Interface
CAD : Computer Aided Design
APC : Armored Personal Carrier

CHAPTER 1

INTRODUCTION

Since the invention of automobile, vehicle handling has always been a topic of research for automotive engineers. With the development of modern computers, and utilization of powerful software tools like MATLAB/Simulink, ADAMS, Dymola/Modelica, etc., computer aided design (CAD) methods started taking part in ground vehicle studies. Testing vehicles in computer environment proved to be a very powerful tool, since it gave valid information about vehicles' dynamic behavior even before road tests, and provided freedom of modification of design parameters just by typing buttons on the keyboard. Further, it became possible to replace road tests with computer simulations. The most important outcome of this development is the reduction of the development cost and time of a new vehicle. Moreover, simulations made it possible to try new ideas which provided valuable information in the research and development stage.

With the ever increasing competition in the design and development of road vehicles, one of the relatively recent popular research subjects has been the four wheel steering (4WS). In the period covering the last twenty five years, researchers have carried out many experimental and theoretical studies on 4WS two-axle vehicles, especially on passenger cars. The handling performance of 4WS two-axle vehicles has been widely investigated in automotive industry as well as in academia, as a means for improving maneuverability, stability, and handling; and a number of steering strategies have been proposed and even implemented. Advantages claimed for these systems include enhanced maneuverability at low speeds and improved handling during high speed maneuvers with increased stability, and reduced sensitivity to lateral wind gusts.

On the other hand, number of published research on multi-axle steered vehicles, such as six (6WS) or eight wheel steering (8WS) vehicles, is surprisingly low.

In this study, lateral dynamics of three and four-axle vehicles, in addition to two-axle vehicles, is investigated. Vehicles are modeled considering sprung and unsprung mass motion, wheel and nonlinear tire dynamics. Dynamic simulation is performed with an integrated performance, ride, and handling model using MATLAB [1]. The differential equations of motion governing the motion of the vehicles are built in SIMULINK.

Various steering strategies are applied to the models. Among those are the ones previously proposed for 4WS vehicles and the ones newly developed for three- and four-axle vehicles.

A graphical user interface (GUI) is built to load and save data, to specify simulation time, to select inputs, namely torque to wheels, drive configuration, steering input, steering strategy, and road profile, to perform the simulation, and to view the results.

Finally, case studies are performed with typical data for a two-axle bus, a three-axle commercial truck, and a four-axle armored personal carrier (APC). The vehicles are simulated with the existing and proposed control laws, and eventually results are discussed in terms of vehicle handling characteristics.

The thesis is composed of seven chapters. In Chapter 2, a literature survey on different multi-axle steering strategies for two, three and four-axle vehicles is presented. In Chapter 3, detailed mathematical modeling of the vehicles is performed. In Chapter 4, the data used in case studies is presented, and the inputs of the simulation, namely torque, drive configuration, steering input and strategies, and road profile are discussed. Further a stability analysis is performed. In Chapter 5, differential equations of motion built in SIMULINK, and some snapshots taken from the graphical user interface (GUI) of the simulation are presented. In Chapter 6, case studies are performed for two, three, and four-axle vehicles, and finally in Chapter 7, conclusions are made on the results of these simulations, and possible future studies are discussed.

CHAPTER 2

LITERATURE REVIEW

2.1 4WS

Since the beginning of the automobile in the late 19th century, front wheel steering (FWS) was almost exclusively used to control the direction of motion of road vehicles. This steering idea, derived from horse-driven carriages, worked rather well, and it was taken for granted that automobiles should be steered by this method.

On the other hand, as vehicle performance improved and designs became more sophisticated, designers began to feel the need for a better response to the steering input by the driver.

During the last twenty five years, a number of significant technologies have developed, enhancing vehicle handling at high speeds. One such advance is the result of the realization that coordinated steering of all four wheels of an automobile can improve its handling and stability. According to Sano et al. [2], Xia et al. [3], and Furukawa et al. [4], when the front wheels of a FWS vehicle are steered, the front wheels change direction and doing so generate lateral forces and tire slip angles. These lateral forces immediately give rise to an angular acceleration about the centre of gravity due to unbalanced yaw moment. The angular acceleration caused by the yawing motion thus enables the vehicle to change direction. Only after the body has started yawing, lateral forces are generated by the rear wheels as they are initially aligned with the body. The vehicle assumes a steady-state motion only after the moment generated by the rear wheels balances the moment generated by the front wheels. This concept led to the idea that if front and rear wheels can move simultaneously in a coordinated manner, then both can generate lateral forces and thus reduce the delay in response by not necessarily having to wait for the vehicle body to start yawing. In other words, if the rear wheels were directly steered as well

to control the sideslip angle, the direction of motion of the vehicle could be changed more quickly. The idea, theoretical in a sense, of steering the rear wheels simultaneously with the front ones as a means of improving the vehicle performance in lateral motion marked an innovative step forward in that technological area based on a different concept.

Studies were made on various 4WS control principles both in feedback and feed-forward compensation configurations. In these control principles, the following steering response characteristics were envisaged as desirable control objectives:

1) Shorter phase lags in lateral acceleration and yaw responses
2) Reduction in sideslip angle (off-tracking) of the vehicle body
3) Stability augmentation
4) Better maneuverability at low speed
5) Achievement of the desired steering responses (model-matching/model-following control)
6) Better responses near the limits of tire adhesion

2.1.1 Historical Developments

The first engineers in history to implement 4WS in a vehicle were working under the structure of Mercedes-Benz [5]. In 1938, they made a cross-country military vehicle called 170VL, which steered the rear wheels in the opposite direction with respect to the front wheels, in order to shorten turning radius. However, Mercedes never applied 4WS in its road cars.

Sato et al. [6] was the first to study 4WS vehicles in detail, in an attempt to obtain desirable vehicle characteristics. He stated: “such vehicle characteristics were considered to be desirable when the velocity vector always agrees with the vehicle longitudinal axis in any running condition”. In other words, zero vehicle sideslip is to be obtained so that the vehicle behavior can be exactly known and suitable handling can be made. This would also ensure a good balance between controllability and stability. This conclusion has provided the first requirement for all 4WS strategies to be developed afterwards.

To analyze the 4WS behavior, Sato et al. [6] proposed a rear wheel controller based on yaw rate feedback together with feed-forward of front steering angle. The gains of the controller were obtained by assuming that centripetal acceleration at the front and rear axles were equal and that at low speeds the lateral slip at both axles was zero. The theoretical and experimental results indicated that 4WS enhanced tracking and steering properties and improved response to external disturbances.

Shibahata et al. [7] emphasized the disadvantages as well as the advantages of 4WS applications. It is interesting to note that, in spite of many different steering strategies proposed so far, the disadvantages indicated by them have not yet been satisfactorily eliminated.

Sano et al. [8] proposed a feed-forward control 4WS designed to steer the rear wheels proportionally in the same direction as the front wheels, in an attempt to reduce the delay in the vehicle's lateral acceleration responses. Moreover they derived an expression for the ratio of the front to the rear wheel steering angle based on achieving zero body sideslip angle in a steady state turn. The expression was a function of the vehicle parameters and forward velocity, and indicated that at high speeds the front and rear wheels must be steered in the same direction, while for low speeds it is just the opposite. This controller was implemented in the Honda Prelude SI in 1988.

The first 4WS mass-production road car was Nissan Skyline in around 1985 [5]. Unlike the Mercedes, it steered the rear wheels in the same direction as the front wheels with a maximum angle of 0.5 degrees, which helped stability. However, Skyline's system did not qualify for the conventional definition of 4WS, because it simply steered the whole rear suspension mounting sub-frame by hydraulic power.

Therefore, the first decent production 4WS car is acknowledged to be the Honda Prelude 1987 [9]. The steering strategy for this model required a rear wheel steering angle depending on the front wheel steering angle. When turning the steering wheel, initially the rear wheels steer slightly, at most 1.7 degree, in the same direction as the front wheels. This improves stability during high speed turning or lane changing. Further turning the steering wheel will reverse the direction of rear wheels. This is used to sharpen the response of low speed cornering or parking. The following diagram shows this characteristic.

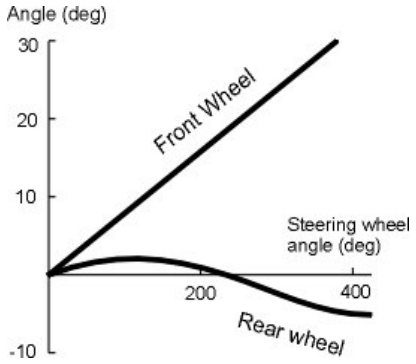

Figure 2.1 Rear and front wheel angles [5]

Takiguchi et al. [10] showed that equalizing the phase between the yaw rate and lateral acceleration while minimizing both phase lags improved vehicle maneuverability. Cars with a minimum difference between phase lag of yaw rate and lateral acceleration received the best subjective ratings. The rear wheel was again steered proportionally to the front wheel. The proportionality factor was a function of forward speed and used steering frequency as input for a particular frequency range. This proportional controller was implemented in 1989 Mazda 625.

Nakaya and Oguchi [11] investigated a rear wheel controller that steered the rear wheels in proportion to the front wheels. This controller affected the phase lag of both yaw rate and lateral acceleration. Step steer and course tracking prototype tests demonstrated that a reduction in phase lag with respect to the steering input for both yaw rate and lateral acceleration improved the controllability of the vehicle.

Whitehead [12] discussed, using a two degree of freedom model, why 4WS vehicles can not give significant improvements in parallel parking. He agreed that high speed motion stability was improved by 4WS, and maintaining zero sideslip angle was desirable; but stated that “It was not known which mode was being stabilized”. A new controller was obtained by setting the rate of change of sideslip angle and sideslip angle to zero, which ultimately resulted in an uncoupled system for sideslip angle. This closed loop law resulted in zero sideslip even during transient motion of the vehicle as opposed to the open loop law. Whitehead later [13] showed numerically that the free steering control problem could be stabilized using 4WS.

Higuchi and Saitoh [14] derived a method which feeds forward the steering wheel angle and feeds back the yaw velocity and the sideslip angle to the front and rear wheel angles, based on optimal control theory. Theoretical studies showed that the sideslip angle is reduced to zero even in the transient state, and the yaw velocity and lateral acceleration responses exhibit first order lag. Further, steering characteristics in terms of frequency response can be changed regardless of the vehicle static margin.

Research on 4WS remained popular from late 80s to early 90s. From late 80s to today, 4WS remained to be uniquely adopted by Japanese car makers. Western car makers did not seem to be very interested (although Audi was rumored to be developing 4WS for A8, but it did not realize). Since the mid-90s, even Japanese themselves started losing interest, dropping 4WS in their models. The main reason for this loss of interest seems to be due to the fact that the early expectations from the application of 4WS have not, so far, been fully realized. Improvements in low speed applications are clear, but at high speeds a conflict is encountered for all steering strategies developed. If sharper response is achieved, this is at the expense of undesirably large vehicle sideslip angle. On the other hand, small vehicle sideslip angles are associated with heavy understeering behavior. In most studies this is interpreted as increased stability, however, it can also be interpreted as sluggish response to steering inputs particularly at high speeds [15].

2.2 6WS and 8WS

As mentioned in the previous section, handling performance of 4WS vehicles has been widely investigated in automotive industry as well as in academia, and a number of steering strategies have been implemented for 4WS vehicles. However, there has been only a few studies and publications related to the applications of the 4WS idea to multi-axle vehicles such as 6WS and 8WS vehicles which constitute a large portion of commercial and military vehicles. Among these, an interesting study was presented by Kageyama and Nagai [16]. They proposed stabilization of tractor-trailer combinations by steering wheels on both axles of the tractor.

Huh et al. [17] investigated the handling performance of a six-wheeled special purpose vehicle in their study. They modeled the vehicle as an 18 degree of freedom system which included non-linear vehicle dynamics, tire models, and kinematical effects. They concluded that steering the wheels on intermediate axles was not negligible from the viewpoint of handling. Further, they extended the theory used for two-axle vehicles and proposed a new control law for the first time in literature to minimize sideslip angle.

Qu et al. [18] examined a three-axle vehicle considering a linear model with front and rear wheel steering and applied the available steering strategies developed for 4WS passenger cars. They found that manoeuvrability and stability of a commercial three-axle vehicle is improved by front and rear wheel steering. They did not, however, consider steered wheels on the intermediate axle.

As mentioned before, in spite of the many steering strategies implemented on 4WS vehicles, the early expectations from the application of 4WS have not been fully realized. Particularly at high speeds, small vehicle side slip angles are associated with heavy understeering behaviour. Therefore, a successful steering strategy needs to provide a means to achieve a low sideslip angle with high yaw velocity and lateral acceleration. The aim of this study is to explore the possibility of a low sideslip angle together with high yaw velocity and lateral acceleration in the case of three and four-axle vehicles, by steering the wheels on intermediate axles. In fact, it is important to see by way of simulation the possibility of realization of the lateral acceleration levels of the neutral steering FWS vehicles by steering the wheels on intermediate axles at reasonable angles, without degrading vehicle sideslip angle.

CHAPTER 3

MODELING

In order to make simulations with valid vehicle data and reach realistic results and conclusions, a detailed model should be developed. The model should include as many as degrees of freedom as needed in order to reflect a real vehicle's behavior. For a rigid body in space, which may be a vehicle for instance, there exist three translational and three rotational degrees of freedom as shown in Figure 3.1.

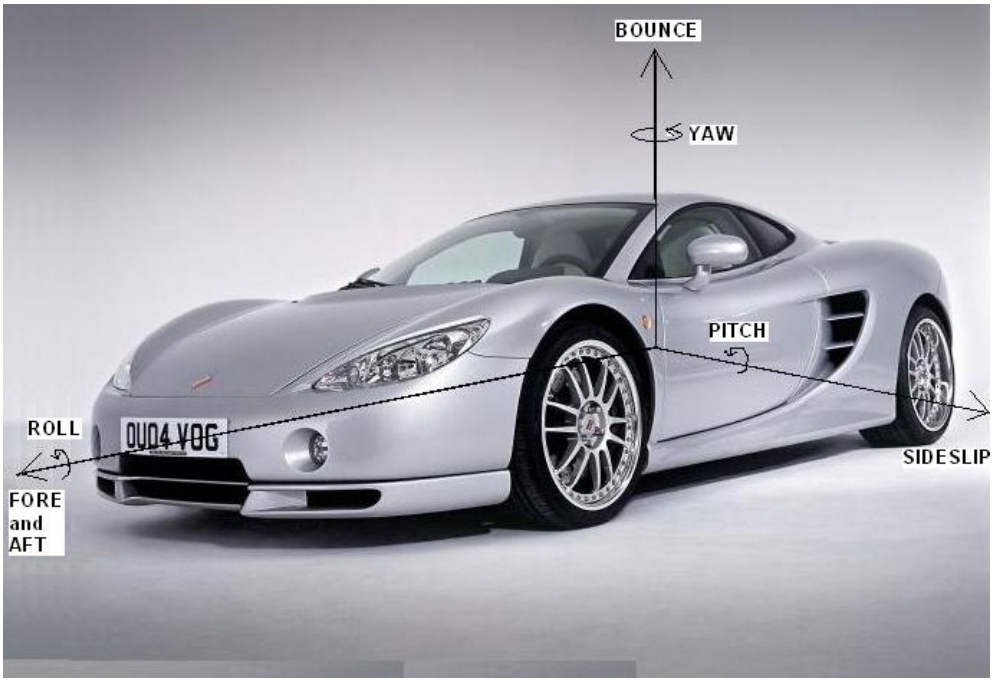

Figure 3.1 Degrees of freedom of a vehicle in space

Table 3.1 shows the degrees of freedom and their relations to subject of study in vehicle dynamics terminology.

Table 3.1 Degrees of freedom of a vehicle and its subject of study [19]

FREEDOM	SUBJECT
BOUNCE	RIDE
SIDE SLIP	HANDLING
FORE AND AFT	PERFORMANCE
YAW	HANDLING
PITCH	RIDE
ROLL	HANDLING, RIDE

Figures 3.2 to 3.4 are built in RHINO [20] environment and are used as mathematical models for two, three, and four-axle vehicles respectively, that are studied in this thesis study.

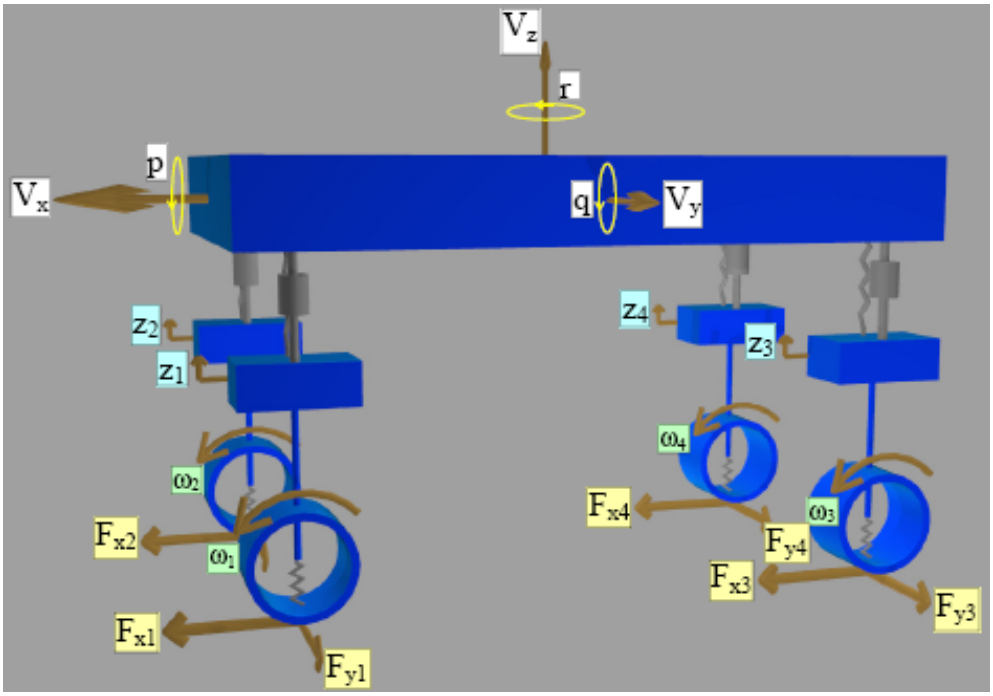

Figure 3.2 Two-axle vehicle model

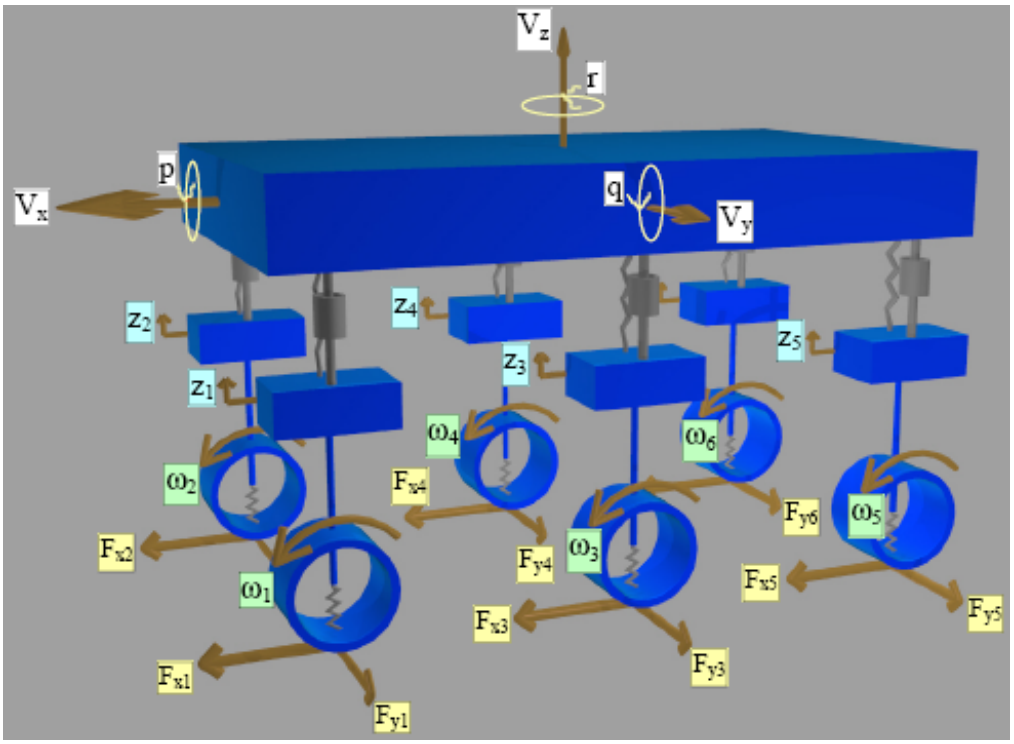

Figure 3.3 Three-axle vehicle model

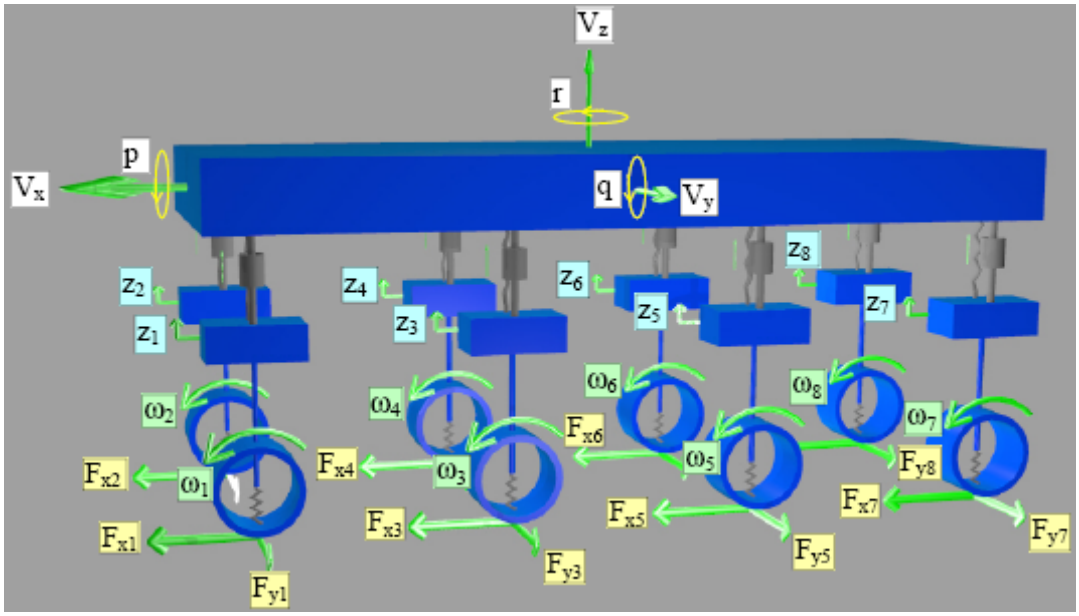

Figure 3.4 Four-axle vehicle model

Note that the models include sprung mass degrees of freedom, unsprung mass motions in vertical direction, wheel rotational dynamics, and lateral and longitudinal forces generated from the nonlinear tire model.

3.1 Equations of Motion for Sprung and Unsprung Masses

As shown in Figures 3.2 to 3.4, the sprung mass possesses three translational and three rotational degrees of freedom which are coupled due to the fact that the body centered reference frame also moves with the vehicle.

In order to write the differential equations of motion describing the motion of the vehicle with respect to ground, a body fixed axis system is represented by Figure 3.5, in which the axes x,y, and z are mutually perpendicular. Consider a typical point *(x, y, z)* and let the point have linear velocity components *a, b, c* relative to the origin and directed parallel to x, y, z axes respectively. In addition, the axes possess rotational velocities *p, q, r* about x, y, z axes, respectively.

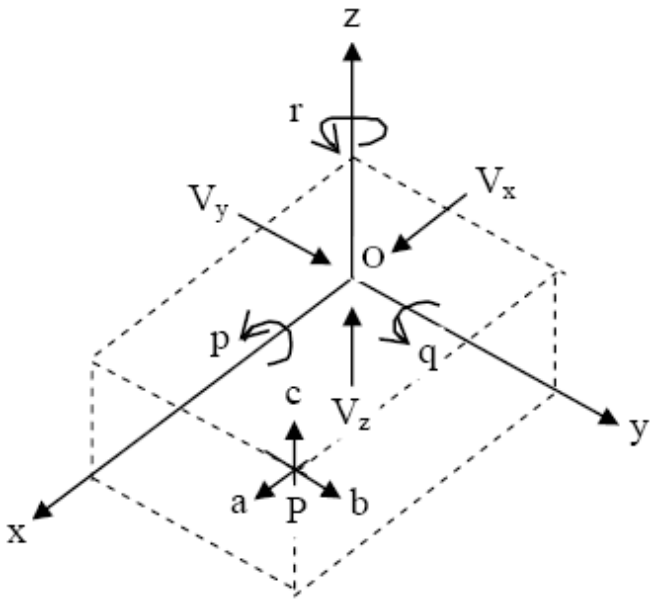

Figure 3.5 The body centered reference system

Let u, v, w be the velocities of the point P parallel to the x, y, z axes, respectively. Then from inspection of Figure 3.5

Velocity parallel to x axis:

$$u = a - ry + qz \tag{3.1}$$

Velocity parallel to y axis:

$$v = b - pz + rx \tag{3.2}$$

Velocity parallel to z axis:

$$w = c - qx + py \tag{3.3}$$

Equations 3.1 to 3.3 define the velocity of a point moving in a reference system of which the origin is fixed with respect to an inertial reference frame.

When the origin is free to move, as it is the case for a reference system fixed to a point on the vehicle, let V_x, V_y, V_z be the instantaneous velocities of the origin in the directions x, y, and z respectively, as shown in figure 3.5. Then the total velocity of P is the sum of the velocities of the origin and the velocity of P relative to the origin. Hence

$$\begin{aligned} u &= V_x + a - ry + qz \\ v &= V_y + b - pz + rx \\ w &= V_z + c - qx + py \end{aligned} \tag{3.4}$$

Equations 3.4 define the velocity of a point moving within a coordinate system which has freedom of translation and rotation. In the special case of a rigid body in which the origin is fixed relative to the body, like the models built for two, three, and four-axle vehicles in this study, $a=b=c=0$. Hence

$$\begin{aligned} u &= V_x - ry + qz \\ v &= V_y - pz + rx \\ w &= V_z - qx + py \end{aligned} \tag{3.5}$$

Let $\dot{u}$, $\dot{v}$, $\dot{w}$ be the accelerations of point P in such a rigid body. Then

$$\begin{aligned}
\dot{u} &= \frac{du}{dt} = \dot{V}_x - r\dot{y} - \dot{r}y + q\dot{z} + \dot{q}z \\
\dot{v} &= \frac{dv}{dt} = \dot{V}_y - p\dot{z} - \dot{p}z + r\dot{x} + \dot{r}x \\
\dot{w} &= \frac{dw}{dt} = \dot{V}_z - q\dot{x} - \dot{q}x + p\dot{y} + \dot{p}y
\end{aligned} \tag{3.6}$$

where $\dot{x} = u$, $\dot{y} = v$, $\dot{z} = w$ and $\dot{p}$, $\dot{q}$, $\dot{r}$ are the angular accelerations about the relevant axes. Substituting these equations in the acceleration equations yields

$$\begin{aligned}
\dot{u} &= \dot{V}_x + V_z q - V_y r - (q^2 + r^2)x + (qp - \dot{r})y + (rp + \dot{q})z \\
\dot{v} &= \dot{V}_y + V_x r - V_z p - (p^2 + r^2)y + (rq - \dot{p})z + (pq + \dot{r})x \\
\dot{w} &= \dot{V}_z + V_y p - V_x q - (p^2 + q^2)z + (pr - \dot{q})x + (qr + \dot{p})y
\end{aligned} \tag{3.7}$$

Equations 3.5 and 3.7 define the velocity and acceleration of a point *P(x, y, z)* in a rigid body when the reference axes are fixed relative to the body and the linear velocities of the axes are V_x, V_y, V_z, and the rotational velocities of the axes are *p, q, r*, respectively.

For a particle of constant mass, the product of the mass and the acceleration of the particle is vectorially equal to the resultant of the forces acting on the particle. By the application of d'Alambert's principle, the external forces and moments acting on a body form a system in equilibrium with the inertia forces. Hence by reference to Figure 3.5

Total external force in x direction $\sum F_x = \sum \delta M \dot{u}$

Total external force in y direction $\sum F_y = \sum \delta M \dot{v}$

Total external force in z direction $\sum F_z = \sum \delta M \dot{w}$ (3.8)

Total external moment about x axis $\sum M_x = \sum \delta M (y\dot{w} - z\dot{v})$

Total external moment about y axis $\sum M_y = \sum \delta M (z\dot{u} - x\dot{w})$

Total external moment about z axis $\sum M_z = \sum \delta M (x\dot{v} - y\dot{u})$

The reference frame may be located in any position provided that appropriate expressions for the accelerations are derived. Equation 3.7 defines the component accelerations for the case of a set of axes fixed in a rigid body. The position of the origin will now be defined as the centre of mass of the body so that:

$$\sum \delta Mx = \sum \delta My = \sum \delta Mz = 0 \tag{3.9}$$

The moments of inertia and products of inertia of the rigid body are now going to be defined:

$M = \sum \delta M$ = total sprung mass

$I_x = \sum \delta M (y^2 + z^2)$ = moment of inertia about 0x

$I_y = \sum \delta M (x^2 + z^2)$ = moment of inertia about 0y

$I_z = \sum \delta M (x^2 + y^2)$ = moment of inertia about 0z (3.10)

$P_{yz} = \sum \delta Myz$ = product of inertia about 0y and 0z

$P_{xz} = \sum \delta Mxz$ = product of inertia about 0x and 0z

$P_{xy} = \sum \delta Mxy$ = product of inertia about 0x and 0y

Note that the sprung mass possesses a plane of symmetry defined by (x, y) axes for the built models, i.e., for every element of mass at a distance +z from the plane, an opposing element exists at –z from the plane of symmetry. Thus, the products of inertia are eliminated. Substitution of Equations 3.7 and 3.8, and collecting the terms

in the form of Equation 3.10 yield the following differential equations of motion for the translational and rotational degrees of freedom of the sprung mass.

Longitudinal motion:

$$\sum F_x = M(\dot{V_x} + V_z q - V_y r) \tag{3.11}$$

Lateral motion:

$$\sum F_y = M(\dot{V_y} + V_x r - V_z p) \tag{3.12}$$

Vertical motion:

$$\sum F_z = M(\dot{V_z} + V_y p - V_x q) \tag{3.13}$$

Roll motion:

$$\sum M_x = I_x \dot{p} + (I_z - I_y) qr \tag{3.14}$$

Pitch motion:

$$\sum M_y = I_y \dot{q} + (I_x - I_z) rp \tag{3.15}$$

Yaw motion:

$$\sum M_z = I_z \dot{r} + (I_y - I_x) pq \tag{3.16}$$

where ΣF_x and ΣF_y, are resultant forces through x and y axes respectively which are composed of tire longitudinal and lateral forces as illustrated in Figures 3.2 to 3.4,

rolling resistance, and aerodynamic drag. ΣF_z is mainly composed of suspension forces; $\Sigma F_z = \Sigma F_{si}$.

Note that rolling resistance for the i^{th} tire is formulated as:

$$R_i = (e + gV_x)F_{zi} \tag{3.17}$$

where e and g are constants obtained from drum tests of a large number of commercial tires in Europe listed in Table 3.2 as follows:

Table 3.2 Average rolling resistance coefficients for commercial vehicle tires [21]

	Single wheel	**Tandem wheel**
e	0.0055	0.0062
g	$2.88\ 10^{-7}$	$7.2\ 10^{-7}$

On the other hand, aerodynamic drag which opposes the longitudinal motion of the vehicle is formulated as [19]:

$$R_a = 0.047 C_D A_f V_x^2 \tag{3.18}$$

where C_D = drag coefficient

A_f = frontal area of the vehicle = 0.9 (maximum height)(track) [m^2]

V_x = forward velocity of the vehicle [kph]

Drag coefficient C_D is selected according to Table 3.3 which gives average values for different type of vehicles:

Table 3.3 Table for the drag coefficient [22]

Vehicle Type	Drag Coefficient (C_D)
Automobile	0.25 - 0.55
Bus	0.5 – 0.7
Tractor- Trailer	0.6 – 1.3
Motorcycle	0.27 – 1.8

Note that Equations 3.11 to 3.16 are valid for two, three and four-axle vehicles investigated in this study. However, ΣF_x, ΣF_y, ΣF_z, ΣM_x, ΣM_y, ΣM_z differ for each of these vehicles, since there are extra forces generated from additional number of axles.

For the two-axle model shown in Figure 3.2,

$$\begin{aligned}\sum F_x = {} & F_{x1}\cos(\delta_f) - F_{y1}\sin(\delta_f) + F_{x2}\cos(\delta_f) - F_{y2}\sin(\delta_f) \\ & + F_{x3}\cos(\delta_r) - F_{y3}\sin(\delta_r) + F_{x4}\cos(\delta_r) - F_{y4}\sin(\delta_r) \\ & - \sum R_i - R_a\end{aligned} \tag{3.19}$$

$$\begin{aligned}\sum F_y = {} & F_{x1}\sin(\delta_f) + F_{y1}\cos(\delta_f) + F_{x2}\sin(\delta_f) + F_{y2}\cos(\delta_f) \\ & + F_{x3}\sin(\delta_r) + F_{y3}\cos(\delta_r) + F_{x4}\sin(\delta_r) + F_{y4}\cos(\delta_r)\end{aligned} \tag{3.20}$$

In writing the suspension force for each suspension, it should be noted that the sprung mass displacement over each suspension is different. For the two-axle vehicle shown in Figure 3.2:

$$
\begin{aligned}
F_{s1} &= k_{s1}(z_1 - \frac{t}{2}\int pdt + a\int qdt - \int V_z dt) + c_1(\dot{z_1} - \frac{t}{2}p + aq - V_z) \\
F_{s2} &= k_{s2}(z_2 + \frac{t}{2}\int pdt + a\int qdt - \int V_z dt) + c_2(\dot{z_2} + \frac{t}{2}p + aq - V_z) \\
F_{s3} &= k_{s3}(z_3 - \frac{t}{2}\int pdt - b\int qdt - \int V_z dt) + c_3(\dot{z_3} - \frac{t}{2}p - bq - V_z) \\
F_{s4} &= k_{s4}(z_4 + \frac{t}{2}\int pdt - b\int qdt - \int V_z dt) + c_4(\dot{z_4} + \frac{t}{2}p - bq - V_z)
\end{aligned}
\tag{3.21}
$$

Other rotational degrees of freedom, namely roll, pitch, and yaw are caused by the resultant moments about x, y and z axes respectively. ΣM_x, ΣM_y and ΣM_z are given as follows for the two-axle vehicle shown in Figure 3.2:

$$
\begin{aligned}
\sum M_x = h(&F_{x1}\sin(\delta_f) + F_{y1}\cos(\delta_f) + F_{x2}\sin(\delta_f) + F_{y2}\cos(\delta_f) \\
&+ F_{x3}\sin(\delta_r) + F_{y3}\cos(\delta_r) + F_{x4}\sin(\delta_r) + F_{y4}\cos(\delta_r)) \\
&+ \frac{t}{2}(F_{s1} - F_{s2} + F_{s3} - F_{s4})
\end{aligned}
\tag{3.22}
$$

$$
\begin{aligned}
\sum M_y = h(&-F_{x1}\cos(\delta_f) + F_{y1}\sin(\delta_f) - F_{x2}\cos(\delta_f) + F_{y2}\sin(\delta_f) \\
&- F_{x3}\cos(\delta_r) + F_{y3}\sin(\delta_r) - F_{x4}\cos(\delta_r) + F_{y4}\sin(\delta_r)) \\
&- a(F_{s1} + F_{s2}) + b(F_{s3} + F_{s4})
\end{aligned}
\tag{3.23}
$$

$$
\begin{aligned}
\sum M_z = &-\frac{t}{2}F_{x1}\cos(\delta_f) + aF_{x1}\sin(\delta_f) + aF_{y1}\cos(\delta_f) + \frac{t}{2}F_{y1}\sin(\delta_f) \\
&+ \frac{t}{2}F_{x2}\cos(\delta_f) + aF_{x2}\sin(\delta_f) + aF_{y2}\cos(\delta_f) - \frac{t}{2}F_{y2}\sin(\delta_f) \\
&- \frac{t}{2}F_{x3}\cos(\delta_r) - bF_{x3}\sin(\delta_r) - bF_{y3}\cos(\delta_r) + \frac{t}{2}F_{y3}\sin(\delta_r) \\
&+ \frac{t}{2}F_{x4}\cos(\delta_r) - bF_{x4}\sin(\delta_r) - bF_{y4}\cos(\delta_r) - \frac{t}{2}F_{y4}\sin(\delta_r)
\end{aligned}
\tag{3.24}
$$

For the three-axle model shown in Figure 3.3,

$$\begin{aligned}\sum F_x = {} & F_{x1}\cos(\delta_f) - F_{y1}\sin(\delta_f) + F_{x2}\cos(\delta_f) - F_{y2}\sin(\delta_f) \\ & + F_{x3}\cos(\delta_m) - F_{y3}\sin(\delta_m) + F_{x4}\cos(\delta_m) - F_{y4}\sin(\delta_m) \\ & + F_{x5}\cos(\delta_r) - F_{y5}\sin(\delta_r) + F_{x6}\cos(\delta_r) - F_{y5}\sin(\delta_r) \\ & - \sum R_i - R_a\end{aligned} \tag{3.25}$$

$$\begin{aligned}\sum F_y = {} & F_{x1}\sin(\delta_f) + F_{y1}\cos(\delta_f) + F_{x2}\sin(\delta_f) + F_{y2}\cos(\delta_f) \\ & + F_{x3}\sin(\delta_m) + F_{y3}\cos(\delta_m) + F_{x4}\sin(\delta_m) + F_{y4}\cos(\delta_m) \\ & + F_{x5}\sin(\delta_r) + F_{y5}\cos(\delta_r) + F_{x6}\sin(\delta_r) + F_{y6}\cos(\delta_r)\end{aligned} \tag{3.26}$$

ΣF_z is composed of suspension forces, as in the two-axle case:

$$\begin{aligned}
F_{s1} &= k_{s1}(z_1 - \frac{t}{2}\int pdt + a\int qdt - \int V_z dt) + c_1(\dot{z}_1 - \frac{t}{2}p + aq - V_z) \\
F_{s2} &= k_{s2}(z_2 + \frac{t}{2}\int pdt + a\int qdt - \int V_z dt) + c_2(\dot{z}_2 + \frac{t}{2}p + aq - V_z) \\
F_{s3} &= k_{s3}(z_3 - \frac{t}{2}\int pdt - b\int qdt - \int V_z dt) + c_3(\dot{z}_3 - \frac{t}{2}p - bq - V_z) \\
F_{s4} &= k_{s4}(z_4 + \frac{t}{2}\int pdt - b\int qdt - \int V_z dt) + c_4(\dot{z}_4 + \frac{t}{2}p - bq - V_z) \\
F_{s5} &= k_{s5}(z_5 - \frac{t}{2}\int pdt - c\int qdt - \int V_z dt) + c_5(\dot{z}_5 - \frac{t}{2}p - cq - V_z) \\
F_{s6} &= k_{s6}(z_6 + \frac{t}{2}\int pdt - c\int qdt - \int V_z dt) + c_6(\dot{z}_6 + \frac{t}{2}p - cq - V_z)
\end{aligned} \tag{3.27}$$

Other rotational degree of freedoms, namely roll, pitch, and yaw are caused by the resultant moments about x, y and z axes respectively, just like the two-axle case:

$$\begin{aligned}\sum M_x = {} & h(F_{x1}\sin(\delta_f) + F_{y1}\cos(\delta_f) + F_{x2}\sin(\delta_f) + F_{y2}\cos(\delta_f) \\ & + F_{x3}\sin(\delta_m) + F_{y3}\cos(\delta_m) + F_{x4}\sin(\delta_m) + F_{y4}\cos(\delta_m) \\ & + F_{x5}\sin(\delta_r) + F_{y5}\cos(\delta_r) + F_{x6}\sin(\delta_r) + F_{y6}\cos(\delta_r)) \\ & + \frac{t}{2}(F_{s1} - F_{s2} + F_{s3} - F_{s4} + F_{s5} - F_{s6})\end{aligned} \tag{3.28}$$

$$\begin{aligned}\sum M_y = h(&-F_{x1}\cos(\delta_f)+F_{y1}\sin(\delta_f)-F_{x2}\cos(\delta_f)+F_{y2}\sin(\delta_f)\\&-F_{x3}\cos(\delta_m)+F_{y3}\sin(\delta_m)-F_{x4}\cos(\delta_m)+F_{y4}\sin(\delta_m)\\&-F_{x5}\cos(\delta_r)+F_{y5}\sin(\delta_r)-F_{x6}\cos(\delta_r)+F_{y6}\sin(\delta_r))\\&-a(F_{s1}+F_{s2})+b(F_{s3}+F_{s4})+c(F_{s5}+F_{s6})\end{aligned} \tag{3.29}$$

$$\begin{aligned}\sum M_z = &-\frac{t}{2}F_{x1}\cos(\delta_f)+aF_{x1}\sin(\delta_f)+aF_{y1}\cos(\delta_f)+\frac{t}{2}F_{y1}\sin(\delta_f)\\&+\frac{t}{2}F_{x2}\cos(\delta_f)+aF_{x2}\sin(\delta_f)+aF_{y2}\cos(\delta_f)-\frac{t}{2}F_{y2}\sin(\delta_f)\\&-\frac{t}{2}F_{x3}\cos(\delta_m)-bF_{x3}\sin(\delta_m)-bF_{y3}\cos(\delta_m)+\frac{t}{2}F_{y3}\sin(\delta_m)\\&+\frac{t}{2}F_{x4}\cos(\delta_m)-bF_{x4}\sin(\delta_m)-bF_{y4}\cos(\delta_m)-\frac{t}{2}F_{y4}\sin(\delta_m)\\&-\frac{t}{2}F_{x5}\cos(\delta_r)-cF_{x5}\sin(\delta_r)-cF_{y5}\cos(\delta_r)+\frac{t}{2}F_{y5}\sin(\delta_r)\\&+\frac{t}{2}F_{x6}\cos(\delta_r)-cF_{x6}\sin(\delta_r)-cF_{y6}\cos(\delta_r)-\frac{t}{2}F_{y6}\sin(\delta_r)\end{aligned} \tag{3.30}$$

For the four-axle model shown in Figure 3.4,

$$\begin{aligned}\sum F_x = &F_{x1}\cos(\delta_1)-F_{y1}\sin(\delta_1)+F_{x2}\cos(\delta_1)-F_{y2}\sin(\delta_1)\\&+F_{x3}\cos(\delta_2)-F_{y3}\sin(\delta_2)+F_{x4}\cos(\delta_2)-F_{y4}\sin(\delta_2)\\&+F_{x5}\cos(\delta_3)-F_{y5}\sin(\delta_3)+F_{x6}\cos(\delta_3)-F_{y6}\sin(\delta_3)\\&+F_{x7}\cos(\delta_4)-F_{y7}\sin(\delta_4)+F_{x8}\cos(\delta_4)-F_{y8}\sin(\delta_4)\\&-\sum R_i - R_a\end{aligned} \tag{3.31}$$

$$\begin{aligned}\sum F_x = &F_{x1}\sin(\delta_1)+F_{y1}\cos(\delta_1)+F_{x2}\sin(\delta_1)+F_{y2}\cos(\delta_1)\\&+F_{x3}\sin(\delta_2)+F_{y3}\cos(\delta_2)+F_{x4}\sin(\delta_2)+F_{y4}\cos(\delta_2)\\&+F_{x5}\sin(\delta_3)+F_{y5}\cos(\delta_3)+F_{x6}\sin(\delta_3)+F_{y6}\cos(\delta_3)\\&+F_{x7}\sin(\delta_4)+F_{y7}\cos(\delta_4)+F_{x8}\sin(\delta_4)+F_{y8}\cos(\delta_4)\end{aligned} \tag{3.32}$$

ΣF_z is composed of suspension forces, as in the two and three-axle cases:

$$
\begin{aligned}
F_{s1} &= k_{s1}(z_1 - \frac{t}{2}\int pdt + a\int qdt - \int V_z dt) + c_1(\dot{z}_1 - \frac{t}{2}p + aq - V_z) \\
F_{s2} &= k_{s2}(z_2 + \frac{t}{2}\int pdt + a\int qdt - \int V_z dt) + c_2(\dot{z}_2 + \frac{t}{2}p + aq - V_z) \\
F_{s3} &= k_{s3}(z_3 - \frac{t}{2}\int pdt + b\int qdt - \int V_z dt) + c_3(\dot{z}_3 - \frac{t}{2}p + bq - V_z) \\
F_{s4} &= k_{s4}(z_4 + \frac{t}{2}\int pdt + b\int qdt - \int V_z dt) + c_4(\dot{z}_4 + \frac{t}{2}p + bq - V_z) \\
F_{s5} &= k_{s5}(z_5 - \frac{t}{2}\int pdt - c\int qdt - \int V_z dt) + c_5(\dot{z}_5 - \frac{t}{2}p - cq - V_z) \\
F_{s6} &= k_{s6}(z_6 + \frac{t}{2}\int pdt - c\int qdt - \int V_z dt) + c_6(\dot{z}_6 + \frac{t}{2}p - cq - V_z) \\
F_{s7} &= k_{s7}(z_7 - \frac{t}{2}\int pdt - d\int qdt - \int V_z dt) + c_7(\dot{z}_7 - \frac{t}{2}p - dq - V_z) \\
F_{s8} &= k_{s8}(z_8 + \frac{t}{2}\int pdt - d\int qdt - \int V_z dt) + c_8(\dot{z}_8 + \frac{t}{2}p - dq - V_z)
\end{aligned}
\tag{3.33}
$$

Other rotational degree of freedoms, namely roll, pitch, and yaw are caused by the resultant moments about x, y and z axes respectively, just like the two and three-axle cases:

$$
\begin{aligned}
\sum M_x = h(&F_{x1}\sin(\delta_1) + F_{y1}\cos(\delta_1) + F_{x2}\sin(\delta_1) + F_{y2}\cos(\delta_1) \\
&+ F_{x3}\sin(\delta_2) + F_{y3}\cos(\delta_2) + F_{x4}\sin(\delta_2) + F_{y4}\cos(\delta_2) \\
&+ F_{x5}\sin(\delta_3) + F_{y5}\cos(\delta_3) + F_{x6}\sin(\delta_3) + F_{y6}\cos(\delta_3) \\
&+ F_{x7}\sin(\delta_4) + F_{y7}\cos(\delta_4) + F_{x8}\sin(\delta_4) + F_{y8}\cos(\delta_4)) \\
&+ \frac{t}{2}(F_{s1} - F_{s2} + F_{s3} - F_{s4} + F_{s5} - F_{s6} + F_{s7} - F_{s8})
\end{aligned}
\tag{3.34}
$$

$$
\begin{aligned}
\sum M_y = h(&-F_{x1}\cos(\delta_1) + F_{y1}\sin(\delta_1) - F_{x2}\cos(\delta_1) + F_{y2}\sin(\delta_1) \\
&- F_{x3}\cos(\delta_2) + F_{y3}\sin(\delta_2) - F_{x4}\cos(\delta_2) + F_{y4}\sin(\delta_2) \\
&- F_{x5}\cos(\delta_3) + F_{y5}\sin(\delta_3) - F_{x6}\cos(\delta_3) + F_{y6}\sin(\delta_3) \\
&- F_{x7}\cos(\delta_4) + F_{y7}\sin(\delta_4) - F_{x8}\cos(\delta_4) + F_{y8}\sin(\delta_4)) \\
&- a(F_{s1} + F_{s2}) - b(F_{s3} + F_{s4}) + c(F_{s5} + F_{s6}) + d(F_{s5} + F_{s6})
\end{aligned}
\tag{3.35}
$$

$$\begin{aligned}\sum M_z = &-\frac{t}{2}F_{x1}\cos(\delta_1)+aF_{x1}\sin(\delta_1)+aF_{y1}\cos(\delta_1)+\frac{t}{2}F_{y1}\sin(\delta_1)\\ &+\frac{t}{2}F_{x2}\cos(\delta_1)+aF_{x2}\sin(\delta_1)+aF_{y2}\cos(\delta_1)-\frac{t}{2}F_{y2}\sin(\delta_1)\\ &-\frac{t}{2}F_{x3}\cos(\delta_2)+bF_{x3}\sin(\delta_2)+bF_{y3}\cos(\delta_2)+\frac{t}{2}F_{y3}\sin(\delta_2)\\ &+\frac{t}{2}F_{x4}\cos(\delta_2)+bF_{x4}\sin(\delta_2)+bF_{y4}\cos(\delta_2)-\frac{t}{2}F_{y4}\sin(\delta_2)\\ &-\frac{t}{2}F_{x5}\cos(\delta_3)-cF_{x5}\sin(\delta_3)-cF_{y5}\cos(\delta_3)+\frac{t}{2}F_{y5}\sin(\delta_3)\\ &+\frac{t}{2}F_{x6}\cos(\delta_3)-cF_{x6}\sin(\delta_3)-cF_{y6}\cos(\delta_3)-\frac{t}{2}F_{y6}\sin(\delta_3)\\ &-\frac{t}{2}F_{x7}\cos(\delta_4)-dF_{x7}\sin(\delta_4)-dF_{y7}\cos(\delta_4)+\frac{t}{2}F_{y7}\sin(\delta_4)\\ &+\frac{t}{2}F_{x8}\cos(\delta_4)-dF_{x8}\sin(\delta_4)-dF_{y8}\cos(\delta_4)-\frac{t}{2}F_{y8}\sin(\delta_4)\end{aligned} \tag{3.36}$$

Unsprung mass motion is simply illustrated in Figure 3.6:

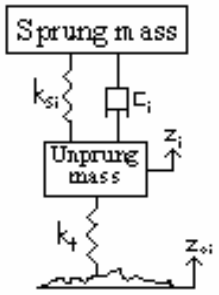

Figure 3.6 Unsprung mass motion

$$m_i \ddot{z}_i = k_t(z_{oi}-z_i)-F_{si}+(-1)^i\frac{K_{ri}}{t} \tag{3.37}$$

where F_{si} values are given in Equations 3.21, 3.27, and 3.33 for the two, three and four-axle vehicles, respectively. K_{ri}/t, on the other hand, represents the force applied by the anti-roll bar in response to body roll.

3.2 Wheel Dynamics

As the tire rolling resistance is lumped and applied to the centre of gravity of the vehicle, the forces and moments applied to the tires are illustrated in figure 3.7.

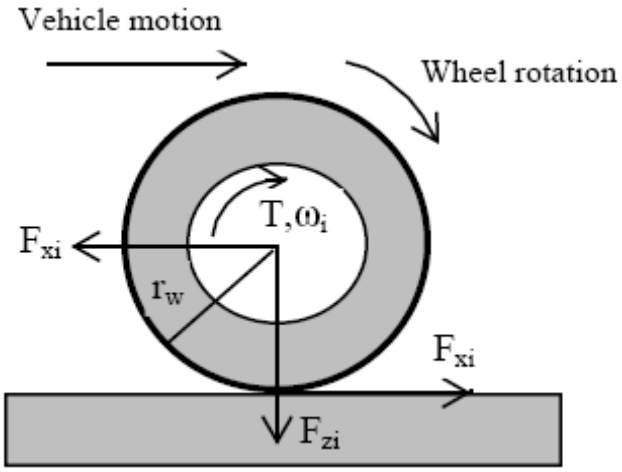

Figure 3.7 Wheel dynamics

The following equations can be written from Figure 3.7:

$$\dot{\omega}_i = \frac{1}{I_\omega}(T - r_w F_{xi}) \tag{3.38}$$

Note that there is a sign change in braking

$$\dot{\omega}_i = \frac{1}{I_\omega}(-T + r_w F_{xi}) \tag{3.39}$$

3.3 Tire Model

Tires generate lateral and longitudinal forces in a nonlinear manner. There are many factors affecting the cornering behavior of tires, such as normal load, slip angle, inflation pressure of the tire, camber angle, traction or braking forces.

Among these factors, the most crucial is certainly the slip angle. Slip angle is defined as the angle between the direction of motion and plane of the wheel. Slip angles for a two axle vehicle are illustrated in Figure 3.8.

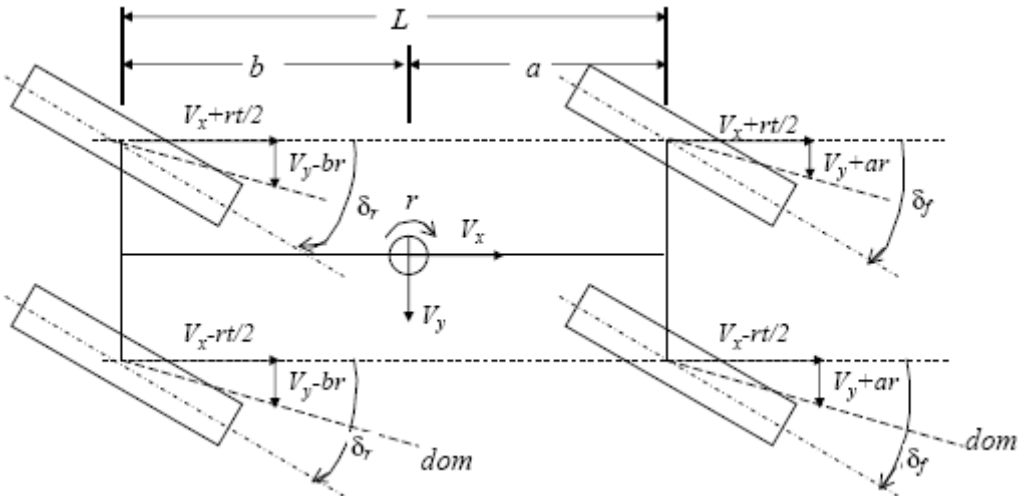

Figure 3.8 Slip angles for a two axle-vehicle

According to the sign convention, if the plane of the wheel is reached by a clockwise rotation from the direction of motion, than the slip angle is negative. Therefore the following equations for the slip angles can be written from Figure 3.8:

$$\alpha_1 = \arctan\left(\frac{V_y + ar}{V_x - \frac{t}{2}r}\right) - \delta_f \qquad \alpha_2 = \arctan\left(\frac{V_y + ar}{V_x + \frac{t}{2}r}\right) - \delta_f$$
$$\alpha_3 = \arctan\left(\frac{V_y - ar}{V_x - \frac{t}{2}r}\right) - \delta_r \qquad \alpha_4 = \arctan\left(\frac{V_y - ar}{V_x + \frac{t}{2}r}\right) - \delta_r \tag{3.40}$$

Figure 3.9 is a typical Cornering (Lateral) Force vs. Slip Angle curve. Note that cornering stiffness is defined as the slope of the linear part of these curves, which lies approximately below a slip angle of 3 or 4 degrees.

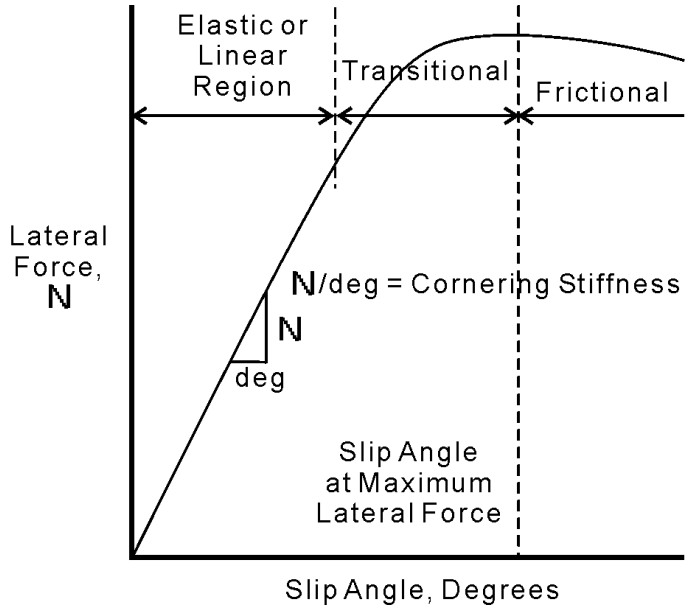

Figure 3.9 A typical tire cornering force characteristic

There exist basically three alternatives in modeling tires for use in full vehicle models [19]:

1) Magic formula: This model, firstly suggested by Pacejka [23], provides many important tire functions accurately. Its mathematical formulation is as follows:

$$Y = S_y + D\sin\left\{C\arctan\left[B(X - S_x)(1-E) + E\arctan(B(X - S_x))\right]\right\} \tag{3.41}$$

where

Y = any tire response quantity (lateral force, longitudinal force, self aligning torque, etc.)

X = lateral slip angle, longitudinal slip angle, or camber angle

and the six constants S_x, S_y, B, C, D, and E must be obtained from some curve fitting procedure.

2) Allen model: It is not a purely analytical tire model. It also makes use of the experimentally obtained CALSPAN parameters [24]. It calculates the instantaneous values of tire forces based on the instantaneous values of forward speed, normal force, longitudinal slip, and lateral slip angle.

3) Dugoff Model: This model is the simplest and is based on tire mechanics analysis [25]. In this study, Dugoff tire model is used since it is mathematically simple and yet it can provide considerable qualitative agreement between theoretical and measured data.

Mathematical formulation of Dugoff model is as follows:

$$\left\{\begin{array}{l} V_s = V\sqrt{s^2+\tan^2\alpha} \\ \mu = \mu_0(1-A_sV_s) \\ z = \dfrac{\mu F_z(1-s)}{2\sqrt{(C_l s)^2+(C_s\tan(\alpha))^2}} \\ f(z) = \left\{\begin{array}{ll} z(2-z) & \text{for } z<1 \\ 1 & \text{for } z\geq 1 \end{array}\right\} \\ F_x = \dfrac{C_l s f(z)}{1-s} \\ F_y = \dfrac{C_s\tan(\alpha) f(z)}{1-s} \end{array}\right\} \tag{3.42}$$

where

α = slip angle [rad]

S = longitudinal slip

V = velocity component in wheel plane [m/s]

V_s = slip velocity [m/s]

μ_o = static tire road friction coefficient

A_s = friction reduction factor [s/m]

C_s = cornering stiffness [N/rad]

C_l = longitudinal stiffness [N/slip]

F_z = normal load on tire [N]

F_x = driving/braking force [N]

F_y = cornering force [N]

Note that longitudinal slip for the i[th] wheel is expressed as

$$s_i = \begin{cases} \dfrac{r_w\omega_i - V_i}{r_w\omega_i} & \text{for } r_w\omega_i \geq V_i \text{ (in acceleration)} \\ \dfrac{V_i - r_w\omega_i}{V_i} & \text{for } r_w\omega_i \leq V_i \text{ (in braking)} \end{cases} \tag{3.43}$$

3.4 Lateral Load Transfers

For the vehicles illustrated in Figures 3.2 to 3.4, the sprung mass rolls and in a left hand turn the rear view of the vehicles is illustrated in Figure 3.10.

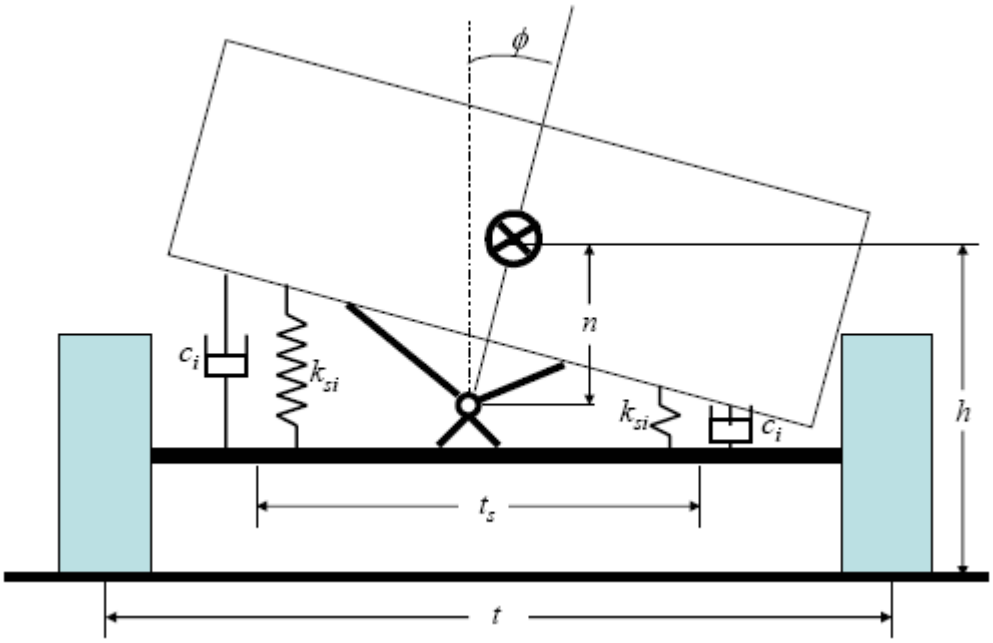

Figure 3.10 Vehicle in a left hand turn

The following equations can be written for the two-axle vehicle according to Figure 3.10 [26].

$$
\begin{aligned}
F_{z1} &= F_{z1s} - \frac{K_{fr}}{K_{fr}+K_{rr}}\left(\frac{Ma_l h + Mgn\phi}{t}\right) \\
F_{z2} &= F_{z2s} + \frac{K_{fr}}{K_{fr}+K_{rr}}\left(\frac{Ma_l h + Mgn\phi}{t}\right) \\
F_{z3} &= F_{z3s} - \frac{K_{rr}}{K_{fr}+K_{rr}}\left(\frac{Ma_l h + Mgn\phi}{t}\right) \\
F_{z4} &= F_{z4s} + \frac{K_{rr}}{K_{fr}+K_{rr}}\left(\frac{Ma_l h + Mgn\phi}{t}\right)
\end{aligned}
\tag{3.44}
$$

where K_{fr} and K_{rr} represent front and rear roll stiffness values. Note that for a beam-axle suspension with leaf springs, the expression for the roll stiffness values can be written as [19]

$$
K_{roll} = \frac{t_s^{\,2}}{2} k_{si} \tag{3.45}
$$

3.5 Assumptions

In spite of the fact that the features of the model are simplified to study the vehicle's handling and ride characteristics, there remain still some more assumptions:

1) The wheels on the same axle are steered at equal angles.

2) Vertical motion of the unsprung mass is along the z direction of the body centered reference frame.

3) The longitudinal load transfers are neglected.

4) Kinematical effects such as self aligning torque, roll steer, camber angle, and tire side force lag are ignored since their effects on the motion of the vehicle are considerably small.

CHAPTER 4

DATA, INPUTS AND STEERING STRATEGIES

4.1 Data

Valid data is very important for a realistic simulation. However, detailed and accurate data is very difficult to obtain, especially for three and four-axle vehicles.

Tables 4.1, 4.2, and 4.3 show sample data used in the case studies for typical examples of a two-axle bus, a three-axle commercial truck, and a four-axle armored personal carrier (APC), respectively.

Table 4.1 Two-axle bus

M	= 18100	sprung mass [kg]
m_f	= 470	unsprung mass for driven wheels [kg]
m_r	= 990	unsprung mass for drive wheels [kg]
I_x	= 15396	moment of inertia through x-axis [kg.m^2]
I_y	= 200551	moment of inertia through y-axis [kg.m^2]
I_z	= 202155	moment of inertia through x-axis [kg.m^2]
a	= 3.557	distance from center of gravity to front axle [m]
b	= 2.523	distance from center of gravity to rear axle [m]
h	= 1.25	height of center of gravity from ground [m]
t	= 1.85	track [m]
$k_{s1,2}$	= 400000	spring coefficient of front suspensions [N/m]
$k_{s3,4}$	= 500000	spring coefficient of rear suspensions [N/m]
c_i	= 50000	damping coefficient of all suspensions [N.s/m]
k_t	= 1082960	spring coefficient for all tires [N/m]
r_w	= 0.5	wheel radius for all wheels [m]
I_w	= 6.25	moment of inertia for all wheels [kg*m^2]
K_{ri}	= 500000	roll bar stiffness of all axles [N.m/rad]
C_f	= -336400	cornering stiffness of front tires [N/rad]
C_r	= -486400	cornering stiffness of rear tires [N/rad]
C_l	= 449000	longitudinal stiffness for all tires [N/unit slip]
C_D	= 0.6	drag coefficient

Table 4.2 Unloaded and loaded 6x4 commercial truck

Symbol	Unloaded	Loaded	Description and unit
M	7565	18435	sprung mass [kg]
F_{z1}	3785	3315	load on 1st axle [kg]
F_{z2}	1890	7610	load on 2nd axle [kg]
F_{z3}	1890	7610	load on 3rd axle [kg]
m_f	390	390	unsprung mass for driven wheels [kg]
m_r	590	590	unsprung mass for drive wheels [kg]
I_x	9569	23317	mass moment of inertia, x-axis [kg.m^2]
I_y	40197	97955	mass moment of inertia, y-axis [kg.m^2]
I_z	38471	93748	mass moment of inertia, z-axis [kg.m^2]
a	2.24	3.51	distance from center of gravity to front axle [m]
b	1.36	0.09	distance from center of gravity to intermediate axle[m]
c	2.71	1.44	distance from center of gravity to rear axle [m]
h	1.25	1.35	height of centre of gravity from ground [m]
t	1.93	1.93	track [m]
k_{si}	200000	200000	spring coefficient of suspension i [N/m]
c_i	30000	30000	damping coefficient of suspension i [N.s/m]
k_t	1082960	1082960	spring coefficient for all tires [N/m]
r_w	0.53	0.53	wheel radius for all wheels [m]
I_w	6.25	6.25	moment of inertia for all wheels [kg.m^2]
K_{ri}	500000	500000	roll bar stiffness of all axles [N.m/rad]
C_f	-176400	-146400	cornering stiffness of front tires [N/rad]
C_m	-100400	-286400	cornering stiffness of tires on intermediate axle [N/rad]
C_r	-100400	-286400	cornering stiffness of rear tires [N/rad]
C_l	239000	319000	longitudinal stiffness for all tires [N/slip]
C_D	0.65	0.7	Drag coefficient

Table 4.3 8x8 APC

M	=	16130	sprung mass [kg]
F_{zi}	=	4032.5	load on all axles [kg]
m	=	390	unsprung mass [kg]
I_x	=	16129	mass moment of inertia through x-axis [kg.m^2]
I_y	=	91498	mass moment of inertia through y-axis [kg.m^2]
I_z	=	94968	mass moment of inertia through z-axis [kg.m^2]
a	=	3.48	distance from center of gravity to 1st axle [m]
b	=	1.16	distance from center of gravity to 2nd axle [m]
c	=	1.16	distance from center of gravity to 3rd axle [m]
d	=	3.48	distance from center of gravity to 4th axle [m]
h	=	1.25	height of center of gravity from ground [m]
t	=	2.3	track [m]
k_{si}	=	200000	spring coefficient of all suspensions [N/m]
c_i	=	30000	damping coefficient of all suspensions [N.s/m]
k_t	=	1082960	spring coefficient of all tires [N/m]
r_w	=	0.55	wheel radius for all wheels [m]
I_w	=	6.25	spin moment of inertia of all wheels [kg.m^2]
K_{ri}	=	500000	roll bar stiffness of all axles [N.m/rad]
C_i	=	-177617	cornering stiffness of all tires [N/rad]
C_l	=	249000	longitudinal stiffness for all tires [N/unit slip]
C_D	=	0.68	drag coefficient

Apart from the data given above, the data

A_s= 0.015 friction reduction factor [s/m], and

μ_o= 0.6 peak static tire/road friction coefficient

are used for all the vehicles.

4.2 Inputs

The model has three main inputs: drive or braking torque, steering input, and road profile.

4.2.1 Torque

Since the performance of the vehicle is not the main object in this study, torque to all wheels is taken as constant for simplicity. If the vehicle is accelerating, the torque is inputted with a positive sign, and if it is braking, this torque is inputted with a negative sign. Besides, a simple proportional feedback cruise control in the form of $T=K(V_{x,\,desired} - V_{x,\,real})$, where K is a constant, can be applied on the vehicle to make its forward velocity constant. This is optional in the simulation; acceleration, braking, or constant velocity operation of the vehicle can be selected. Note that the option of constant forward velocity is implemented because handling improvement studies are usually performed using the bicycle model with the assumption of constant velocity. Bicycle model is going to be discussed in the coming chapters.

It is also possible in the simulation to select the drive configuration of the vehicles; whether the vehicle is front, rear, or four wheel drive for the two-axle vehicle, or 6x2, 6x4, or 6x6 for the three-axle vehicle, or 8x2, 8x4, 8x6, or 8x8 for the four-axle vehicle.

4.2.2 Road Profile

The road surface profile is mostly described by spectral density $S(\omega)$ in ride studies, assuming that the road surface profile is a stationary random process i.e. statistical characteristics such as mean, variance, etc. of the road profile do not

change with time. Moreover the road surface roughness is assumed to be ergodic [19], i.e. the left and right wheels can be subjected to identical inputs. Thus a single sample of the random process representing the road surface profile is sufficient for the simulations.

It is not easy to define $S(\omega)$ for a given road with great precision. Profile records must be of finite length and therefore it should be assumed that road profiles are realizations of stationary random processes. However high accuracy is rarely essential since the aim is to establish a spectral description which can be typically taken for a given class of roads, rather than to describe a particular road with precision. Where profile measurements are not available, and a spectrum representative of a class of roads is required; or where analytical convenience is important, it may be useful to employ a mathematical model.

A previously developed algorithm [27] is used to obtain time functions of the road surface profile for different road surfaces with known power spectral density functions. Three road input model alternatives, i.e. three power spectral density formulas are available in the simulation. These are:

$$\left\{ \begin{array}{l} S_1(\omega) = \dfrac{2\alpha V\sigma^2}{\pi} \cdot \dfrac{1}{(\alpha V)^2 + \omega^2} \\ S_2(\omega) = \dfrac{2\alpha V\sigma^2}{\pi} \cdot \dfrac{(\alpha V)^2 + \omega^2 + (\beta V)^2}{\left[\omega^2 + (\alpha^2 + \beta^2)V^2\right]^2 + (2\alpha V)^2 \omega^2} \\ S_3(\omega) = \dfrac{\sigma_1^{\,2}}{\pi} \cdot \dfrac{\alpha_1 V}{\omega^2 + (\alpha_1 V)^2} + \dfrac{\sigma_2^{\,2}}{\pi} \dfrac{\alpha_2 V\left[\omega^2 + V^2(\alpha_2^2 + \beta^2)\right]}{\left[\omega^2 + V^2(\alpha_2^2 - \beta^2)\right]^2 + (2\alpha_2 \beta V^2)^2} \end{array} \right\} \tag{4.1}$$

where

$S_i(\omega)$ = Single-sided spatial power spectral density,

α = breakaway frequency,

σ^2 = variance of road irregularity,

V = forward velocity of the vehicle

and all others are specified constants. Those constants are given in Table 4.1:

Table 4.1 Road input model constants [19]

$S_1(\omega)$			$S_2(\omega)$			
Road type	α [m^{-1}]	σ [m]	**Road type**	α [m^{-1}]	σ [m]	β [m^{-1}]
Asphalt	0.15	0.0033	Asphalt	0.15	0.0033	0.6
Concrete	0.2	0.0056	Paved	0.2	0.0056	2
Rough	0.4	0.012	Dirt	0.4	0.012	1.1

$S_3(\omega)$					
Road Type	α_1 [m^{-1}]	α_2 [m^{-1}]	β [m^{-1}]	σ_1^2 [m^2]	σ_2^2 [m^2]
Asphalt	0.2	0.05	0.6	$7.65.10^{-6}$	$1.35.10^{-6}$
Paved	0.5	0.2	2.0	$2.55.10^{-4}$	$4.5.10^{-4}$
Dirt	0.8	0.5	0.5	$7.5.10^{-4}$	$2.5.10^{-4}$

4.2.3 Steering Input

Two options are offered for the steering input of the front wheels in the simulation, which are adjustable sinusoidal (frequency and amplitude) and ramped step (slope and amplitude) inputs, as illustrated in Figure 4.1.

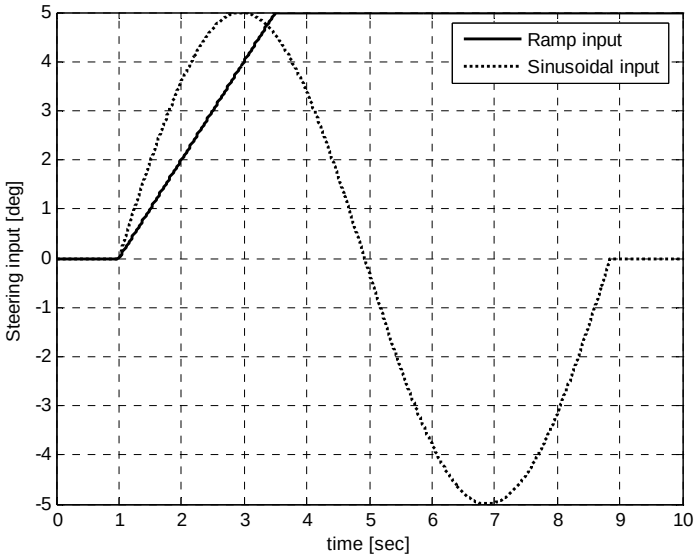

Figure 4.1 Steering input options

4.3 Steering Strategies

Various steering strategies need to be constructed to be able to find the one which will give the desired handling behavior. A number of steering strategies have been proposed in literature for the two-axle vehicles.

4.3.1 Steering Strategies for the Two-Axle Vehicle

Since the main concern in handling studies is the yaw rate and lateral acceleration, one needs to construct a simpler model in order to accomplish the generation of steering strategies easier. The choice is usually the single track model commonly named as bicycle model. The bicycle model for a two-axle vehicle is illustrated in Figure 4.2 together with the forces acting on the vehicle.

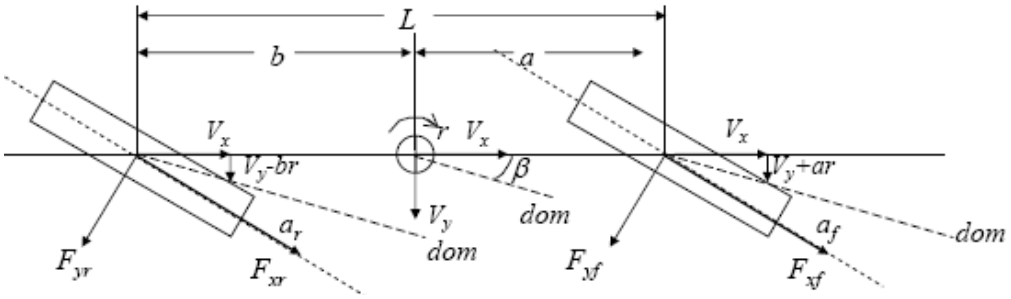

Figure 4.2 Bicycle model for two-axle vehicle

Note that bicycle model is obtained by lumping the two wheels on the same axle into a single wheel.

The following differential equations of motion can be written from Figure 4.2:

$$
\begin{aligned}
M(\dot{V}_x - V_y r) &= F_{xf}\cos(\delta_f) - F_{yf}\sin(\delta_f) + F_{xr}\cos(\delta_r) - F_{yr}\sin(\delta_r) \\
M(\dot{V}_y + V_x r) &= F_{xf}\sin(\delta_f) + F_{yf}\cos(\delta_f) + F_{xr}\sin(\delta_r) + F_{yr}\cos(\delta_r) \\
I_z \dot{r} &= a(F_{xf}\sin(\delta_f) + F_{yf}\cos(\delta_f)) - b(F_{xr}\sin(\delta_r) + F_{yr}\cos(\delta_r))
\end{aligned}
\tag{4.2}
$$

Note that the acceleration terms in Equations 3.11 to 3.16 simplify to the acceleration terms above, since there is no vertical motion, roll and pitch motion in planar bicycle model, i.e. V_z, p, q are ignored.

If the steering angles of the front and rear wheels are assumed to be small, such that $\cos(\delta) \cong 1$ and $\sin(\delta) \cong 0$, then Equations 4.2 reduce to:

$$\begin{aligned} M(\dot{V}_x - V_y r) &= F_{xf} + F_{xr} \\ M(\dot{V}_y + V_x r) &= F_{yf} + F_{yr} \\ I_z \dot{r} &= aF_{yf} - bF_{yr} \end{aligned} \tag{4.3}$$

The term $V_y r$ on the left hand side of the first equation above is a product of two variables of small magnitude and hence can be neglected [19]. Then the equation reduces to $M\dot{V}_x = F_{xf} + F_{xr}$ which is uncoupled from other two equations and can be used to study the acceleration performance of the vehicle in straight motion.

Treating the forward velocity of the vehicle V_x as a parameter, the degrees of freedom of the system reduce to two, namely sideslip and yaw and formulated as:

$$\begin{aligned} M(\dot{V}_y + V_x r) &= F_{yf} + F_{yr} \\ I_z \dot{r} &= aF_{yf} - bF_{yr} \end{aligned} \tag{4.4}$$

With the knowledge that under normal driving conditions, slip angles are usually smaller than four degree, the bicycle model assumes the Cornering Force vs. Slip Angle relation in the linear range.

$$\begin{aligned} F_{yf} &= C_f^{right}\alpha_f + C_f^{left}\alpha_f \\ F_{yr} &= C_r^{right}\alpha_r + C_r^{left}\alpha_r \end{aligned} \tag{4.5}$$

Assuming the cornering stiffness values of tires on the same axle are equal

$$C_f^{right} = C_f^{left} = C_f$$
$$C_r^{right} = C_r^{left} = C_r \tag{4.6}$$

one may arrive at:

$$F_{yf} = 2C_f \alpha_f$$
$$F_{yr} = 2C_r \alpha_r \tag{4.7}$$

Substituting the above equations into Equation 4.4 yields:

$$M(\dot{V}_y + V_x r) = 2C_f \alpha_f + 2C_r \alpha_r$$
$$I_z \dot{r} = 2aC_f \alpha_f - 2bC_r \alpha_r \tag{4.8}$$

The slip angle expressions which can be written from Figure 4.2 as:

$$\alpha_f = \arctan\left(\frac{V_y + ar}{V_x}\right) - \delta_f \quad \cong \quad \frac{V_y + ar}{V_x} - \delta_f$$
$$\alpha_r = \arctan\left(\frac{V_y - br}{V_x}\right) - \delta_r \quad \cong \quad \frac{V_y - br}{V_x} - \delta_r \tag{4.9}$$

Substitution of the above equations into equation 4.8 yields:

$$M\dot{V}_y = 2(C_f + C_r)\frac{V_y}{V_x} + (2aC_f - 2bC_r - MV_x^2)\frac{r}{V_x} - 2C_f\delta_f - 2C_r\delta_r$$
$$I_z \dot{r} = 2(aC_f - bC_r)\frac{V_y}{V_x} + (a^2C_f + b^2C_r)\frac{r}{V_x} - 2aC_f\delta_f - 2bC_r\delta_r \tag{4.10}$$

or in state space representation with V_y and r as the state variables :

$$\begin{Bmatrix} \dot{V}_y \\ \dot{r} \end{Bmatrix} = \begin{bmatrix} \frac{2(C_f + C_r)}{MV_x} & \frac{2(aC_f - bC_r)}{MV_x} - V_x \\ \frac{2(aC_f - bC_r)}{JV_x} & \frac{2(a^2C_f + b^2C_r)}{JV_x} \end{bmatrix} \begin{Bmatrix} V_y \\ r \end{Bmatrix} + \begin{bmatrix} \frac{-2C_f}{M} & \frac{-2C_r}{M} \\ \frac{-2aC_f}{J} & \frac{2bC_r}{J} \end{bmatrix} \begin{Bmatrix} \delta_f \\ \delta_r \end{Bmatrix} \quad (4.11)$$

Driver obviously can not control the front and rear wheel steering angles simultaneously. Therefore the simplest idea to relate rear wheel steering angle to the front wheel steering angle is through the relation $\delta_r = k\delta_r$, where k can be a constant, or a function of vehicle parameters and speed.

The commonly used condition to determine the expression for the parameter k, is to set the vehicle sideslip angle to zero. Vehicle side slip angle, β in Figure 4.2, is defined as the angle between the longitudinal axis of the vehicle, and the velocity vector at the center of gravity.

$$\beta = \arctan(\frac{V_y}{V_x}) \cong \frac{V_y}{V_x} \quad (4.12)$$

Substitution of the above equation into Equation 4.11 yields:

$$\begin{Bmatrix} \dot{\beta} \\ \dot{r} \end{Bmatrix} = \begin{bmatrix} \frac{2(C_f + C_r)}{MV_x} & -1 + \frac{2(aC_f - bC_r)}{MV_x{}^2} \\ \frac{2(aC_f - bC_r)}{I_z} & \frac{2(a^2C_f + b^2C_r)}{I_zV_x} \end{bmatrix} \begin{Bmatrix} \beta \\ r \end{Bmatrix} + \begin{bmatrix} \frac{-2C_f}{MV_x} & \frac{-2C_r}{MV_x} \\ \frac{-2aC_f}{I_z} & \frac{2bC_r}{I_z} \end{bmatrix} \begin{Bmatrix} \delta_f \\ \delta_r \end{Bmatrix} \quad (4.13)$$

The 1st strategy implemented for the two-axle vehicle is FWS, which is used as a reference for evaluating other strategies.

The 2nd approach for the two-axle vehicle is an open loop control law. It is obtained by eliminating r from the steady state equations of motion (i.e. after assigning $\dot{\beta} = \dot{r} = 0$), and setting the numerator of the expression for sideslip angle to zero, after substituting $\delta_r = k\delta_f$ into Equation 4.13 [8].

$$\delta_r = \left(\frac{bL + M\frac{a}{2C_r}V_x^{\,2}}{-aL + M\frac{b}{2C_f}V_x^{\,2}} \right) \delta_f \tag{4.14}$$

The 3rd strategy uses a rear wheel steering angle as some function of front wheel steering angle. A sample function is illustrated in Figure 4.3.

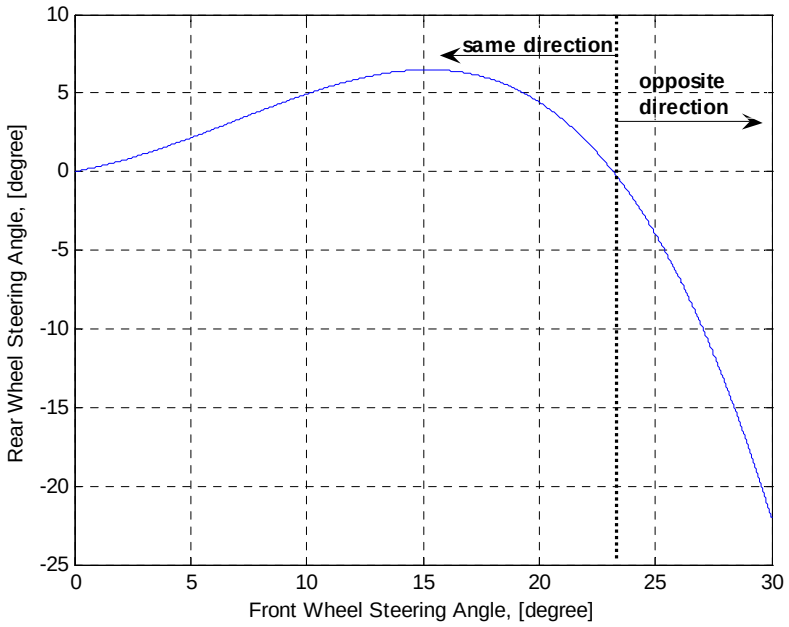

Figure 4.3 Strategy 3 for two-axle vehicle

The sample function in Figure 4.3 is a polynomial [19] given by the expression:

$$\delta_r = \left(0.25733 + 0.04286\delta_f - 0.00163\delta_f^{\,2} - 0.00003\delta_f^{\,3}\right)\delta_f \tag{4.15}$$

It provides steering of the front and rear wheels in the same direction for small steering inputs, which is the case at high speeds, during which small steering angles are sufficient for lane changes or taking gentle curves, and steering of the front and rear wheels in the opposite direction for large steering inputs, which is the case in city traffic or parking, during which large steering angles are required.

4th Strategy, described by Whitehead [12], provides zero sideslip angle even in the transient part of cornering. It includes proportional plus yaw velocity feedback and is obtained by equating sideslip angle and its derivative to zero in the first part of Equation 4.13, and directly deriving δ_r in terms of vehicle parameters, r and δ_f. Its formulation is:

$$\delta_r = \frac{2(aC_f - bC_r) - MV_x^2}{2C_r V_x} r - \frac{C_f}{C_r}\delta_f \tag{4.16}$$

The 4WS vehicle will always be stable irrespective of the forward speed with the application of this strategy.

Strategy 5 is simply yaw velocity feedback [19] and is formulated as follows:

$$\delta_r = \frac{M}{L}\left(\frac{b}{2C_f} - \frac{a}{2C_r}\right) V_x r \delta_f \tag{4.17}$$

An interesting property of this control strategy is that the resulting vehicle will be stable if it is originally neutral steer or oversteer; and unstable if it is originally understeer.

All the strategies considered for the two-axle vehicle are summarized in the Appendix.

4.3.2 Steering Strategies for the Three-Axle Vehicle

The bicycle model for a three-axle vehicle is shown in Figure 4.4.

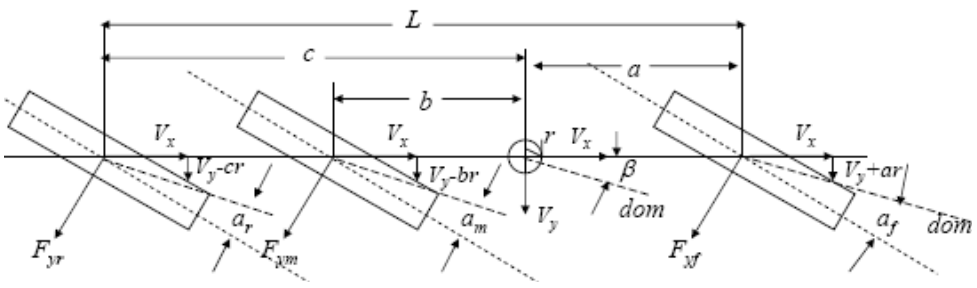

Figure 4.4 Bicycle model for three-axle vehicle

Using a similar procedure as in the case of two-axle vehicle; with the same assumptions and addition of an extra axle, the following equations are derived from the bicycle model of Figure 4.4 for a three-axle vehicle:

$$\begin{Bmatrix} \dot{\beta} \\ \dot{r} \end{Bmatrix} = \begin{bmatrix} \frac{2(C_f + C_m + C_r)}{MV_x} & -1 + \frac{2(aC_f - bC_m - cC_r)}{MV_x^2} \\ \frac{2(aC_f - bC_m - cC_r)}{I_z} & \frac{2(a^2C_f + b^2C_m + c^2C_r)}{I_z V_x} \end{bmatrix} \begin{Bmatrix} \beta \\ r \end{Bmatrix} + \begin{bmatrix} \frac{-2C_f}{MV_x} & \frac{-2C_m}{MV_x} & \frac{-2C_r}{MV_x} \\ \frac{-2aC_f}{I_z} & \frac{2bC_m}{I_z} & \frac{2cC_r}{I_z} \end{bmatrix} \begin{Bmatrix} \delta_f \\ \delta_m \\ \delta_r \end{Bmatrix} \tag{4.18}$$

The 1st strategy implemented for the three-axle vehicle is FWS, which is used as a reference for evaluating other strategies.

Strategies 2 to 5 are empirical strategies offered by Huh et al. [17] to observe the benefits and disadvantages of multi-axle steering for a three-axle vehicle.

Strategy 2 called as 1st Crab Mode is simply:

$$\begin{aligned} \delta_m &= 0.5\delta_f \\ \delta_r &= 0 \end{aligned} \tag{4.19}$$

Strategy 3 called as Front Mode is simply

$$\begin{aligned} \delta_m &= 0 \\ \delta_r &= -0.5\delta_f \end{aligned} \tag{4.20}$$

Strategy 4 called as 2nd Crab Mode is simply

$$\begin{aligned} \delta_m &= 0.5\delta_f \\ \delta_r &= -0.5\delta_f \end{aligned} \tag{4.21}$$

Strategy 5 called as Coordinate Mode is simply

$$\begin{aligned} \delta_m &= -0.5\delta_f \\ \delta_r &= -0.5\delta_f \end{aligned} \tag{4.22}$$

Strategy 6, again offered by Huh et. al. [17] is the direct application of Strategy 4 for the two-axle vehicle to the three-axle vehicle. It is formulated as:

$$\left\{\begin{array}{l}\delta_m = 0 \\ \delta_r = \left(\dfrac{2(aC_f - cC_r) - MV_x^2}{2C_r V_x}\right) r - \left(\dfrac{C_f + C_m}{C_r}\right)\delta_f\end{array}\right\} \tag{4.23}$$

7th and 8th strategies which are proposed in this thesis study are applications of the 4WS algorithms to three-axle vehicle; to achieve zero steady state, and transient sideslip angles, respectively. Strategy 7 is the extension of an algorithm applied to a two-axle vehicle previously [8]. It is derived by eliminating r from the steady state mode of Equation 4.18, and equating the coefficient of sideslip angle to zero, after substituting $\delta_m = k_m \delta_f$ and $\delta_r = k_r \delta_f$ into the equations. In other words, it is derived by eliminating r from Equation 4.24, and equating the coefficient of β to zero.

$$\begin{array}{l}\dfrac{2(C_f + C_m + C_r)}{MV_x}\beta + \left(-1 + \dfrac{2(aC_f - bC_m - cC_r)}{MV_x^2}\right)\mathrm{r} - \left(\dfrac{2C_f + 2C_m k_m + 2C_r k_r}{MV_x}\right)\delta_f = 0 \\ \dfrac{2(aC_f - bC_m - cC_r)}{I_z}\beta + \dfrac{2(a^2 C_f + b^2 C_m + c^2 C_r)}{I_z V_x} r + \left(\dfrac{-2aC_f + 2bC_m k_m + 2cC_r k_r}{I_z}\right)\delta_f = 0\end{array} \tag{4.24}$$

Its formulation is:

$$\left\{\begin{array}{l}\delta_m = k_m \delta_f \\ \qquad -C_f[2(bC_m(a+b) + cC_r(a+c)) + aMV_x^2] \\ \delta_r = \dfrac{-k_m C_m[2(aC_f(a+b) + cC_r(-b+c)) - bMV_x^2]}{C_r[2(aC_f(a+c) + bC_m(b-c)) - cMV_x^2]}\delta_f\end{array}\right\} \tag{4.25}$$

Likewise 8th strategy is the extension of a logic applied to a two-axle vehicle previously [12]. It includes proportional plus yaw velocity feedback and is obtained by equating sideslip angle and its derivative to zero in the first part of Equation 4.18, and directly deriving δ_r in terms of vehicle parameters, r, δ_m and δ_f. Its formulation is:

$$\begin{Bmatrix} \delta_m = k_m \delta_f \\ \delta_r = \left(\dfrac{2(aC_f - bC_m - cC_r) - MV_x^2}{2C_r V_x} \right) r - \left(\dfrac{C_f + C_m k_m}{C_r} \right) \delta_f \end{Bmatrix} \tag{4.26}$$

All the strategies considered for the three-axle vehicle are summarized in the Appendix.

4.3.3 Steering Strategies for the Four-Axle Vehicle

Four-axle bicycle model is illustrated in Figure 4.5.

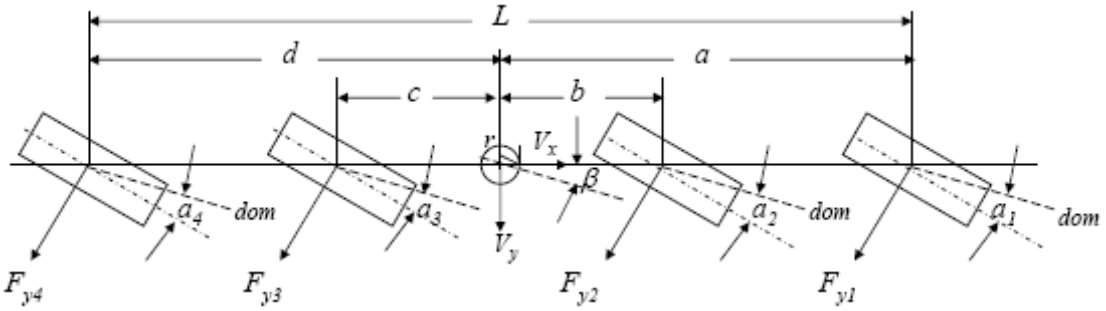

Figure 4.5 Bicycle model for four-axle vehicle

Following a similar procedure as in the cases of two and three-axle vehicles, using the same assumptions, the following equations are derived for the bicycle model of Figure 4.5 for a four-axle vehicle:

$$\begin{Bmatrix} \dot{\beta} \\ \dot{r} \end{Bmatrix} = \begin{bmatrix} \dfrac{2(C_1 + C_2 + C_3 + C_4)}{MV_x} & -1 + \dfrac{2(aC_1 + bC_2 - cC_3 - dC_4)}{MV_x^2} \\ \dfrac{2(aC_1 + bC_2 - cC_3 - dC_4)}{I_z} & \dfrac{2(a^2C_1 + b^2C_2 + c^2C_3 + d^2C_4)}{I_z V_x} \end{bmatrix} \begin{Bmatrix} \beta \\ r \end{Bmatrix} + \begin{bmatrix} \dfrac{-2C_1}{MV_x} & \dfrac{-2C_2}{MV_x} & \dfrac{-2C_3}{MV_x} & \dfrac{-2C_3}{MV_x} \\ \dfrac{-2aC_1}{I_z} & \dfrac{-2bC_2}{I_z} & \dfrac{2cC_3}{I_z} & \dfrac{2dC_4}{I_z} \end{bmatrix} \begin{Bmatrix} \delta_1 \\ \delta_2 \\ \delta_3 \\ \delta_4 \end{Bmatrix} \tag{4.27}$$

The 1st strategy implemented for the four-axle vehicle is FWS, which is used as a reference for evaluating other strategies, just like the two and three-axle cases.

2nd, 3rd, 4th and 5th strategies are empirical strategies simulated to see whether steering the wheels on intermediate axles is advantageous or not.

The 2nd strategy is simply:

$$\begin{aligned}\delta_2 &= 0\delta_1 \\ \delta_3 &= 0\delta_1 \\ \delta_4 &= -0.5\delta_1\end{aligned} \tag{4.28}$$

The 3rd strategy is simply:

$$\begin{aligned}\delta_2 &= 0.5\delta_1 \\ \delta_3 &= 0.5\delta_1 \\ \delta_4 &= -0.5\delta_1\end{aligned} \tag{4.29}$$

The 4th strategy is simply:

$$\begin{aligned}\delta_2 &= 0.5\delta_1 \\ \delta_3 &= -0.5\delta_1 \\ \delta_4 &= -0.5\delta_1\end{aligned} \tag{4.30}$$

The 5th strategy is simply:

$$\begin{aligned}\delta_2 &= -0.5\delta_1 \\ \delta_3 &= -0.5\delta_1 \\ \delta_4 &= -0.5\delta_1\end{aligned} \tag{4.31}$$

6th and 7th strategies, which are proposed in this thesis study, are applications of 4WS algorithms to achieve zero steady state and transient sideslip angles.

The 6th strategy, which is the extension of a previously introduced algorithm [8] aims to achieve zero steady state vehicle sideslip angle. It is derived by eliminating r from the steady state mode of Equation 4.27, and equating the coefficient of sideslip angle to zero, after substituting $\delta_2=k_2\delta_1$, $\delta_3=k_3\delta_1$, and $\delta_4=k_4\delta_1$ into the equations:

$$\left\{\begin{array}{l}\delta_2 = k_2\delta_1 \\ \delta_3 = k_3\delta_1 \\ \\ \delta_4 = \dfrac{\begin{array}{l} -C_1[2(bC_2(-a+b)+cC_3(a+c)+dC_4(a+d))+aMV_x^2] \\ -k_2C_2[2(aC_1(a-b)+cC_3(b+c)+dC_4(b+d))+bMV_x^2] \\ -k_3C_3[2(aC_1(a+c)+bC_2(b+c)+dC_4(-c+d))-cMV_x^2] \end{array}}{C_4[2(aC_1(a+d)+bC_2(b+d)+cC_3(c-d))-dMV_x^2}\delta_1 \end{array}\right\} \tag{4.32}$$

Likewise 7th strategy is the extension of a logic applied to a two-axle vehicle previously [12]. It includes proportional plus yaw velocity feedback and is obtained by equating sideslip angle and its derivative to zero in the first part of Equation 4.27, and directly deriving δ_4 in terms of vehicle parameters, r, δ_1, δ_2, and δ_3. Its formulation is:

$$\left\{\begin{array}{l}\delta_2 = k_2\delta_1 \\ \delta_3 = k_3\delta_1 \\ \\ \delta_4 = \left(\dfrac{2(aC_1+bC_2-cC_3-dC_4)-MV_x^2}{2C_rV_x}\right)r - \left(\dfrac{C_1+C_2k_2+C_3k_3}{C_r}\right)\delta_1 \end{array}\right\} \tag{4.33}$$

All the strategies considered for the four-axle vehicle are summarized in the Appendix.

4.4 Stability Analysis

It is important to define the limits of stability for three and four-axle vehicles, since the vehicles can give unexpected responses under ordinary driving conditions.

With the utilization of the bicycle model of a two-axle vehicle, it is well known [19] that the condition for stability for a two-axle vehicle is:

$$2L^2C_fC_r + (aC_f - bC_r)MV_x^2 > 0 \tag{4.34}$$

and if:

1) $aC_f > bC_r$ or $|aC_f| < |bC_r|$ then the vehicle is said to be understeer, and it is unconditionally stable.

2) $aC_f = bC_r$ then the vehicle is said to be neutral steer, and it is again unconditionally stable.

3) $aC_f < bC_r$ or $|aC_f| > |bC_r|$ then the vehicle is said to be oversteer, and it is unstable over a certain speed, namely critical speed expressed as

$$V_{x,critical} = \sqrt{\frac{2L^2 C_f C_r}{(-aC_f + bC_r)M}} \tag{4.35}$$

Further, it is well known that [19] characteristic speed for a two-axle vehicle is defined as the speed at which the understeer vehicle gives the maximum yaw velocity response, and it is formulated as:

$$V_{x,characteristic} = \sqrt{\frac{2L^2 C_f C_r}{(aC_f - bC_r)M}} \tag{4.36}$$

To define these terms for the three and four-axle vehicles, it should be borne in mind that for a system with a quadratic characteristic equation, the necessary and sufficient condition is that all three coefficients should be of the same sign, i.e. the real parts of the eigenvalues of the system matrix should be negative.

Recall that Equation 4.18 was derived from the bicycle model of a three-axle vehicle. The characteristic equation of the system is obtained by:

$$\det(\lambda[I]-[A]) = \begin{vmatrix} \lambda - \dfrac{2(C_f + C_m + C_r)}{MV_x} & 1 - \dfrac{2(aC_f - bC_m - cC_r)}{MV_x^2} \\ -\dfrac{2(aC_f - bC_m - cC_r)}{I_z} & \lambda - \dfrac{2(a^2C_f + b^2C_m + c^2C_r)}{I_zV_x} \end{vmatrix}$$

$$= \lambda^2 - \left(\frac{2(a^2C_f + b^2C_m + c^2C_r)}{I_zV_x} + \frac{2(C_f + C_m + C_r)}{MV_x}\right)\lambda + \left(\frac{2(C_f + C_m + C_r)}{MV_x}\right)\left(\frac{2(a^2C_f + b^2C_m + c^2C_r)}{I_zV_x}\right) + \left(\frac{2(aC_f - bC_m - cC_r)}{I_z}\right)\left(1 - \frac{2(aC_f - bC_m - cC_r)}{MV_x^2}\right) \quad (4.37)$$

It is obvious that the coefficient of λ is positive, since the cornering stiffness values are negative. Therefore the necessary condition for stability is:

$$\left(\frac{2(C_f + C_m + C_r)}{MV_x}\right)\left(\frac{2(a^2C_f + b^2C_m + c^2C_r)}{I_zV_x}\right) + \left(\frac{2(aC_f - bC_m - cC_r)}{I_z}\right)\left(1 - \frac{2(aC_f - bC_m - cC_r)}{MV_x^2}\right) > 0 \quad (4.38)$$

After some manipulations, the above equation is reduced to the following equation:

$$\frac{2\left[C_fC_m(a+b)^2 + C_fC_r(a+c)^2 + C_mC_r(b-c)^2\right] + MV_x^2(aC_f - bC_m - cC_r)}{2MI_zV_x} > 0 \quad (4.39)$$

For the above equation to be valid, the necessary condition is:

$$2\left[C_fC_m(a+b)^2 + C_fC_r(a+c)^2 + C_mC_r(b-c)^2\right] + MV_x^2(aC_f - bC_m - cC_r) > 0 \quad (4.40)$$

Therefore handling characteristics for a three-axle vehicle can be defined as:

1) Neutral steer for $aC_f = bC_m + cC_r$ which gives unconditional stability

2) Understeer for $aC_f > bC_m + cC_r$ or $|aC_f| < |bC_m + cC_r|$ which gives unconditional stability

3) Oversteer for $aC_f < bC_m + cC_r$ or $|aC_f| > |bC_m + cC_r|$ which gives instability over

a critical speed defined as:

$$V_{x,critical} = \sqrt{\frac{-2\left[C_f C_m (a+b)^2 + C_f C_r (a+c)^2 + C_m C_r (b-c)^2\right]}{M\left(aC_f - bC_m - cC_r\right)}} \tag{4.41}$$

Recall Equation 4.24. If β is eliminated from these steady state equations, then the yaw velocity gain at steady state is obtained as:

$$\frac{r}{\delta_f} = \frac{2\left[\left(C_f + C_m + C_r\right)\left(aC_f - bC_m k_m - cC_r k_r\right) - \left(aC_f - bC_m - cC_r\right)\left(C_f + C_m k_m + C_r k_r\right)\right]V_x}{\left(aC_f - bC_m - cC_r\right)MV_x^2 + 2\left[\left(a^2 C_f + b^2 C_m + c^2 C_r\right)\left(C_f + C_m + C_r\right) - \left(aC_f - bC_m - cC_r\right)^2\right]} \tag{4.42}$$

and lateral acceleration gain at steady state (since $a_l = V_x r$)

$$\frac{a_l}{\delta_f} = \frac{2\left[\left(C_f + C_m + C_r\right)\left(aC_f - bC_m k_m - cC_r k_r\right) - \left(aC_f - bC_m - cC_r\right)\left(C_f + C_m k_m + C_r k_r\right)\right]V_x^2}{\left(aC_f - bC_m - cC_r\right)MV_x^2 + 2\left[\left(a^2 C_f + b^2 C_m + c^2 C_r\right)\left(C_f + C_m + C_r\right) - \left(aC_f - bC_m - cC_r\right)^2\right]} \tag{4.43}$$

For a neutral steer three-axle vehicle for which $aC_f = bC_m + cC_r$ holds, the above equations reduce to

$$\begin{aligned} \frac{r}{\delta_f} &= \frac{\left(aC_f - bC_m k_m - cC_r k_r\right)V_x}{\left(a^2 C_f + b^2 C_m + c^2 C_r\right)} \\ \frac{a_l}{\delta_f} &= \frac{\left(aC_f - bC_m k_m - cC_r k_r\right)V_x^2}{\left(a^2 C_f + b^2 C_m + c^2 C_r\right)} \end{aligned} \tag{4.44}$$

and if it is a FWS vehicle, i.e. $k_m = k_r = 0$

$$\begin{aligned} \frac{r}{\delta_f} &= \frac{aC_f V_x}{a^2 C_f + b^2 C_m + c^2 C_r} \\ \frac{a_l}{\delta_f} &= \frac{aC_f V_x^2}{a^2 C_f + b^2 C_m + c^2 C_r} \end{aligned} \tag{4.45}$$

Note that characteristic speed can also be defined for a three-axle vehicle for which the vehicle gives the maximum yaw velocity response. It can be found by equating the derivative of Equation 4.42 with respect to V_x to zero:

$$V_{x,characteristic} = \sqrt{\frac{2\left[C_f C_m (a+b)^2 + C_f C_r (a+c)^2 + C_m C_r (b-c)^2\right]}{M\left(aC_f - bC_m - cC_r\right)}} \tag{4.46}$$

Note that characteristic and critical speeds are the same except a minus sign, just like the two-axle case.

With a similar procedure, one can derive from the bicycle model of a four-axle vehicle shown in Figure 4.5, that if:

1) $aC_1 + bC_2 = cC_3 + dC_4$ then the vehicle is neutral steer and it is unconditionally stable

2) $aC_1 + bC_2 > cC_3 + dC_4$ or $|aC_1 + bC_2| < |cC_3 + dC_4|$ then the vehicle is said to be understeer and it is again unconditionally stable

3) $aC_1 + bC_2 < cC_3 + dC_4$ or $|aC_1 + bC_2| > |cC_3 + dC_4|$ then the vehicle is said to be oversteer and it is instable over a certain critical speed defined as:

$$V_{x,critical} = \sqrt{\frac{-2\left[\begin{array}{c} C_1C_2(a-b)^2 + C_1C_3(a+c)^2 + C_1C_4(a+d)^2 \\ +C_2C_3(b+c)^2 + C_2C_4(b+d)^2 + C_3C_4(c-d)^2 \end{array}\right]}{M\left(aC_1 + bC_2 - cC_3 - dC_4\right)}} \tag{4.47}$$

For the characteristic speed, the expression is:

$$V_{x,characteristic} = \sqrt{\frac{2\left[\begin{array}{c} C_1C_2(a-b)^2 + C_1C_3(a+c)^2 + C_1C_4(a+d)^2 \\ +C_2C_3(b+c)^2 + C_2C_4(b+d)^2 + C_3C_4(c-d)^2 \end{array}\right]}{M\left(aC_1 + bC_2 - cC_3 - dC_4\right)}} \tag{4.48}$$

The yaw velocity and lateral acceleration gains (at steady state) that a four-axle, neutral steer, FWS vehicle will produce can be obtained as:

$$\frac{r}{\delta_f} = \frac{aC_1V_x}{a^2C_1 + b^2C_2 + c^2C_3 + d^2C_4}$$
$$\frac{a_l}{\delta_f} = \frac{aC_1V_x^2}{a^2C_1 + b^2C_2 + c^2C_3 + d^2C_4} \quad (4.49)$$

CHAPTER 5

SIMULATION TOOL

The mathematical tool used in this study to solve the equations of motion is MATLAB. The equations are modeled in SIMULINK. Figures 5.1 to 5.12 illustrate the generation of the mathematical model for a two-axle vehicle in SIMULINK. The integrator used in the simulation is ode5 (Dormand-Price), with a fixed step size of 0.001.

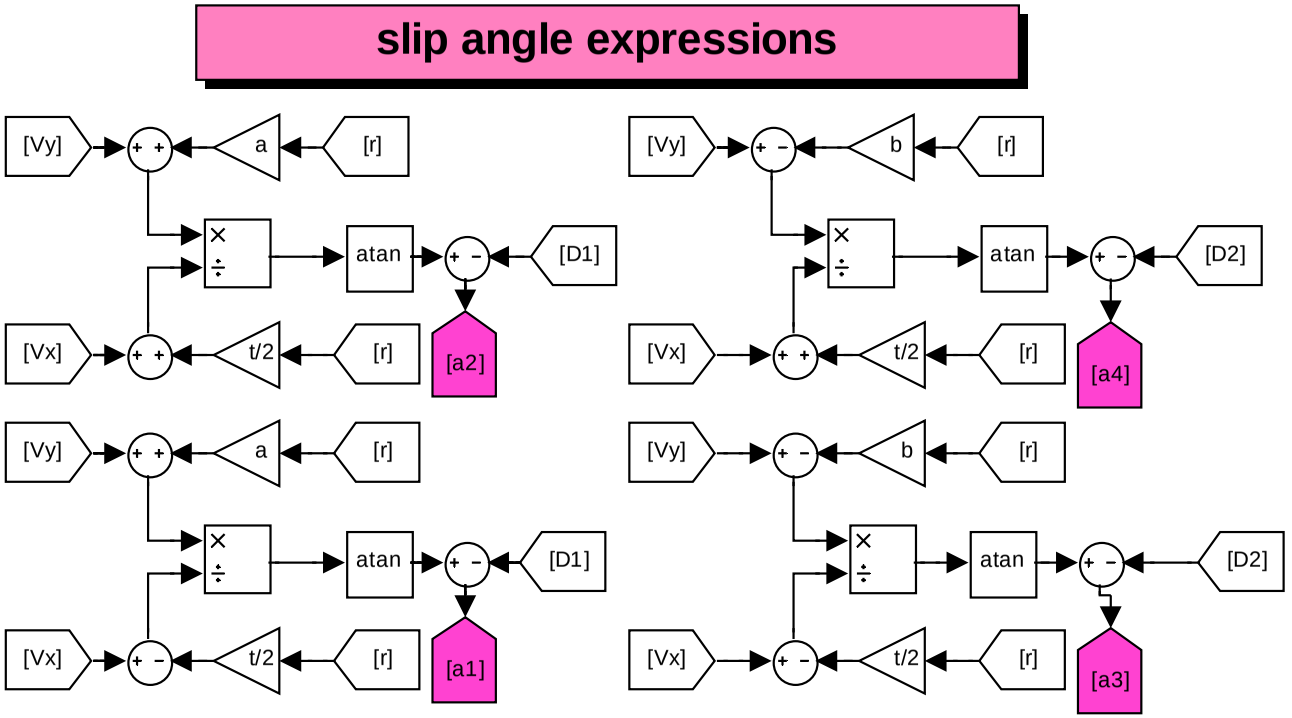

Figure 5.1 Slip angle expressions

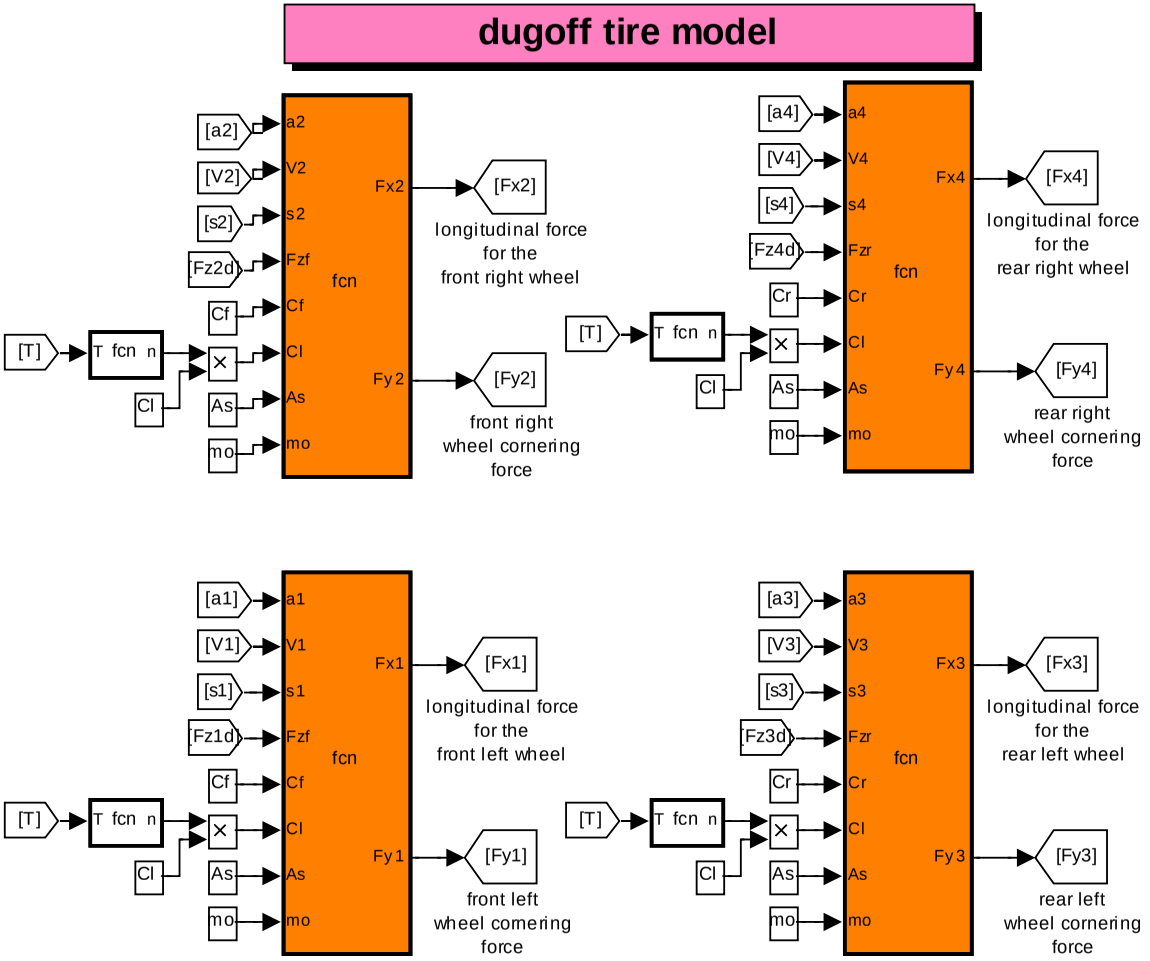

Figure 5.2 Dugoff tire model

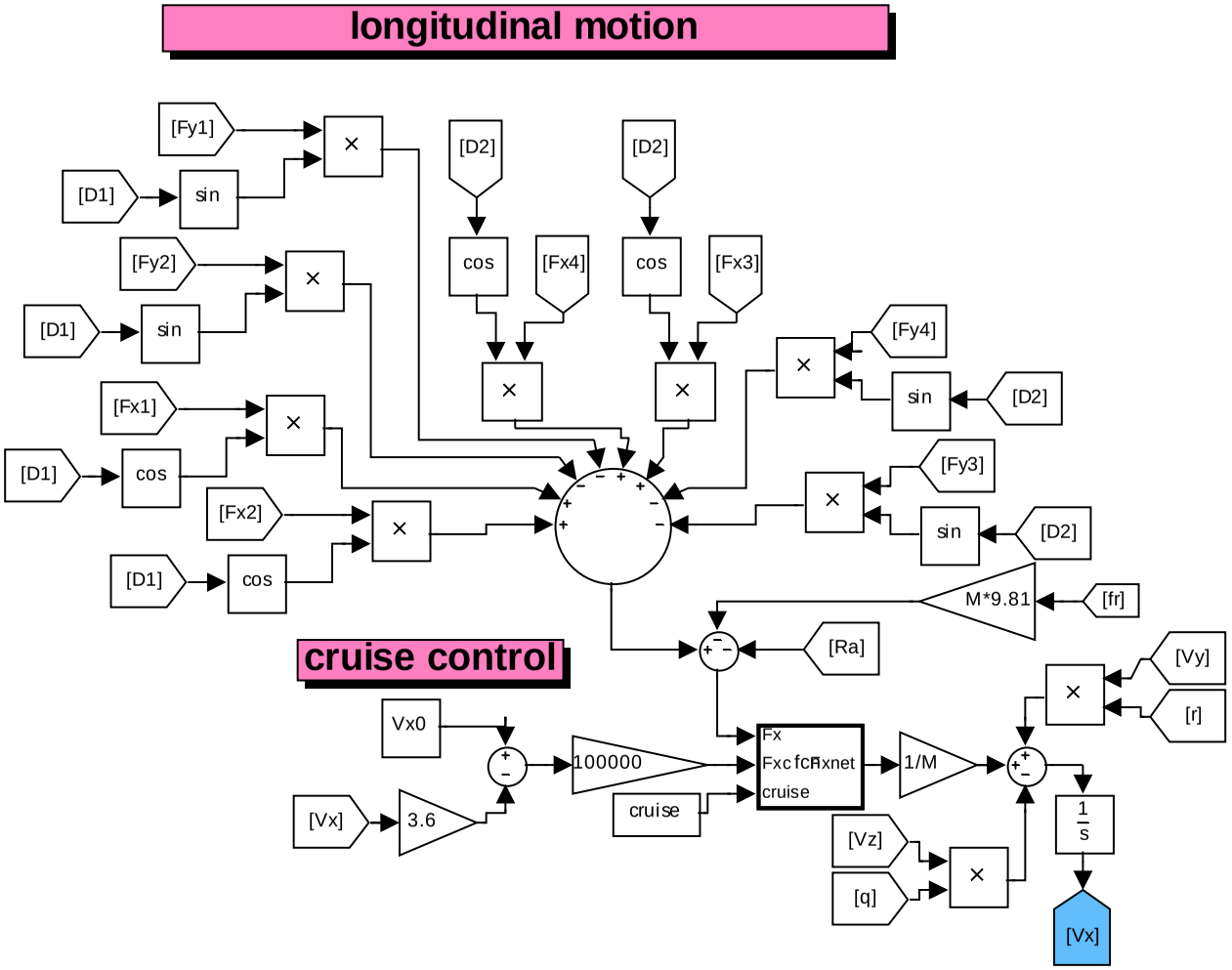

Figure 5.3 Longitudinal motion

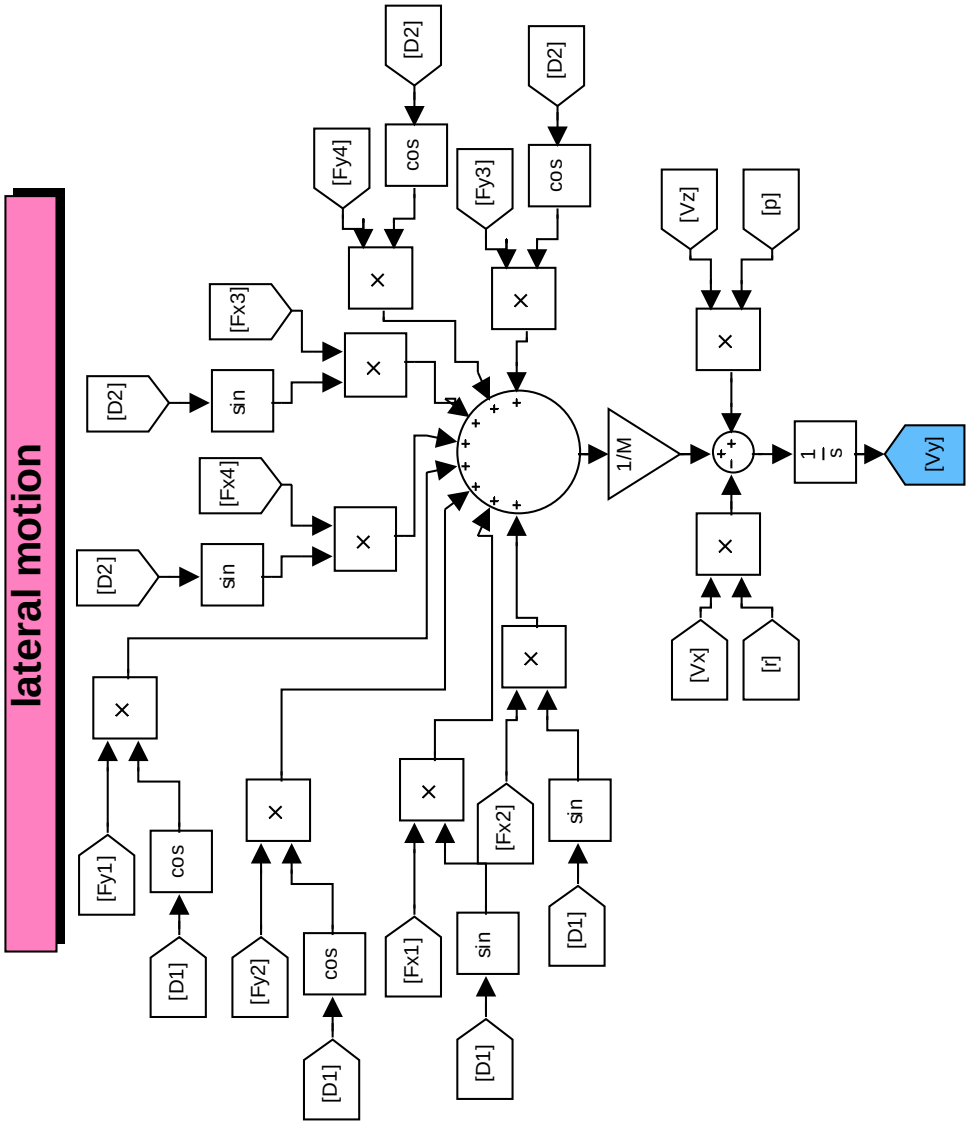

Figure 5.4 Lateral motion

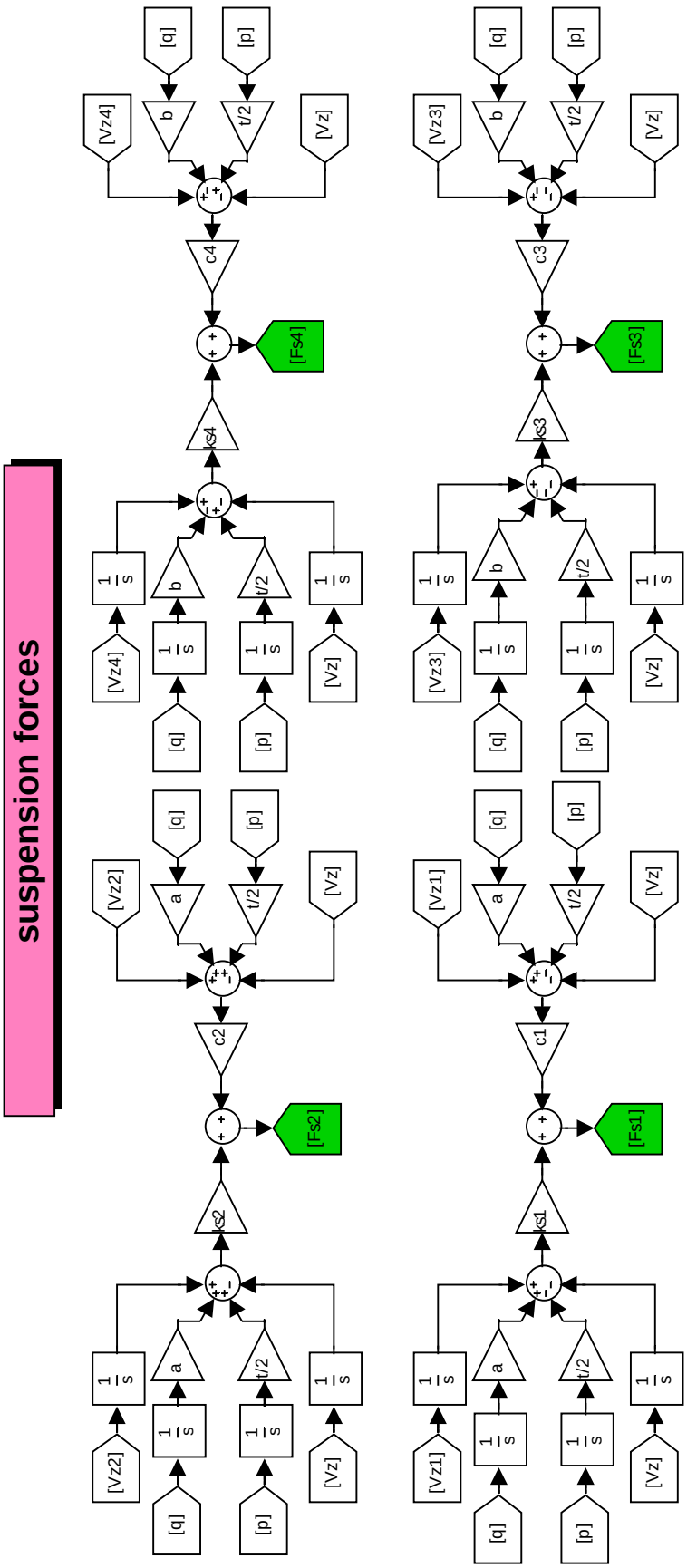

Figure 5.5 Suspension forces

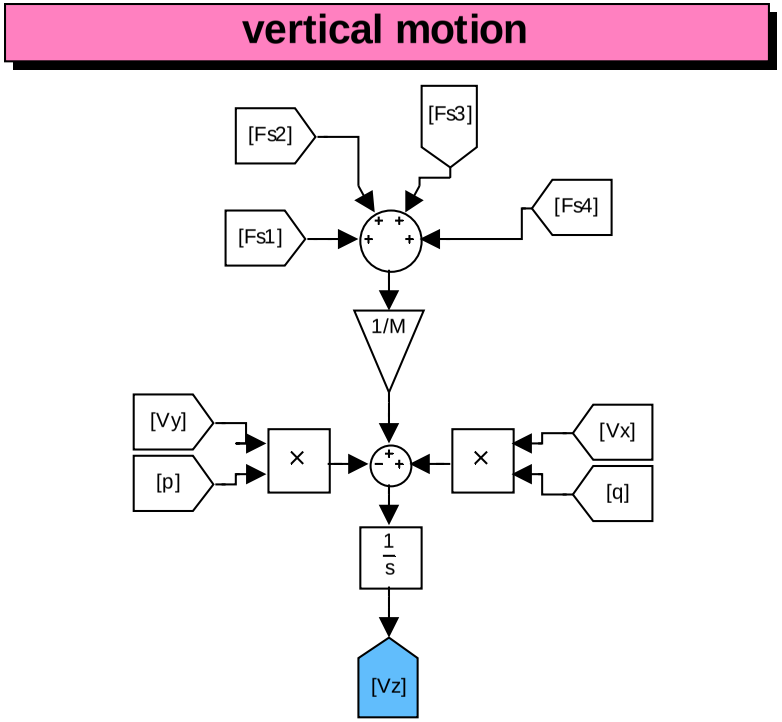

Figure 5.6 Vertical motion

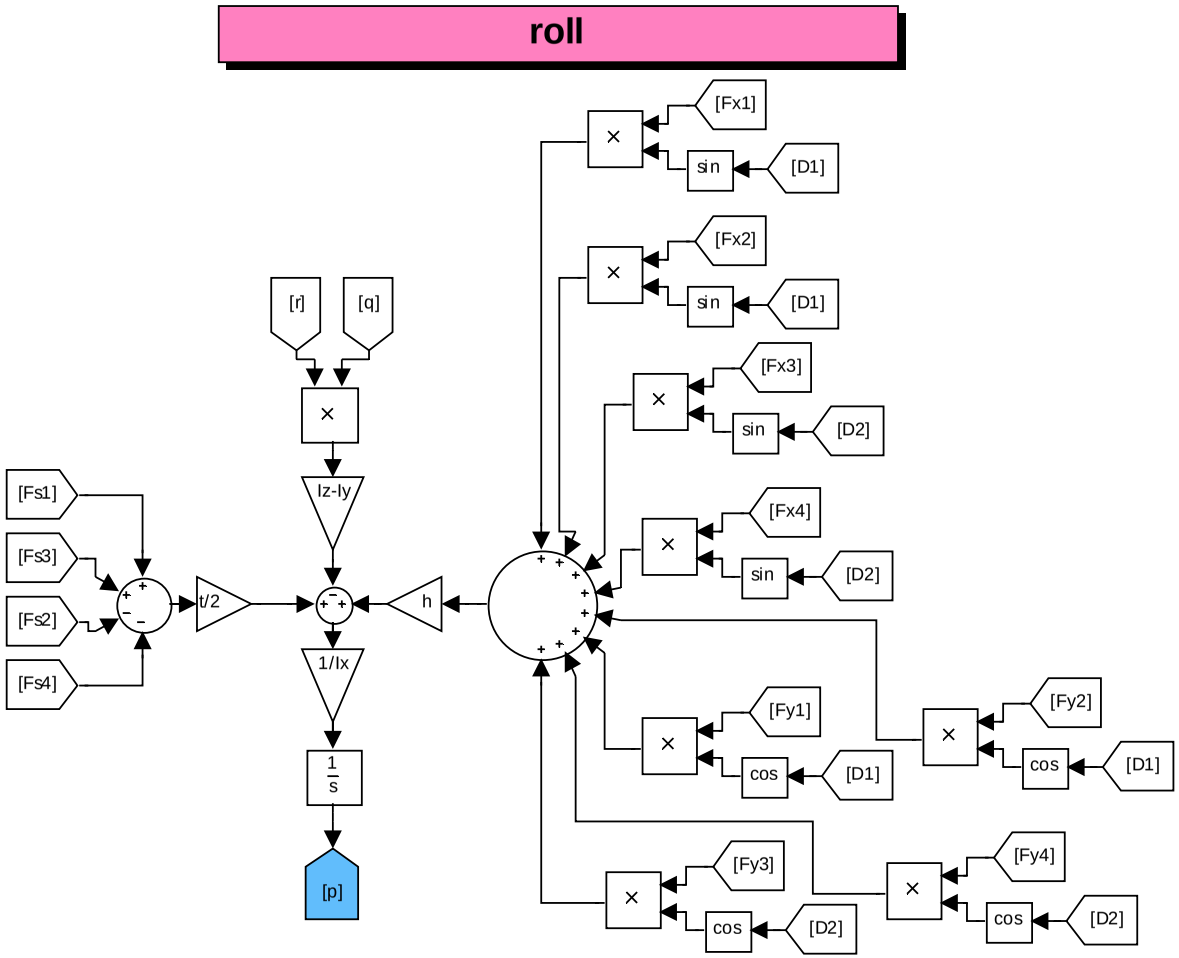

Figure 5.7 Roll velocity

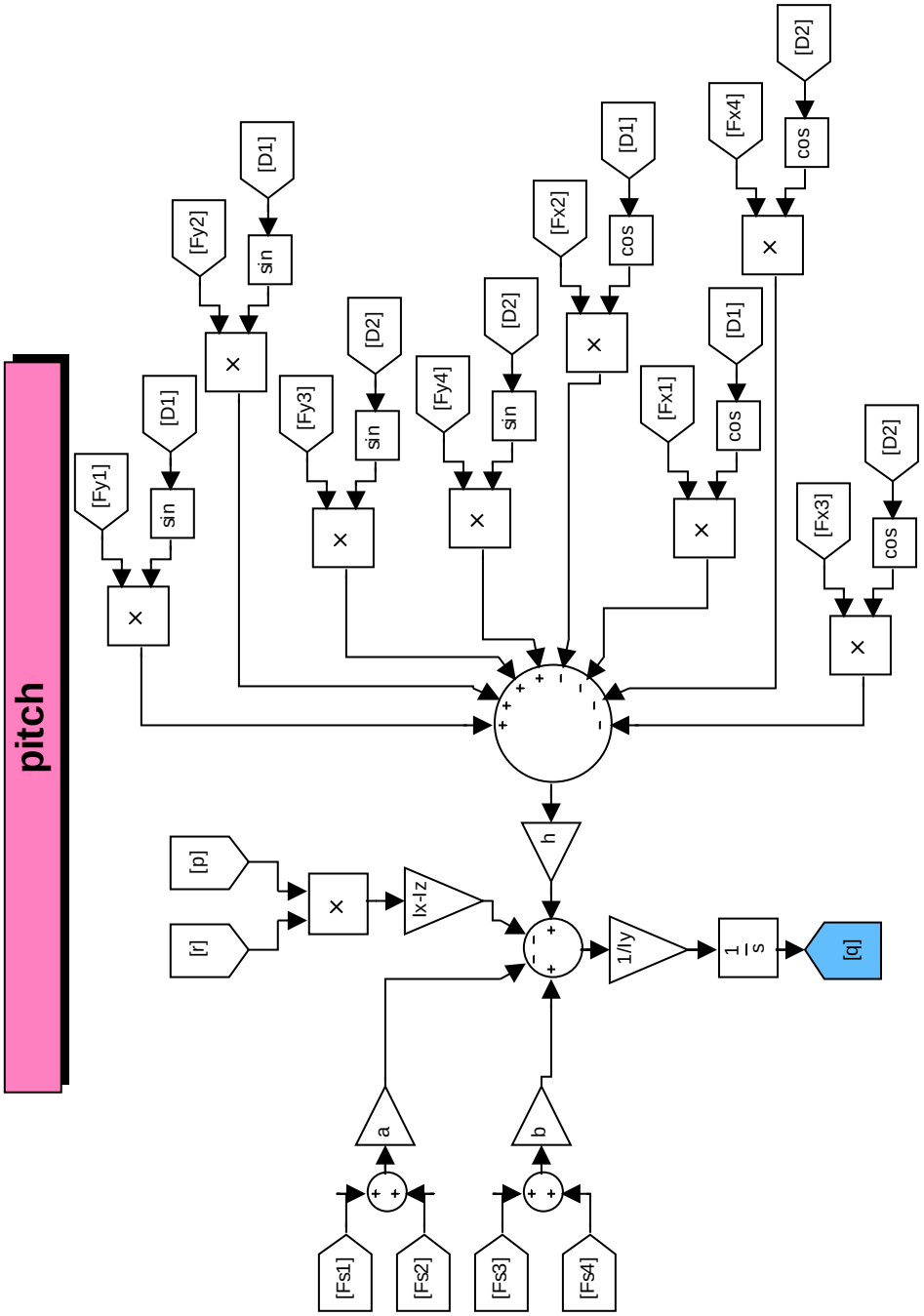

Figure 5.8 Pitch velocity

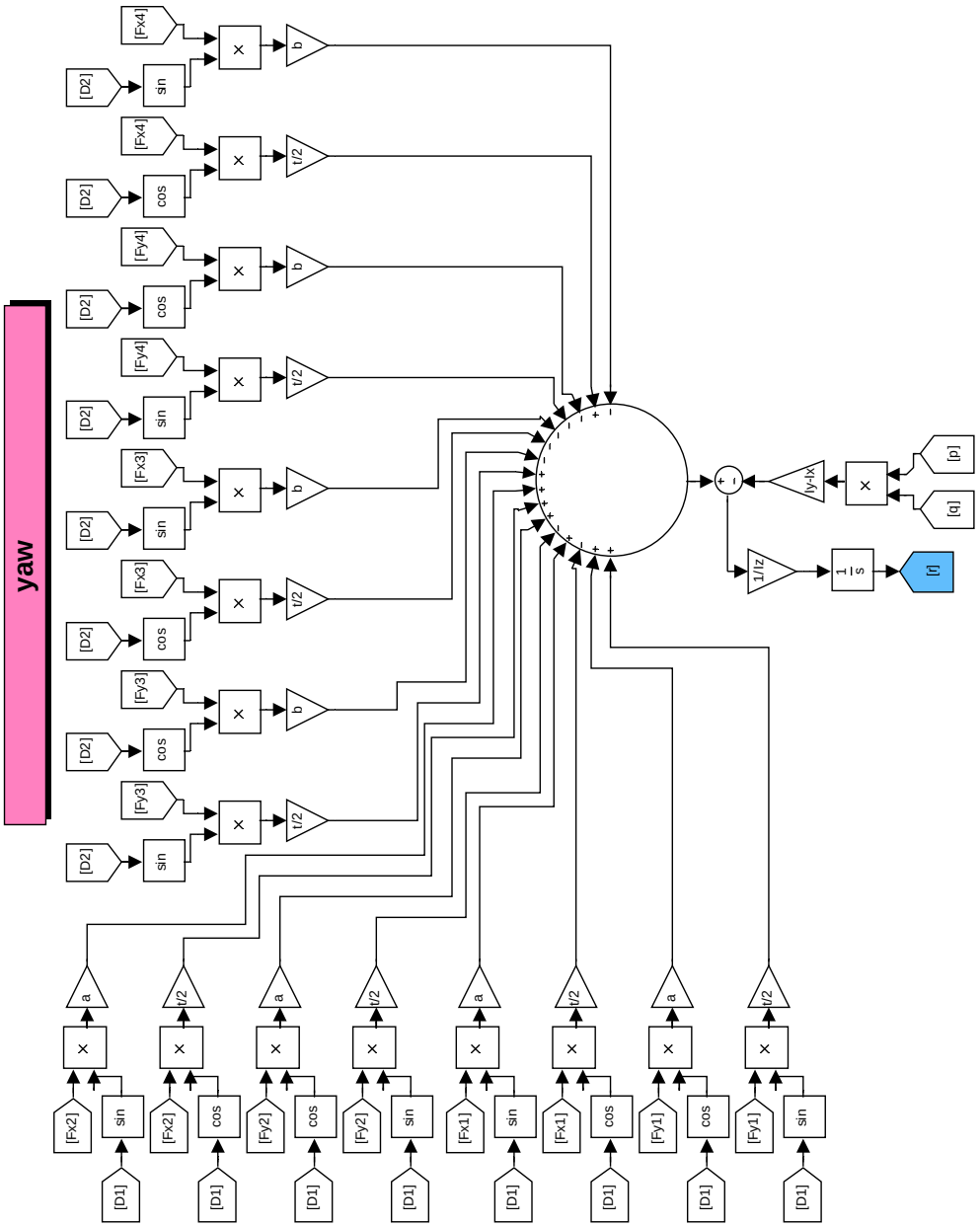

Figure 5.9 Yaw velocity

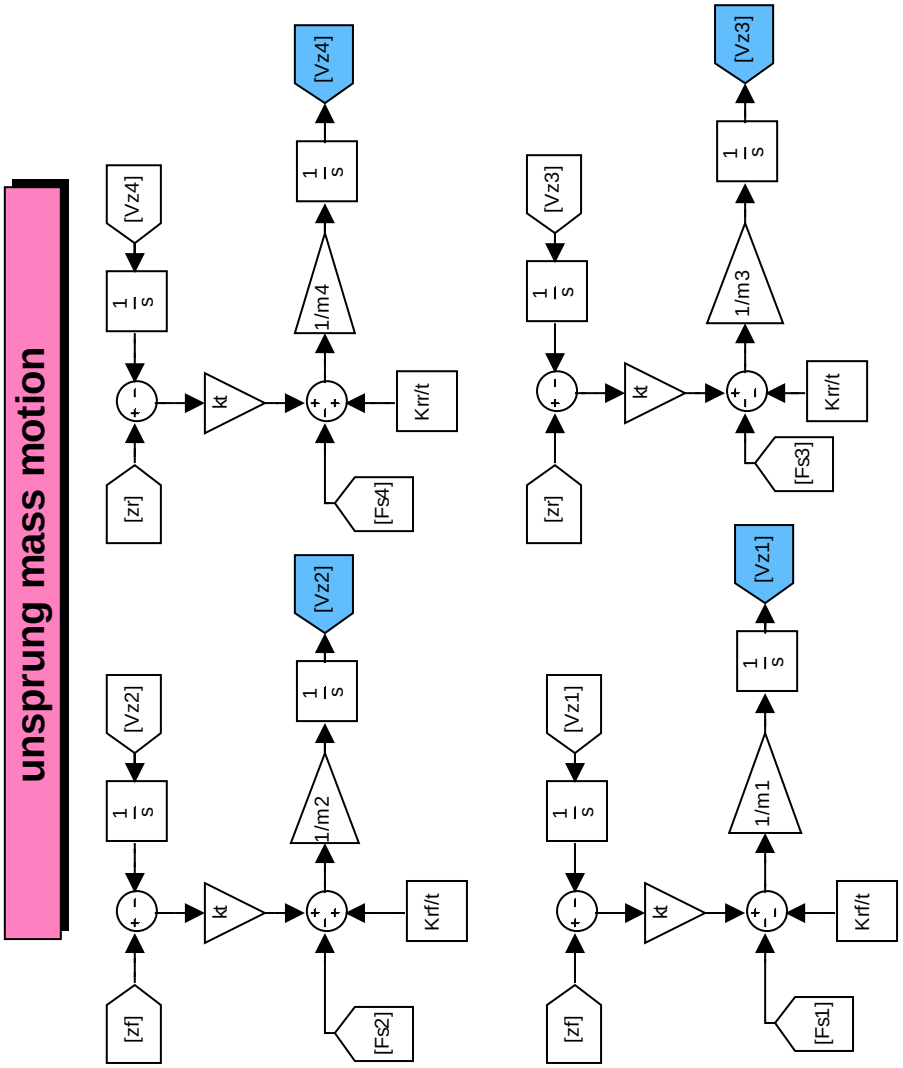

Figure 5.10 Unsprung mass motion

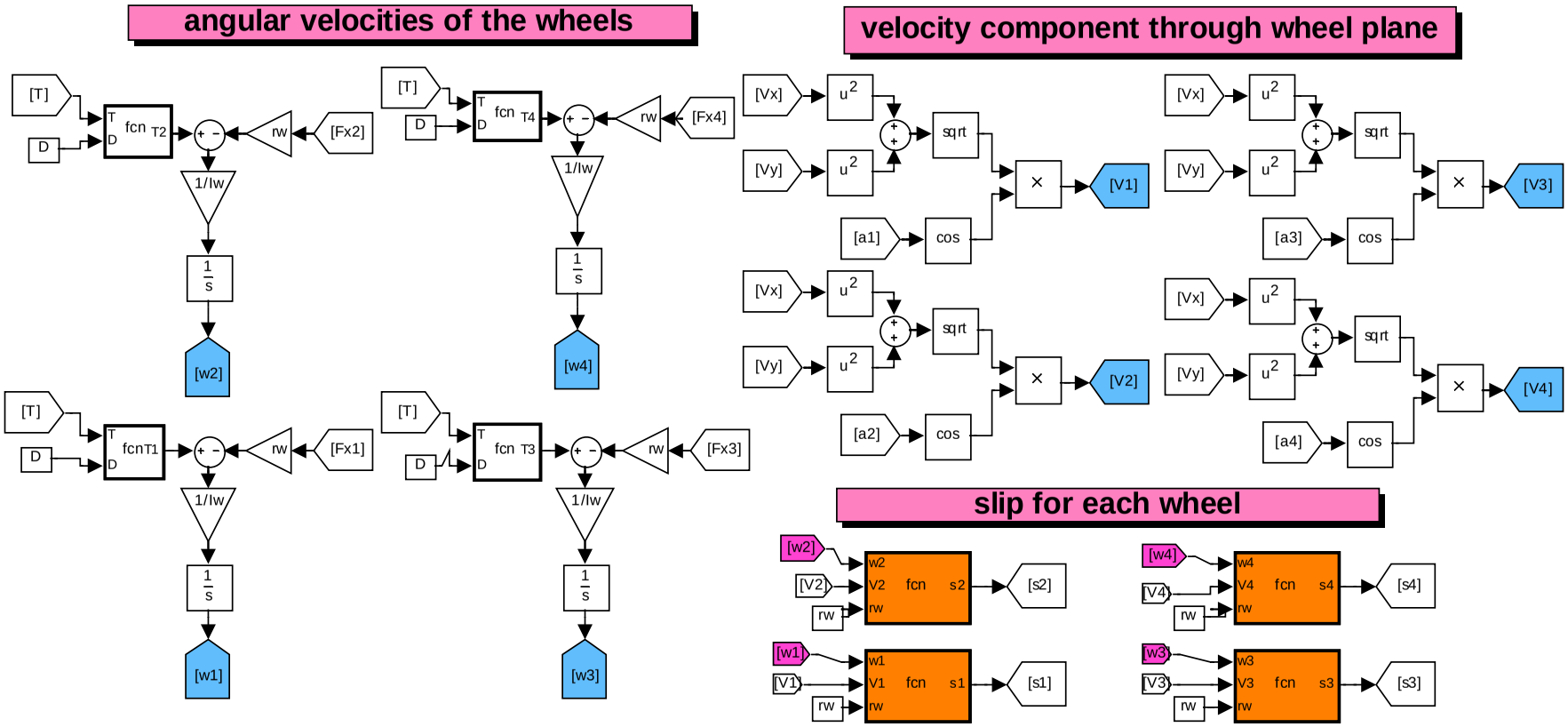

Figure 5.11 Some wheel dynamics expressions

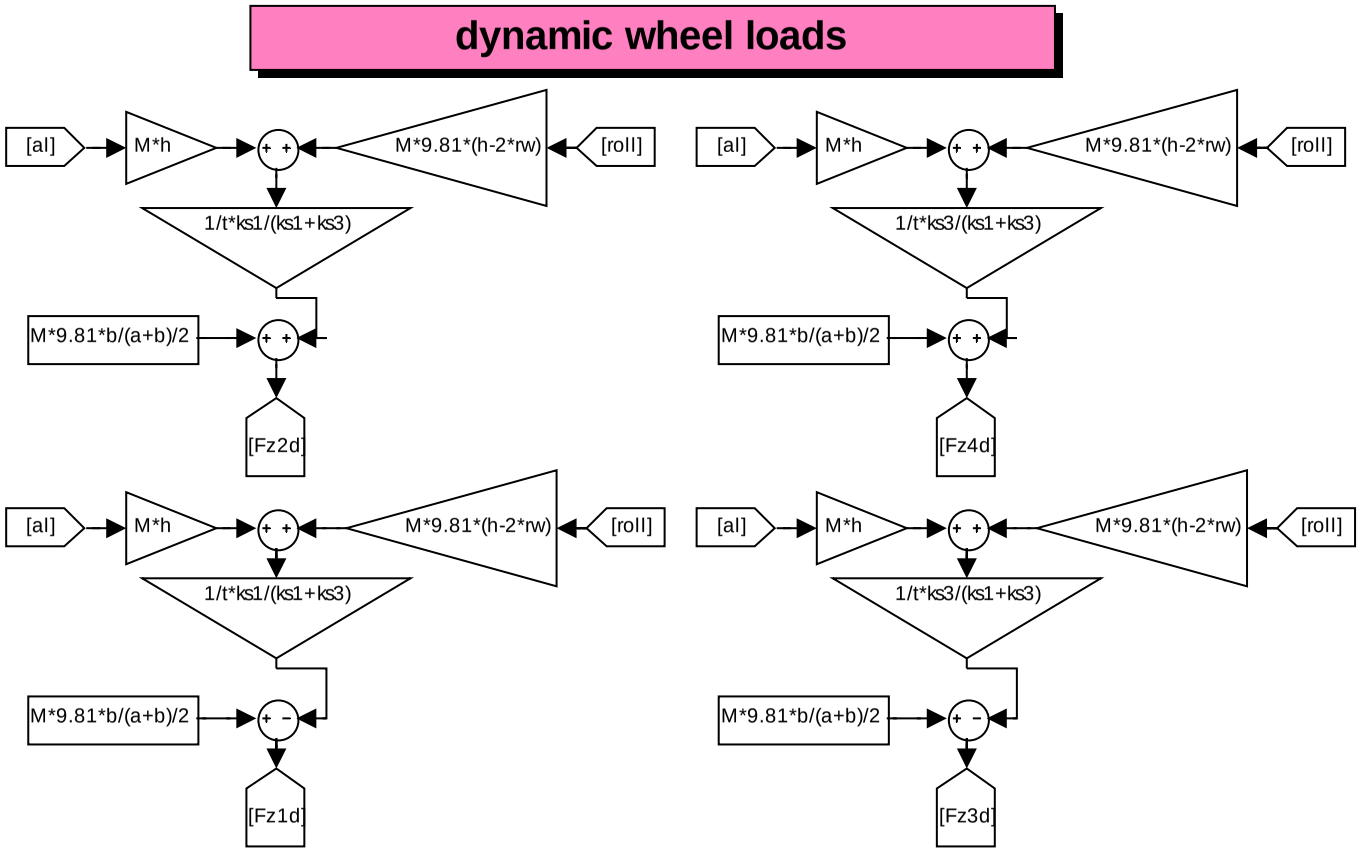

Figure 5.12 Wheel loads with lateral load transfer

A graphical user interface (GUI) is built to:

1) load and save data
2) specify simulation time
3) select inputs; namely torque to wheels, drive configuration, steering input and strategy, and road profile
4) perform the simulation
5) view the results.

Figure 5.13 shows the main window of the GUI. It is used to select the number of axles, and it leads to other windows which are explained below. It is also used to start the simulation.

Figure 5.14 shows the window to load and save vehicle data, select drive configuration, decide on whether the vehicle is braking, accelerating, or moving with constant velocity, and input simulation time.

Figure 5.15 shows the window to specify steering input and select steering strategy. Figure 5.16 shows the window to select road profile [27]. Finally Figure 5.17 shows the window to see the results.

Figure 5.13 The main GUI window

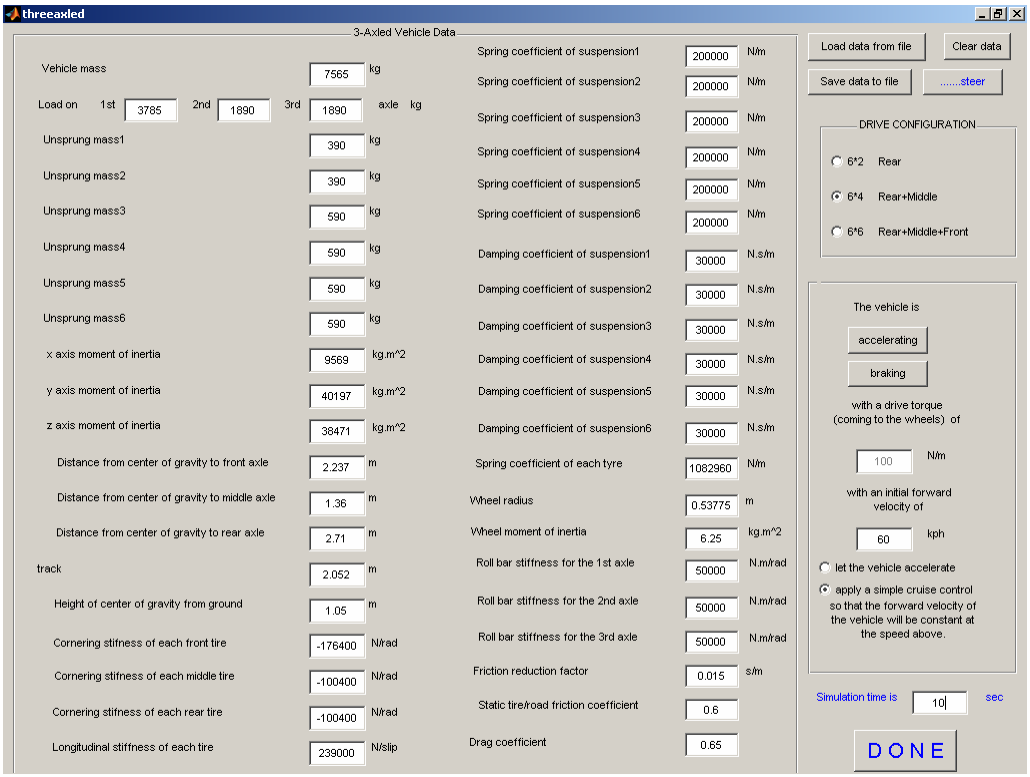

Figure 5.14 Data and drive configuration

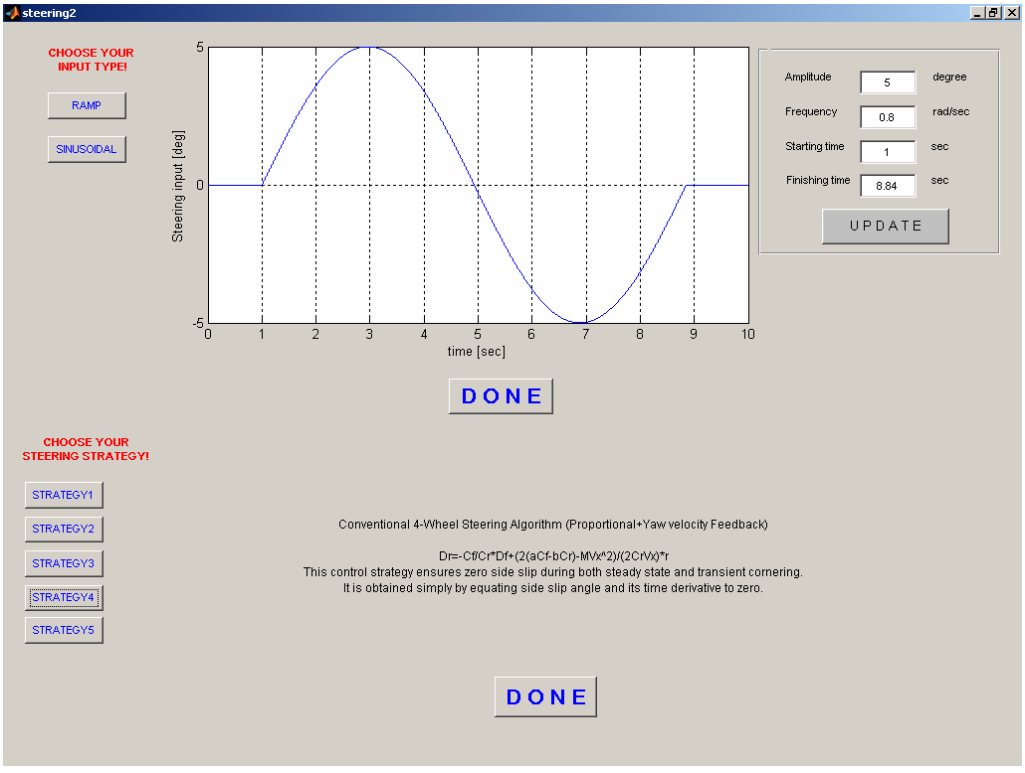

Figure 5.15 Steering input selection

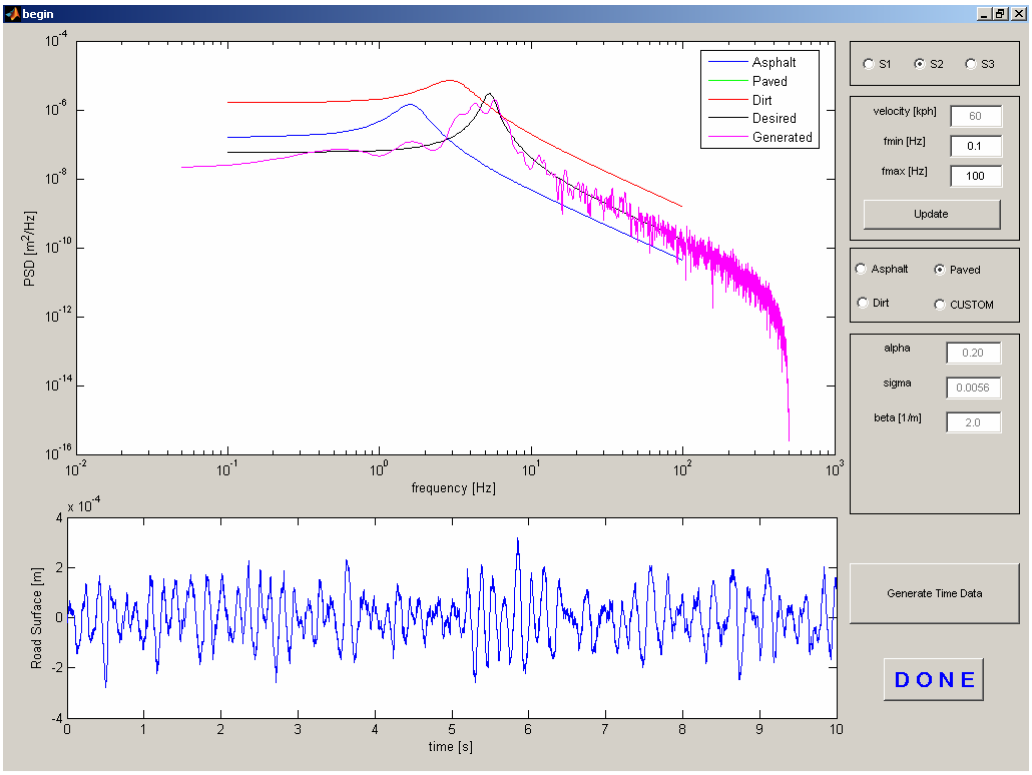

Figure 5.16 Road profile selection

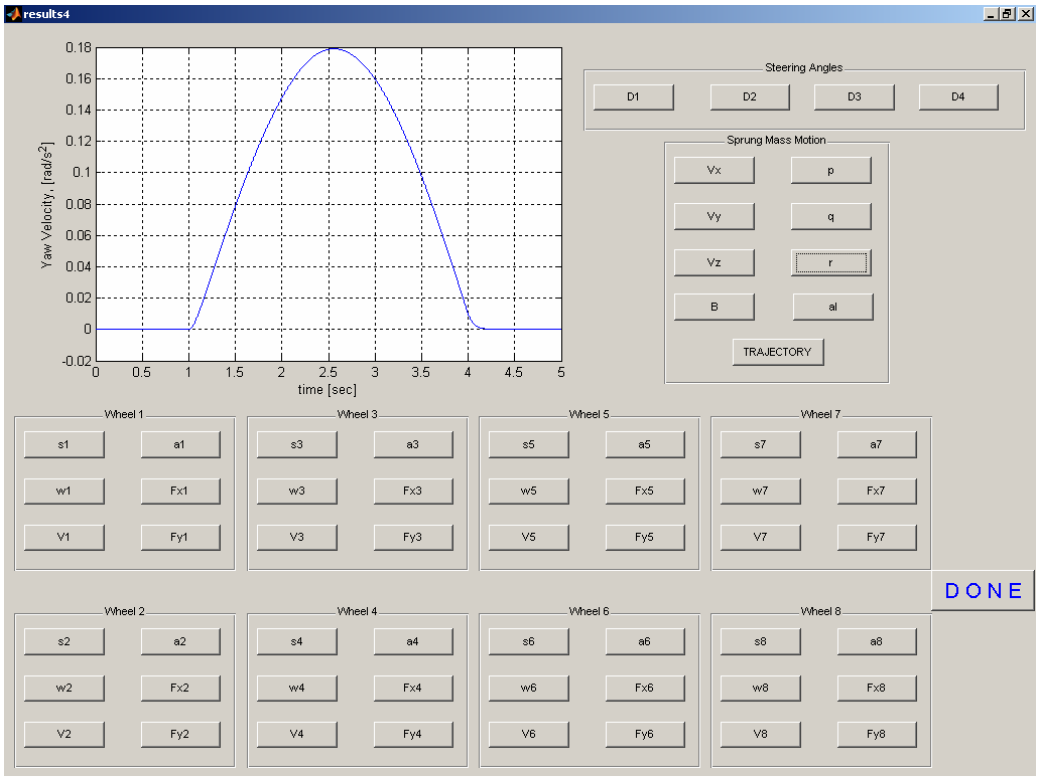

Figure 5.17 Results

Note that Figures 5.13 and 5.16 are common for all two, three and four-axle vehicles. However, Figures. 5.14, 5.15, and 5.17 are separate for two, three, and four-axle vehicles, for which the written code is different; since the data specifications, number of steering strategies, number of results, etc. all differ with a different number of axles.

CHAPTER 6

CASE STUDIES

6.1 Two-Axle Vehicle

Data given in Table 4.1 for the two-axle bus is used for the simulation at a constant speed of 75 kph, with the steering input and the road profile as given in Figure 6.1. Results obtained for the sideslip angle, yaw velocity, and lateral acceleration for the five steering strategies discussed in Section 4.3.1 for the two-axle vehicle are presented in Figure 6.2.

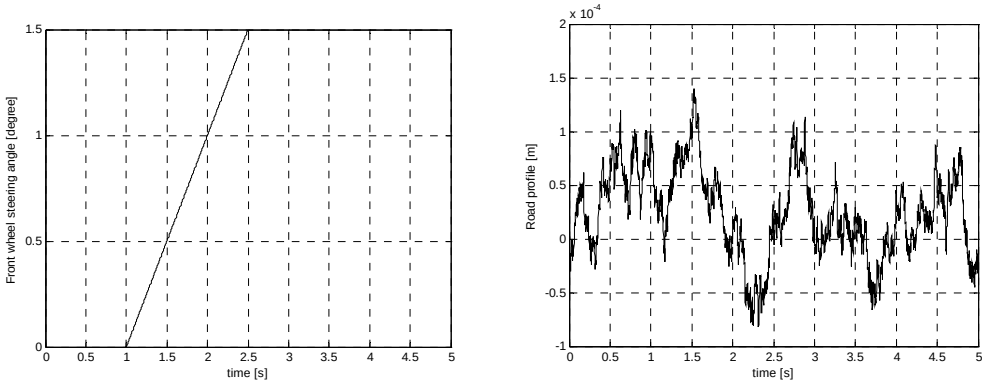

(a) (b)

Figure 6.1 (a) Steering input, (b) Asphalt road profile

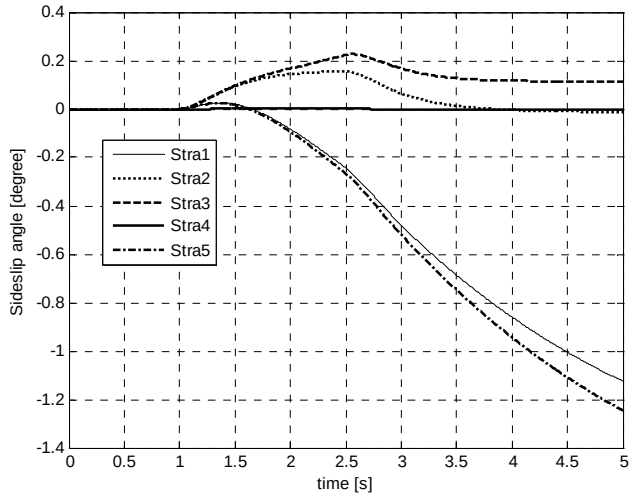

(a)

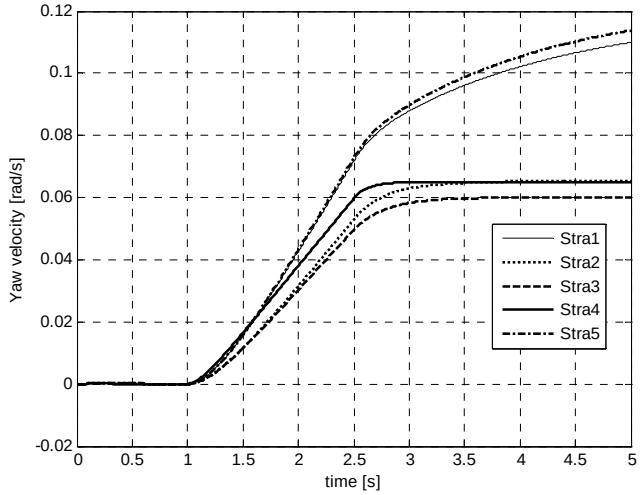

(b)

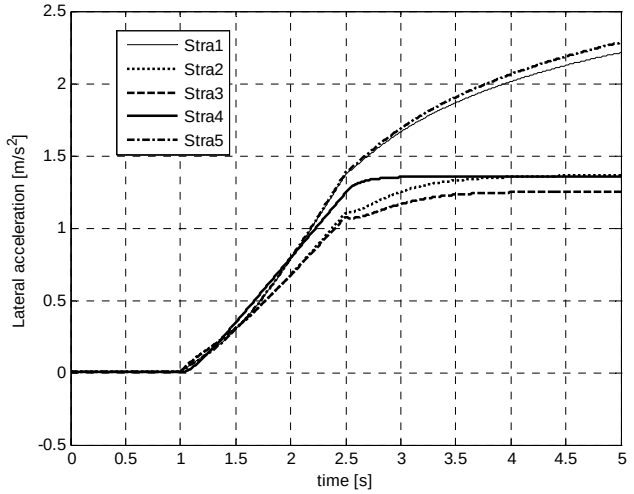

(c)

Figure 6.2 (a) Sideslip angle, (b) yaw velocity, (c) lateral acceleration for the bus

Note that the best strategy in terms of sideslip angle is Strategy 4, which gives zero sideslip angle even in the transient part of cornering. Strategy 2 coincides with Strategy 4 as the motion settles to steady state, as expected.

It is also observed from the yaw velocity and lateral acceleration curves that Strategy 4 gives a slightly quicker response than the other strategies, which is favorable. On the contrary, Strategy 2 gives a sluggish response.

Strategy 1 and Strategy 5 give higher yaw velocity and lateral acceleration responses, but their sideslip angle response is unsatisfactory. Strategy 5 is best in terms of yaw velocity and lateral acceleration gains, but it does not leave a favorable subjective impression for ordinary passengers, since the amount of vehicle sideslip angle is excessive.

6.2 Three-Axle Vehicle

Before testing all strategies, the first five empirical strategies are simulated for the three-axle truck firstly, in order to observe whether steering the wheels on intermediate and rear axles for a three axle vehicle is beneficial in terms of vehicle handling characteristics or not. The first five strategies as explained in Section 4.3.2 are illustrated in Figure 6.3 as follows:

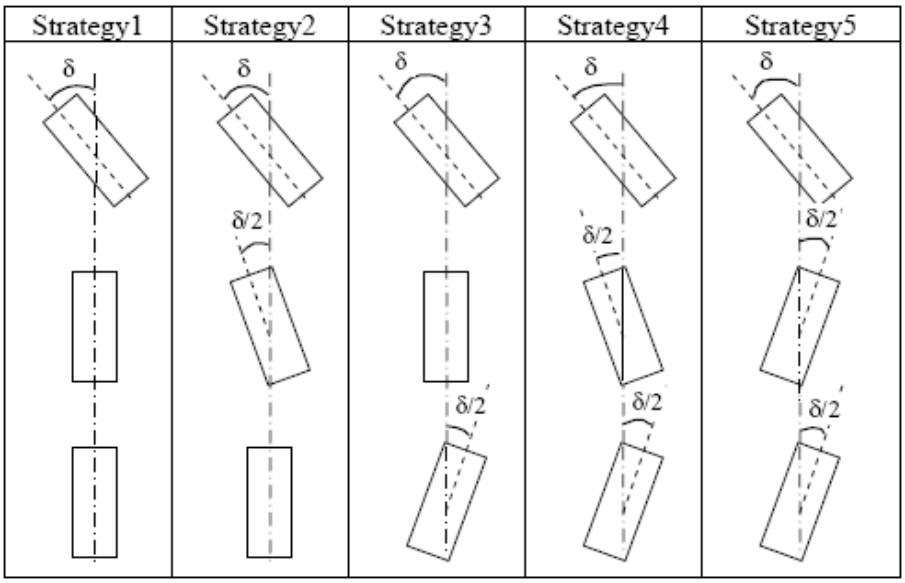

Figure 6.3 First five steering strategies for the three-axle vehicle

With the data given in Table 4.2 for an unloaded commercial truck, at a constant velocity of 55 kph, and with the steering input and the road profile as given in Figure 6.4; the simulation results for the sideslip angle, yaw velocity, and lateral acceleration for the first five steering strategies are presented in Figure 6.5.

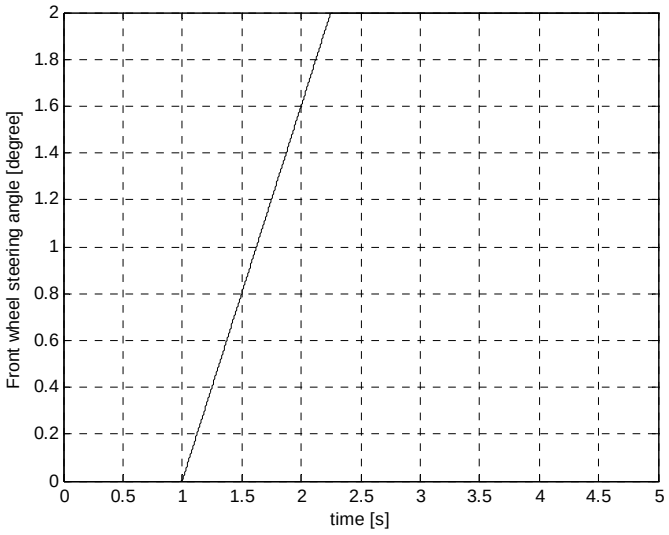

(a)

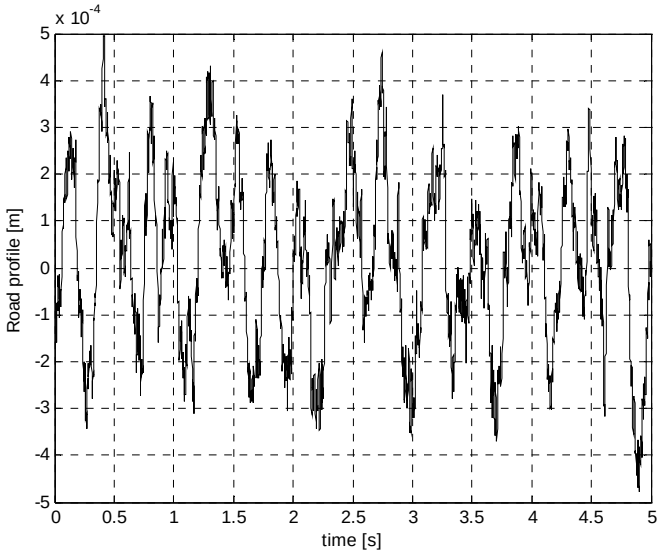

(b)

Figure 6.4 (a) Steering input and (b) dirt road profile

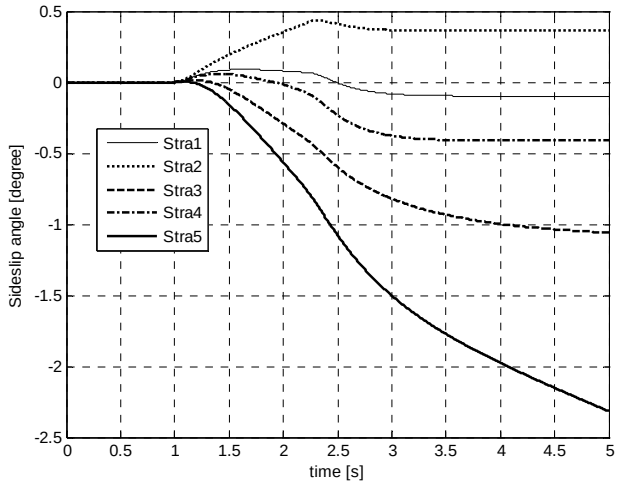

(a)

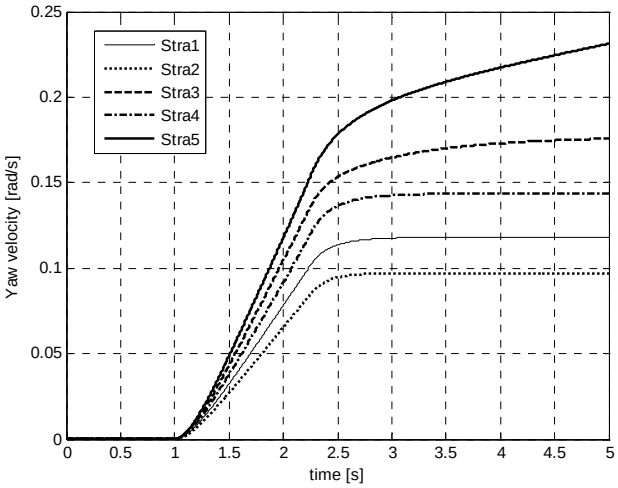

(b)

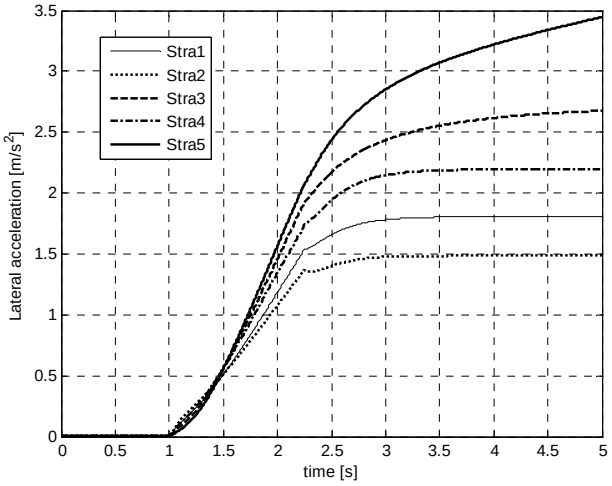

(c)

Figure 6.5 (a) Sideslip angle, (b) yaw velocity, (c) lateral acceleration responses for the 1st five steering strategies for the unloaded truck

It is observed that steering the wheels on intermediate axle in the same direction with the front wheels has no use in terms of sideslip angle, yaw velocity, and lateral acceleration, at the specified forward speed of 55 kph. For example Strategy 2 gives a higher sideslip angle, and lower yaw velocity and lateral acceleration responses that Strategy 1, which means that steering the wheels on the intermediate axle in the same direction with the front wheel gives no use; on the contrary, it degrades vehicle handling characteristics, at least at the mentioned speed.

It is also observed that Strategy 3 gives a higher sideslip angle response than that of Strategy 4, which is worse, but also higher yaw velocity and lateral acceleration responses than those of Strategy 4, which is favorable. Note that Strategy 5 gives the best yaw velocity and lateral acceleration responses, but the worst sideslip angle response.

As a general trend, as yaw velocity and lateral acceleration responses increase, so does sideslip angle response. Therefore, a means to achieve high yaw velocity and lateral acceleration responses while keeping a low sideslip angle is required.

With the data given in Table 4.2, at a constant velocity of 55 kph, and with the steering input and the road profile as given in Figure 6.4 again, the simulation results for the sideslip angle, yaw velocity, and lateral acceleration for Strategies 1, 6, 7 and 8 ($\delta_m=0$ for Strategies 7 and 8) for the unloaded and loaded trucks are presented in Figures 6.6 and 6.7.

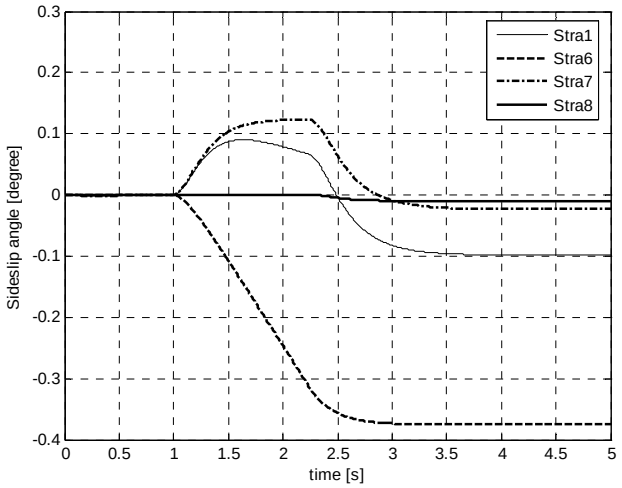

(a)

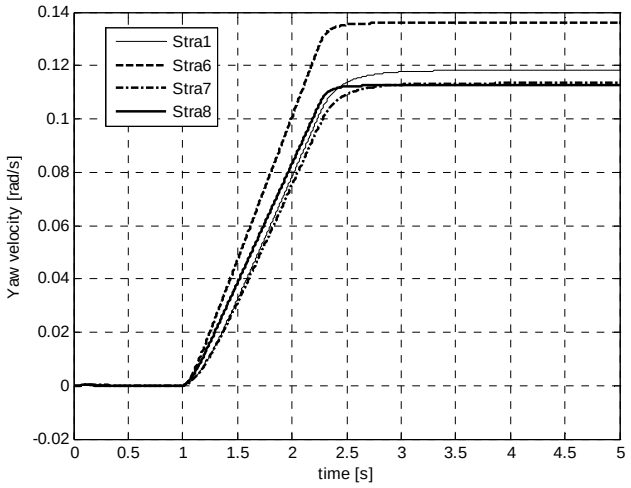

(b)

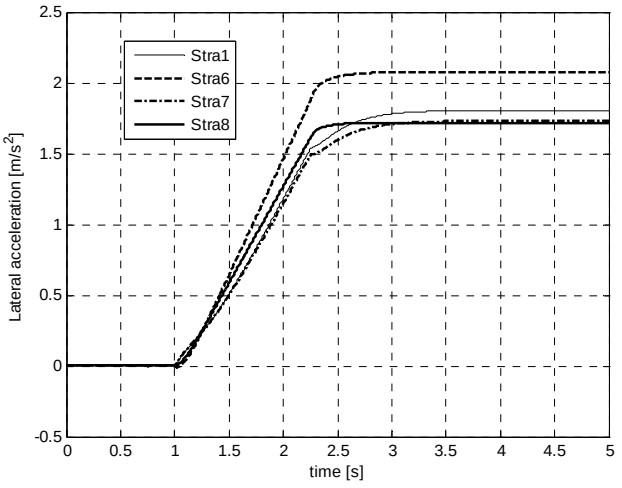

(c)

Figure 6.6 Simulation results for the unloaded truck for (a) sideslip angle, (b) yaw velocity, (c) lateral acceleration

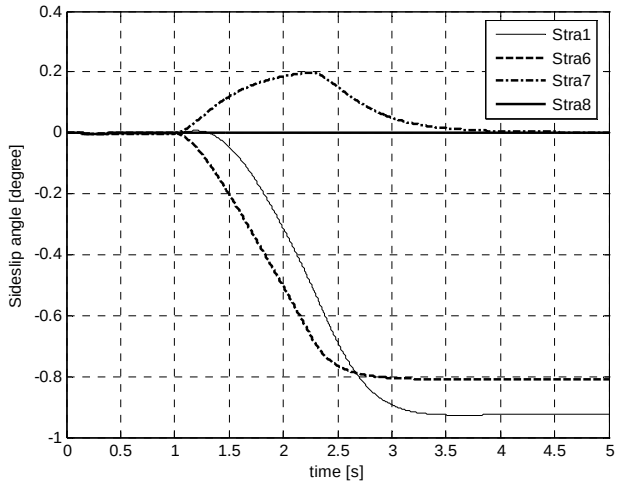

(a)

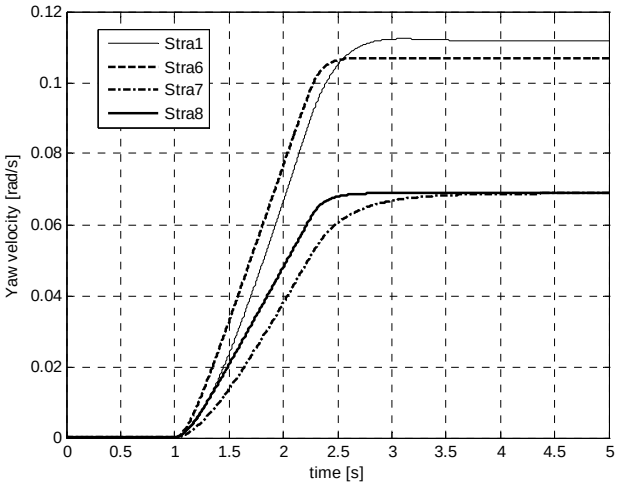

(b)

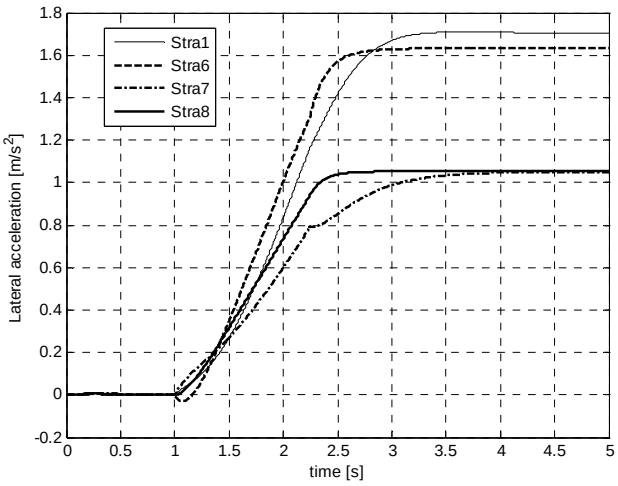

(c)

Figure 6.7 Simulation results for the loaded truck for (a) sideslip angle, (b) yaw velocity, (c) lateral acceleration

Note that the best strategy in terms of sideslip angle for both unloaded and loaded trucks is Strategy 8, which gives (almost) zero sideslip angle even in the transient part of cornering. Strategy 8 coincides with Strategy 7 as the motion settles to steady state, as expected.

On the other hand, Strategy 1 and Strategy 6 give higher yaw velocity and lateral acceleration responses, especially for the loaded truck, but poor sideslip angle response.

Note that the disadvantage of Strategy 8, which is the low yaw velocity and lateral acceleration responses, can be improved by steering the wheels on intermediate axle too. The results in Figure 6.8 are applications of Strategy 8 with different intermediate axle steering schemes for the unloaded and loaded trucks. On these figures, steady state lateral acceleration levels for the neutral steer FWS configurations of the vehicles are also indicated.

Recall from the stability analysis for a three-axle vehicle in Section 4.4 that for a neutral steer, FWS three-axle vehicle for which the relation $aC_f = bC_m + cC_r$ holds, the lateral acceleration at steady state was derived as:

$$(a_l)_{\substack{neutral \\ steady}} = \frac{aC_f V_x^2}{a^2 C_f + b^2 C_m + c^2 C_r} \delta_f \tag{6.1}$$

Consider the unloaded truck whose data is given in Table 4.2. If the cornering stiffness of the front wheels are increased from *176400 N/rad* to *182423 N/rad* in magnitude, then the vehicle obeys the relation $aC_f = bC_m + cC_r$ and it becomes neutral steer. In such a case, when the appropriate values are substituted into Equation 6.1, lateral acceleration for the neutral steer, FWS three-axle unloaded commercial truck for the steady state is found to be 1.81 m/s^2. Likewise if the cornering stiffness values of the wheels on intermediate and rear axles are increased from *286400 N/rad* to *335859 N/rad* in magnitude for the loaded truck whose data is provided in Table 4.2, the vehicle becomes neutral steer and the steady state lateral acceleration is found to be 1.67 m/s^2 according to Equation 6.1.

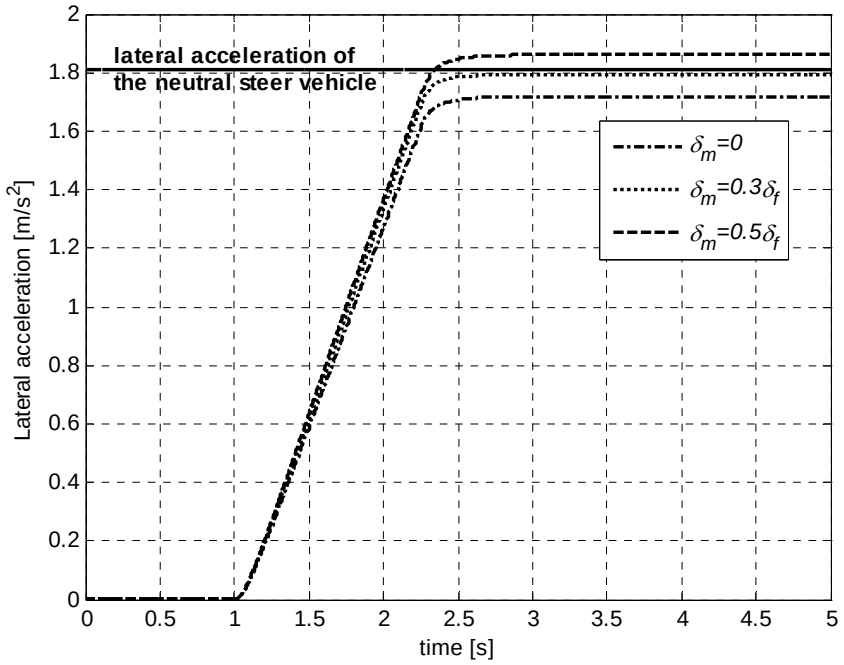

(a)

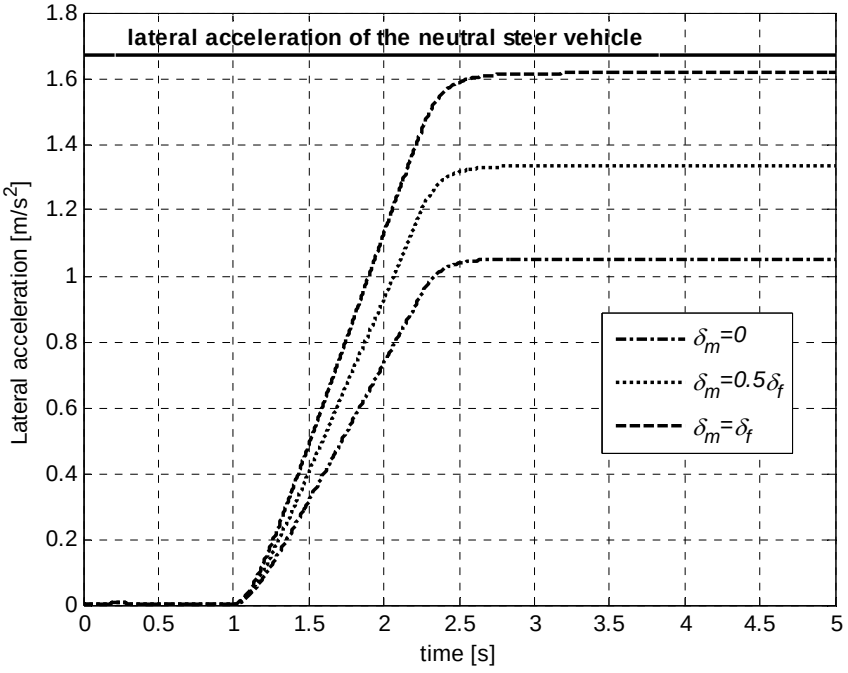

(b)

Figure 6.8 Application of Strategy 8 with increasing intermediate axle steering for (a) the unloaded truck, (b) the loaded truck

As seen in these figures, yaw velocity and lateral acceleration responses increase as the intermediate axle steering increases, without degrading sideslip angle, with the utilization of Strategy 8.

Note that for the unloaded truck, steering the intermediate axle at an amount of $0.3\delta_f$ is sufficient to reach the lateral acceleration of the neutral steer FWS vehicle's lateral acceleration. Lateral acceleration response can be further improved by steering the intermediate axle through a larger angle, for instance at $0.5\delta_f$, as shown in Figure 6.8. On the other hand, for the loaded truck, it is not possible to reach to the neutral steer FWS vehicle's lateral acceleration, even by steering the wheels on intermediate axle at an equal amount to the front wheels, as seen in Figure 6.8. That is normal since, the heavier the vehicle, the more sluggishly it responds, and the harder to reach the neutral steer vehicle's lateral acceleration.

6.3 Four-Axle Vehicle

Recall from Section 4.3.3 that 2nd, 3rd, 4th and 5th strategies are empirical strategies simulated to see whether steering the wheels on intermediate axles is advantageous or not for a four-axle vehicle. First five strategies are illustrated in Figure 6.9:

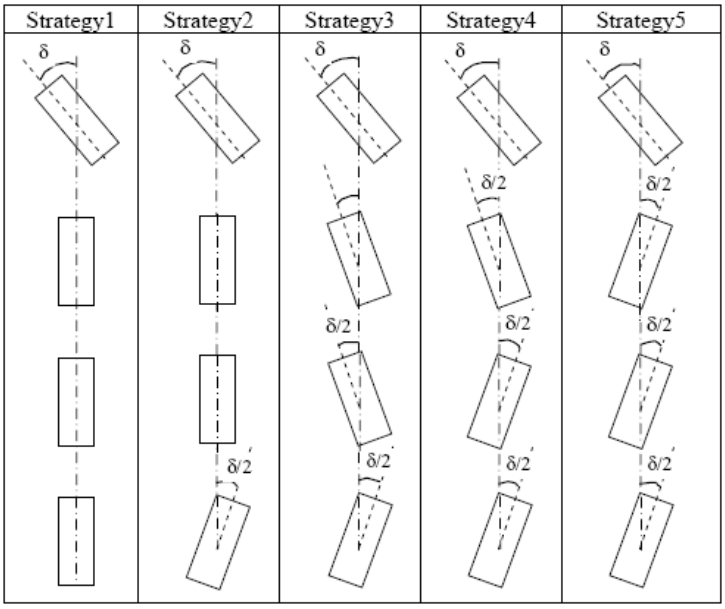

Figure 6.9 First five steering strategies for the four-axle vehicle

With the data given in Table 4.3 for the four-axle APC, at a constant velocity of 50 kph, and with the steering input and road profile as given in Figure 6.10, results obtained for sideslip angle, yaw velocity, and lateral acceleration for the first five steering strategies are presented in Figure 6.11.

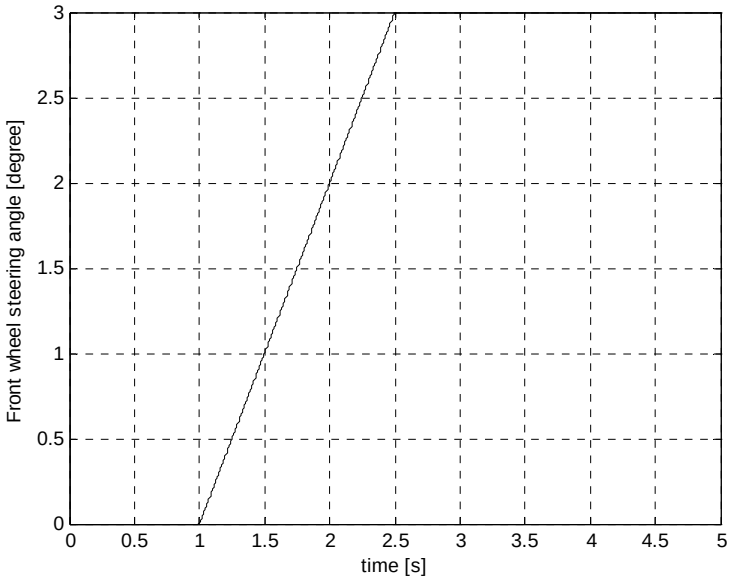

(a)

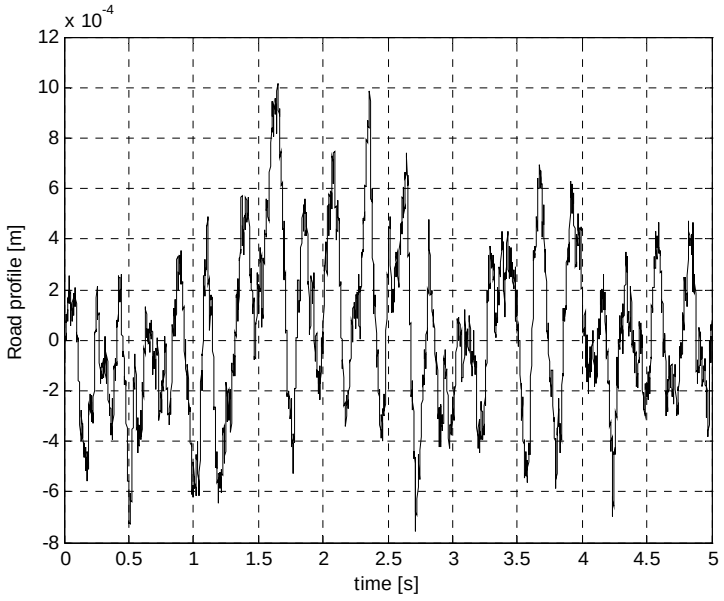

(b)

Figure 6.10 (a) Steering input and (b) paved road profile

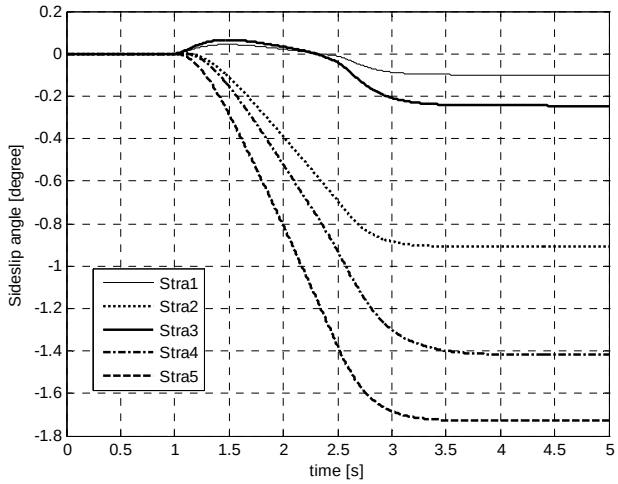

(a)

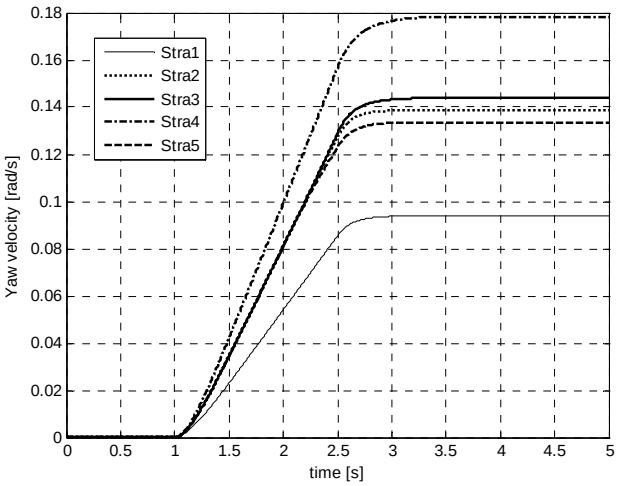

(b)

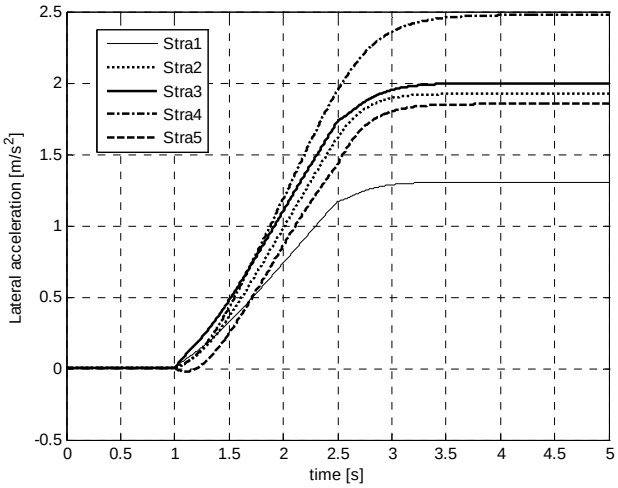

(c)

Figure 6.11 Simulation results for the first five steering strategies for (a) sideslip angle, (b) yaw velocity, (c) lateral acceleration

It is observed that Strategy 5 is the worst strategy since it gives the highest sideslip angle response, together with lower yaw velocity and lateral acceleration responses. On the other hand, Strategy 4 seems to be the best in terms of yaw velocity and lateral acceleration responses. Strategy 2 and Strategy 3 give quite similar yaw velocity and lateral acceleration responses.

Note that as in the three-axle case, the higher the yaw velocity and lateral acceleration responses, the higher the sideslip angle response. Therefore again a means to achieve the best handling characteristics is required, which will ensure high yaw velocity and lateral acceleration responses, and a low sideslip angle response.

With the same steering input and road profile as given in Figure 6.10, and at a constant velocity of 50 kph, the results of the simulation performed for Strategies1, 6 and 7 ($\delta_2 = \delta_3 = 0$ for Strategies 6 and 7) are given in Figure 6.12 as follows:

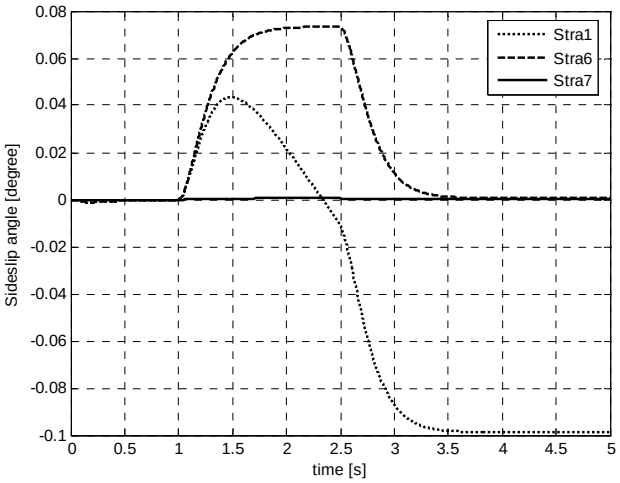

(a)

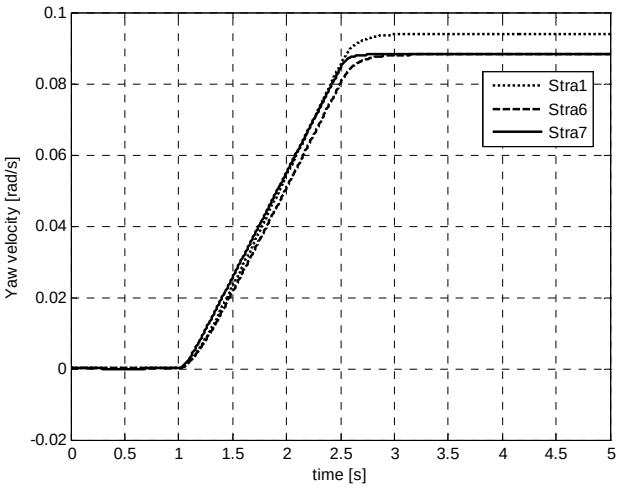

(b)

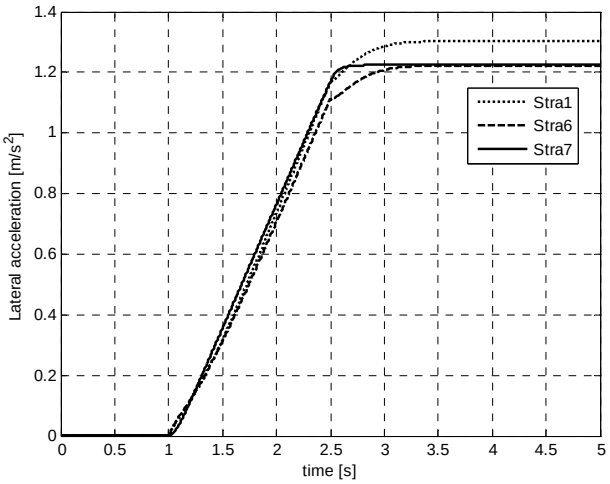

(c)

Figure 6.12 Simulation results for Strategies 1, 6 and 7 for (a) sideslip angle, (b) yaw velocity, (c) lateral acceleration

Note that the best strategy in terms of sideslip angle is Strategy 7, which gives zero sideslip angle even in the transient part of cornering. Strategy 6 coincides with Strategy 7 as the motion settles to steady state as expected, just like the two and three-axle cases.

Strategy 1, namely FWS gives a slightly higher sideslip angle, yaw velocity, and lateral acceleration responses than those of Strategy 6 and Strategy 7.

As in the three-axle case, the low amount of yaw and lateral acceleration responses that are obtained from Strategy 7 can be improved by steering the wheels on intermediate axles. The results in Figure 6.13 are applications of Strategy 7 with different intermediate axle steering schemes. On this figure, steady state lateral acceleration levels for the neutral steer FWS configuration of the vehicle is also indicated.

Recall from Section 4.4 that for a neutral steer, FWS four-axle vehicle, the lateral acceleration at steady state was derived to be

$$(a_l)_{\substack{neutral \\ steady}} = \frac{aC_1V_x^2}{a^2C_1 + b^2C_2 + c^2C_3 + d^2C_4}\delta_f \tag{6.2}$$

For the vehicle used in this simulation which is already neutral steer, that value is calculated to be 1.31 m/sec^2, which can also be checked from Figure 6.11 (c) and 6.12 (c).

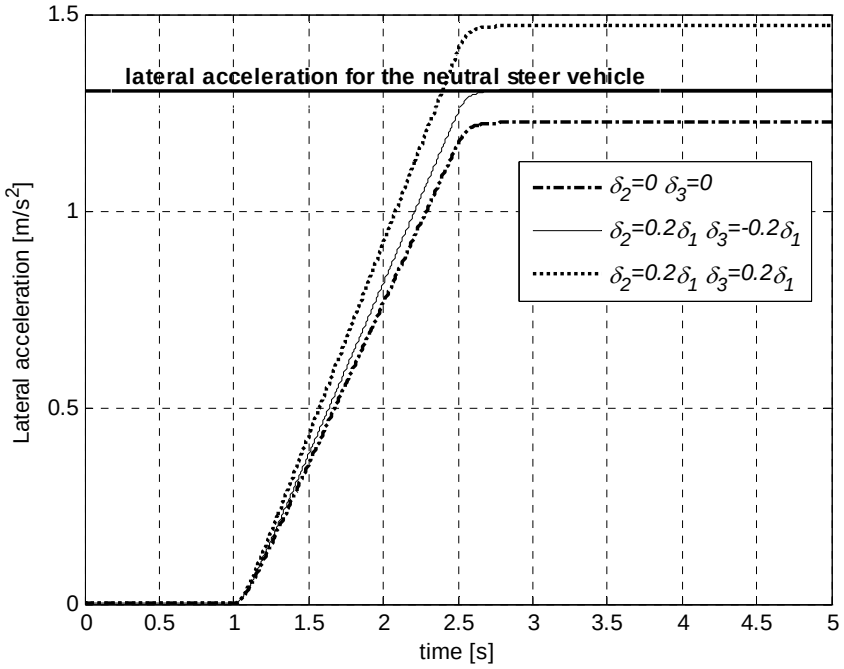

Figure 6.13 Application of Strategy 7 with various intermediate axle steering

It is again noted that yaw velocity and lateral acceleration responses increase without degrading sideslip angle with the application of Strategy 7 together with steering the wheels on intermediate axles. Note that the lateral acceleration at steady state generated by the FWS neutral steer configuration of the vehicle can be achieved by steering the wheels on the first intermediate axle at an amount of $0.2\delta_1$, and the ones on second intermediate axle at an amount of $-0.2\delta_1$ as seen in Figure 6.13. Lateral acceleration can further be increased by steering the wheels on both intermediate axles at an amount of $0.2\delta_1$.

CHAPTER 7

CONCLUSIONS AND FUTURE WORK

The handling characteristics of three and four-axle vehicles in addition to two-axle vehicles are investigated in this study. The mathematical models of the vehicles in this thesis study are built in 3-D space without neglecting any significant degrees of freedom as much as possible, considering the sprung mass degrees of freedom, unsprung mass motions in vertical direction, wheel rotational dynamics, and a nonlinear tire model generating longitudinal and lateral forces.

The differential equations of motion governing the motion of sprung mass, unsprung mass, and wheels are modeled in MATLAB / SIMULINK. A graphical user interface (GUI) is built in MATLAB in order to control the simulation in a broader respect. For the case studies, data for a typical two-axle bus, a three-axle commercial truck, and a four-axle APC are selected.

Existing steering strategies previously developed for two-axle vehicles are applied to the two-axle bus. The simulation results confirmed the results previously found which indicates that it is not possible to reduce the vehicle side slip angle and increase the yaw velocity and lateral acceleration responses of a vehicle simultaneously.

As the next step, the focus of the study is directed upon three and four-axle vehicles, on which only a few results are reported. New strategies to decrease sideslip angle and increase yaw velocity and lateral acceleration responses are derived by extending the theory used for two-axle vehicles, with the utilization of the planar bicycle model. Further, a stability analysis is performed on three and four-axle vehicles, and limits of stability are derived. Terms like neutral steer, understeer, oversteer, critical speed, characteristic speed, etc. which are used in handling studies

for two-axle vehicles are defined for three and four-axle vehicles, and these terms are derived explicitly in terms of vehicle parameters and forward speed.

The simulation results show that the problem with 4WS two-axle vehicles can be solved and a means to achieve low sideslip angle together with high yaw velocity and lateral acceleration is available in the case of three and four-axle vehicles. The solution is steering the wheels on intermediate axles.

It is shown that steering the wheels on intermediate axles at reasonable (construction wise) angles, namely at one third or one fourth of those of front wheels; yaw velocity and lateral acceleration responses can be increased without degrading vehicle sideslip angle. In fact it is possible to realize the lateral acceleration levels of the neutral steer, FWS unloaded three-axle commercial truck and four-axle APC using steering Strategy 8 and Strategy 7 for three and four-axle vehicles respectively. However, for the loaded truck, it was not possible to reach to the neutral steer vehicle's lateral acceleration, even by steering the wheels on intermediate axle at an equal amount to the front wheels, due to the inadequacy of the selected vehicle specifications.

Note that the models built in this thesis study include all degrees of freedom in space. Therefore, these models are open to further studies of performance and ride comfort, in addition to lateral dynamics. For instance, it is also possible for the user to test the handling characteristics of the vehicles under different suspension types, or under acceleration or braking of the vehicles, or under different drive conditions; for a passenger car which is a front wheel drive one, or for a four-axle 8x4 bus, etc. since these are all implemented to the simulation as inputs and options, for future studies. Simple lane changes, or complex driving cycles which can last as much as the user desires, can be performed using the simulation, since the user inputs the simulation time.

The final step in this future study should obviously be the practical application of the developed strategies to real three and four-axle vehicles. This may lead to new problems related to the implementation of control units to the vehicle, in terms of the control methods and equipment; whether mechanical, hydraulic, or electronic control components to be used. But despite the difficulties involved in implementation, it would be invaluable to see how well the proposed control laws work on real vehicles.

REFERENCES

[1] **MATLAB** by "The MathWorks, Inc." Version 7.0.0.19920 (R14), May 06, 2004.

[2] Sano, S., Miyoshi, T., and Furukawa, Y., "**Steer-Angle-Dependent Four-Wheel Steering System-Honda 4WS",** JSAE Review, Vol. 8, No. 1, pp. 80-82, January 1987.

[3] Xia, X., and Law, E. H., **"Non-linear Analysis of Closed Loop Driver / Vehicle Performance with Four Wheel Steering Control",** SAE Transactions, No: 920055, pp. 79-86, 1992.

[4] Furukawa, Y., Yuhara, N., Sano, S., Takeda, H., and Matsushita, Y., **"A review of Four-Wheel Steering Studies from the Viewpoint of Vehicle Dynamics and Control"** Vehicle System Dynamics, Vol. 18, pp. 151-186, 1989.

[5] Wan, M., **"Electronic Traction & Braking Aid",** last access: July, 2006, http://www.autozine.org/technical_school/traction/tech_traction_other.htm
last update: 2003.

[6] Sato, H., Hirota, A., Yanagisawa, H., and Fukushima, T., **"Dynamic Characteristic of a Whole Wheel steering Vehicle with Yaw Velocity Feedback Rear Wheel Steering",** I. Mech. E., 124/83, Road Vehicle Handling, pp. 147-156, 1983.

[7] Shibahata, Y., Irie, N., Ito, H., and Nakamura, K., **"The Development for an Experimental Four-Wheel-Steering Vehicle",** SAE Paper 860623, 1986

[8] Sano, S., Furukawa, Y., and Shiraishi, S. **"Four Wheel Steering System with Rear Wheel steer Angle Controlled as a Function of Steering Wheel Angle",** SAE Paper 860625, 1986.

[9] Yamaguchi, J., **"Four Wheel Steering Blossoms in Japan"**, Automotive Engineering, Vol. 95, No. 7, pp. 60-62, 1987.

[10] Takiguchi T., Yasuda, N., Furutani, S., Kazanawa, H., and Inoue, H., **"Improvement of Vehicle dynamics by Vehicle-Speed-Sensing Four Wheel Steering System",** SAE Transactions, Vol. 95, No. 860624, pp. 870-879, 1986.

[11] Nakaya, H., and Oguchi, Y., **"Characteristic of Four-Wheel Steering Vehicle and its Future Prospect",** International Journal of Vehicle Design, Vol. 8, No. 3, pp. 314-325, 1987.

[12] Whitehead, J. C., **"Four Wheel Steering: Maneuverability and High Speed Stabilization",** SAE Paper, 880642, 1988.

[13] Whitehead, J. C., **"Stabilizing the Weave Mode",** SAE Transactions, Vol. 97, No. 881136, pp. 1-7, 1988.

[14] Higuchi, A. and Saitoh, Y., **"Optimal Control of Four-Wheel Steering Vehicle"**, Vehicle System Dynamics**,** Vol. 22, pp. 397-410, 1993.

[15] Ünlüsoy, Y. S., "Otomobillerde Dört Tekerlekten Doğrultu Kontrolü", **Mühendis ve Makina,** c.40 (1999), n.477, s.25-30.

[16] Kageyama, I., and Nagai, R. **"Stabilization of passenger car-caravan combination using four wheel steering control",** Vehicle System Dynamics, Vol. 24, pp 313-327, 1995.

[17] Huh, K., Kim, J. and Hong, J. **"Handling and driving characteristics for six-wheeled vehicles",** Proceedings of IMechE, Part D, 214**,** 159-170, 2000.

[18] Qu, Q. Z., Liu, Y. Z., and Zhang, J. W., **"Control Strategies of Steering Characteristics of Commercial Three-Axle Vehicle For Front and Rear Wheels Steering",** Int. J. of Vehicle Design, 26, Nos. 2/3, 2001.

[19] Ünlüsoy, Y. S., **"Unpublished ME 513 Vehicle Dynamics Lecture Notes"**, METU, 2004.

[20] **Rhinoceros** by "Robert McNeel & Associates", Version 3.0 SR3, February, 2006.

[21] Risse, H. J. **"Rollwiderstand und Kraftsoffverbrauch",** Automobiltechnische Zeitschrift (.atz), v88, n6, pp. 383-388, 1988.

[22] Chen, A., **"Road Vehicle Performance",** last access: July, 2006, http://www.engineering.usu.edu/cee/transportation/cee3210/Doc/CN2_1.pdf, last update: 2005.

[23] Bakker, E., Nyborg, L., and Pacejka, H.B., **"Tire Modelling for Use in Vehicle Dynamics Studies",** SAE Technical Paper 870432, 1987.

[24] Allen, R., W., and Rosenthal, T., J., **"Steady State and Transient Analysis of Ground Vehicle Handling",** SAE Transactions, 870495, 1987.

[25] Dugoff, H., Fancher, P.S., and Segel, L., **"An Analysis of Tire Traction Properties and Their Influence on Vehicle Dynamic Performance",** SAE paper 700377, 1970.

[26] Jang, B., and Karnopp, D., **"Simulation of Vehicle and Power Steering Dynamics Using Tire Model Parameters Matched to Whole Vehicle Experimental Results",** Vehicle System Dynamics, 33, pp. 121-133, 2000.

[27] Kılıç, V. **"Generation of Deterministic Data From Signals of Known Power Spectral Density",** ME 513 Vehicle Dynamics Term Project, METU, 2003.

APPENDIX

STEERING STRATEGIES

Table A.1 Steering strategies for two-axle vehicle

Two-Axle Vehicle	δ_r
Strategy 1	0
Strategy 2	$\left(\dfrac{bL + M\dfrac{a}{2C_r}V_x^{\,2}}{-aL + M\dfrac{b}{2C_f}V_x^{\,2}} \right)\delta_f$
Strategy 3	$\left(0.25733 + 0.04286\delta_f - 0.00163\delta_f^{\,2} - 0.00003\delta_f^{\,3}\right)\delta_f$
Strategy 4	$\dfrac{2(aC_f - bC_r) - MV_x^{\,2}}{2C_rV_x}r - \dfrac{C_f}{C_r}\delta_f$
Strategy 5	$\dfrac{M}{L}\left(\dfrac{b}{2C_f} - \dfrac{a}{2C_r}\right)V_x r\delta_f$

Table A.2 Steering strategies for three-axle vehicle

Three-Axle Vehicle	δ_m	δ_r
Strategy 1	0	0
Strategy 2	$0.5\delta_f$	0
Strategy 3	0	$-0.5\delta_f$
Strategy 4	$0.5\delta_f$	$-0.5\delta_f$
Strategy 5	$-0.5\delta_f$	$-0.5\delta_f$
Strategy 6	0	$\left(\dfrac{2(aC_f - cC_r) - MV_x^{\,2}}{2C_rV_x}\right)r - \left(\dfrac{C_f + C_m}{C_r}\right)\delta_f$
Strategy 7	$k_m\delta_f$	$\dfrac{-C_f[2(bC_m(a+b) + cC_r(a+c)) + aMV_x^{\,2}] - k_mC_m[2(aC_f(a+b) + cC_r(-b+c)) - bMV_x^{\,2}]}{C_r[2(aC_f(a+c) + bC_m(b-c)) - cMV_x^{\,2}]}\delta_f$
Strategy 8	$k_m\delta_f$	$\left(\dfrac{2(aC_f - bC_m - cC_r) - MV_x^{\,2}}{2C_rV_x}\right)r - \left(\dfrac{C_f + C_mk_m}{C_r}\right)\delta_f$

Table A.3 Steering strategies for four-axle vehicle

Four-Axle Vehicle	δ_2	δ_3	δ_4
Strategy 1	0	0	0
Strategy 2	0	0	$-0.5\delta_1$
Strategy 3	$0.5\delta_1$	$0.5\delta_1$	$-0.5\delta_1$
Strategy 4	$0.5\delta_1$	$-0.5\delta_1$	$-0.5\delta_1$
Strategy 5	$-0.5\delta_1$	$-0.5\delta_1$	$-0.5\delta_1$
Strategy 6	$k_2\delta_1$	$k_3\delta_1$	$-C_1[2(bC_2(-a+b)+cC_3(a+c)+dC_4(a+d))+aMV_x^2]$ $-k_2C_2[2(aC_1(a-b)+cC_3(b+c)+dC_4(b+d))+bMV_x^2]$ $\frac{-k_3C_3[2(aC_1(a+c)+bC_2(b+c)+dC_4(-c+d))-cMV_x^2]}{C_4[2(aC_1(a+d)+bC_2(b+d)+cC_3(c-d))-dMV_x^2}$
Strategy 7	$k_2\delta_1$	$k_3\delta_1$	$\left(\frac{2(aC_1+bC_2-cC_3-dC_4)-MV_x^2}{2C_rV_x}\right)r-\left(\frac{C_1+C_2k_2+C_3k_3}{C_r}\right)\delta_1$